Molecular properties in relativistic electronic structure theory

Joost van Stralen

16 November 2004

Molecular properties in relativistic electronic structure theory

This work was financially supported by the Netherlands Organization for Scientific Research (NWO) through the 'Jonge Chemici' program.

VRIJE UNIVERSITEIT

Molecular properties in relativistic electronic structure theory

ACADEMISCH PROEFSCHRIFT

ter verkrijging van de graad van doctor aan
de Vrije Universiteit Amsterdam,
op gezag van de rector magnificus
prof.dr. T. Sminia,
in het openbaar te verdedigen
ten overstaan van de promotiecommissie
van de faculteit der Exacte Wetenschappen
op dinsdag 16 november 2004 om 15.45 uur
in de aula van de universiteit,
De Boelelaan 1105

door

Johannes Nicolaas Petrus van Stralen

geboren te Heerhugowaard

promotor:	prof.dr. E.J. Baerends
copromotor:	dr. L. Visscher

Contents

Chapter 1

Introduction

The scientific field of electronic structure theory concerns the motion of electrons in the frame of nuclei. The equations that describe this motion result from quantum mechanics. Unfortunately these equations are so complicated that, except for the simplest systems, they cannot be solved exactly. Approximations have to be made. This has resulted in a large arsenal of different electronic structure methods, each with its own advantages and disadvantages, and tailored to specific aims.

One is often not interested in the motion of the electrons themselves, but in quantities (properties) that result from it. The aim of the work described in this thesis is to calculate properties of small molecules as accurately as possible. Most of these molecules contain one or more heavy elements. In the vicinity of heavy nuclei, electrons might obtain such high velocities that the theory of special relativity has to be included in the model used. Otherwise, obtaining high accuracy is doomed to fail. An adequate description of the effects of relativity must, however, take consideration of the two other main 'dimensions' needed for an accurate theoretical description of molecular properties: electron correlation and the basis set.

The molecular properties discussed in this thesis have either a complementary or a predictive value for experiments. In section 1.1 these properties are introduced. In the following sections of this introductary chapter, the three main factors involved in obtaining accurate theoretical values of these molecular properties are described. In section 1.5 an overview of the other chapters of this thesis is given.

1.1 Molecular properties

A classification of quantities that allow a fruitful interplay between theory and experiment has been made by Gauss[1]. For a molecule in a given electronic state, quantities of interest are:

1. Properties involving *different* points on the Born-Oppenheimer potential energy surface. Examples are reaction energies, dissociation energies, energy differences between different isomers, etc.

2. Properties that require information of one electronic state at a *single* point on the potential energy surface. Examples of this kind of quantities are the equilibrium structure, dipole moment, NMR parameters, etc.

3. Properties that characterize transitions between *different* electronic states. Examples of these are electronic excitation energies, radiative life times, electron affinities, etc.

In this thesis we will focus on properties of the second kind, although we sometimes also consider several points of the Born-Oppenheimer potential energy surface. For calculations of properties of this kind, a distinction can be made between frequency-independent and frequency-dependent properties. In this thesis only frequency-independent properties will be considered.

Applying a set of frequency independent perturbations, with field strengths $\boldsymbol{\lambda}$, to a molecular electronic system, its energy can be written as

$$E\left(\boldsymbol{\lambda}\right) = E^{(0)} + \boldsymbol{\lambda}^T \mathbf{E}^{(1)} + \frac{1}{2}\boldsymbol{\lambda}^T \mathbf{E}^{(2)} \boldsymbol{\lambda} + \ldots \,. \tag{1.1}$$

The expansion coefficients $\mathbf{E}^{(n)}$ are the molecular properties of interest and describe the response of the molecular electronic system to the external perturbations. $E^{(0)}$ corresponds to the unperturbed energy of the system, $\mathbf{E}^{(1)}$ corresponds to first-order properties and can be obtained by differentiation of the energy at perturbation strength zero

$$\mathbf{E}^{(1)} = \left.\frac{\mathrm{d}E}{\mathrm{d}\boldsymbol{\lambda}}\right|_{\boldsymbol{\lambda}=0} . \tag{1.2}$$

Differentiation of the energy to second order gives us second-order properties

$$\mathbf{E}^{(2)} = \left.\frac{\mathrm{d}^2E}{\mathrm{d}\boldsymbol{\lambda}^2}\right|_{\boldsymbol{\lambda}=0} , \tag{1.3}$$

etc.

Examples of first-order properties are the molecular gradient, electric field gradient, multipole moments, i.e. the dipole moment, quadrupole moment, octupole moment, etc. Examples of second-order properties are the nuclear magnetic shielding, indirect spin-spin coupling constant, dipole-polarizability, etc.

In this thesis the calculation of first-order molecular properties is discussed. Two properties for which calculations have been performed have already been mentioned in the previous paragraph: the electric field gradient, and the dipole moment. Another property that has been tackled is parity-violation energy. These properties will be described in some detail in the following subsections. In each case the basis functions do not depend on the perturbation that is applied, in contrast to, for example, the molecular gradient. However, before introducing these properties we will briefly say something about the way static molecular properties are calculated.

There are two approaches to the calculation of static molecular properties: numerical and analytical[1]. Both methods are used in the applications described in this thesis. Advantages and disadvantages of each approach can be found in reference [1] and [2]. In the numerical method the derivatives are calculated via finite-differentiation techniques, *e.g.* in the case of a first-order property:

$$\left.\frac{\mathrm{d}E}{\mathrm{d}\lambda}\right|_{\lambda=0} = \frac{E(+\Delta\lambda) - E(-\Delta\lambda)}{2\Delta\lambda}, \tag{1.4}$$

where $\Delta\lambda$ is an appropriately chosen field strength[2].

In the analytical method, an analytical expression for the corresponding derivative is derived and subsequently implemented within a computer code. An abundance of information on this topic can be found in the literature (see, for example, [1], [2] and [3]) and in chapter 2 of this thesis. In the analytical method, a distinction has to be made between so called variational and non-variational methods. For variational methods, like Hartree-Fock, density functional theory and the multi-configuration self consistent field method, the electronic energy is fully optimized with respect to the electronic parameters that describe the wavefunction. First-order molecular properties are very simple to calculate with variational methods since no evaluation of the response of the wavefunction is needed. First-order properties can simply be calculated as expectation values. In the case of a non-variational method, like Møller-Plesset second-order perturbation theory and coupled-cluster theory, the electronic energy is not variational with respect to the

[1] A combination of these methods is also possible.

[2] Note that in equation (1.4), for sake of convenience, λ is a scalar. We apply only one perturbation. In equation (1.2) it is a vector.

electronic parameters that describe the wavefunction. Within these methods the calculation of first-order molecular properties requires extra work. An extra perturbation-independent equation has to be solved to include the response of the wavefunction to the applied perturbation.

1.1.1 Electric field gradients

A nucleus with a spin quantum number greater than $\frac{1}{2}$ possesses an electric quadrupole moment. One can think of this in terms of an ellipsoidal charge distribution of the nucleus. Electric quadrupoles do not interact with spatially uniform electric fields, but with the gradient of an electric field[4]. The electric field gradient at a nucleus is a measure of a *non-spherically symmetric* distribution of local electronic charge.

The nuclear quadrupole coupling energy, in atomic units, due to the quadrupole moment of nucleus X is given by the relationship

$$E\left(X\right) = \frac{1}{2}\mathrm{Tr}\left(\mathbf{q}\left(X\right)\mathbf{Q}\left(X\right)\right), \tag{1.5}$$

where $\mathbf{q}\left(X\right)$ is the electric field gradient tensor at nucleus X and $\mathbf{Q}\left(X\right)$ the nuclear quadrupole moment tensor of this nucleus.

The operator for the electric field gradient (EFG) at nucleus X is given by

$$\begin{aligned} \hat{q}_{\alpha\beta}\left(X\right) &= \sum_{Y\neq X} Z_Y \frac{3R_{XY\alpha}R_{XY\beta} - \delta_{\alpha\beta}R_{XY}^2}{R_{XY}^5} \\ &- \sum_i \frac{3r_{iX\alpha}r_{iX\beta} - \delta_{\alpha\beta}r_{iX}^2}{r_{iX}^5}, \end{aligned} \tag{1.6}$$

where Z_Y is the charge of the neighbouring atom Y, $\mathbf{R}_{XY}$ is the position vector of nucleus X relative to Y and $\mathbf{r}_{iX}$ the position vector of electron i relative to X. Greek letter subscripts represent Cartesian directions.

For diatomic molecules the energy expression, equation (1.5), reduces to

$$E\left(X\right) = \frac{1}{4}q_{zz}\left(X\right)Q\left(X\right), \tag{1.7}$$

with the z-axis chosen along the molecular bond. It is customary to call the quantity $Q = 2Q_{zz} - Q_{xx} - Q_{yy}$ simply the 'nuclear quadrupole moment' (NQM)[4].

Quadrupolar nuclei are relatively unpopular in nuclear magnetic resonance (NMR) studies since the coupling of the quadrupole moment with the

EFG causes efficient spin relaxation, which results in linebroadening. Another major consequence of quadrupolar relaxation is the loss of multiplet structure for spins that are scalar-coupled to quadrupolar nuclei[5].

The most common experimental techniques where the coupling of the quadrupolar nuclei with the EFG is used are nuclear quadrupole resonance (NQR) (solids, oriented molecules in liquid crystals), Mössbauer spectroscopy (solids) and microwave spectroscopy (gas phase molecules). The advantage of the EFG is that it is very sensitive to changes of the electron distribution. A spectacular example of this was recently shown by Evans *et al.*[6] in microwave spectra of AuCl, Ar-AuCl and Kr-AuCl. While the nuclear quadrupole couplings constant (NQCC) of Au has the value +9.6 MHz in AuCl it changes sign in the noble gas-AuCl complexes, being -259.8 MHz and -349.9 MHz for Ar-AuCl and Kr-AuCl respectively.

The availability of accurate nuclear quadrupole moments is important for several reasons: to test nuclear models for stable isotopes in nuclear physics, in studies of molecular dynamics in systems where nuclear quadrupole effects determine the spin-lattice relaxation time, and simply since it allows an accurate experimental determination of the EFG. Reference values of NQMs have been tabulated by Pyykkö in 2001[7]. A method that has become popular for the accurate determination of NQMs in recent years is the combination of NQCCs from high-resolution spectroscopy with accurate EFGs from quantum chemical calculations on diatomic molecules, an example of this can be found in references [8] and [9] and in chapters 3 and 4 of this thesis.

1.1.2 Dipole moments

When a uniform electric field, $\mathbf{F}$, is present the energy of a molecular system can be written as

$$E(\mathbf{F}) = E^{(0)} - \mathbf{F}^T\boldsymbol{\mu} - \frac{1}{2}\mathbf{F}^T\boldsymbol{\alpha}\mathbf{F} + \ldots , \tag{1.8}$$

where $\boldsymbol{\mu}$ is the permanent dipole moment at zero field:

$$\boldsymbol{\mu} = -\left.\frac{\mathrm{d}E}{\mathrm{d}\mathbf{F}}\right|_{\mathbf{F}=0} \tag{1.9}$$

and $\boldsymbol{\alpha}$ is the dipole-polarizability.

The operator we need to calculate the dipole moment in direction α is the dipolar operator

$$\hat{\mu}_\alpha = \sum_K Z_K R_{K\alpha} - \sum_i r_{i\alpha}, \tag{1.10}$$

where the first summation is over the nuclei with charges Z_K and position vectors $\mathbf{R}_K$, and the second summation is over the electrons with position vectors $\mathbf{r}_i$.

Calculating the dipole moment for a whole range of internal coordinates makes it possible to construct a dipole moment surface, $\boldsymbol{\mu}(\mathbf{R})$. Obtaining wavefunctions for the nuclear motion on the Born-Oppenheimer surface, together with the dipole moment surface, allows for subsequent calculation of rotation-vibration transition intensities[10, 11], and hence the rotation-vibration spectrum can be simulated. Calculation of a whole dipole moment surface and the solution of the quantum mechanical nuclear motion problem is however restricted to few atom systems. An example of this is the water molecule, see references [12] and [13] and chapter 6. However, to simulate the intensities of the vibrational spectrum it is often sufficient to calculate the first derivative of the dipole moment with respect to the modes of interest[14, 15].

1.1.3 Parity-violation energies

A molecule is said to be chiral if it is not superposable with its mirror image. Chirality is one of the most important phenomena in molecular sciences. It was not without reason that in 2001, exactly 100 years after the first Noble prize in chemistry was given to the Dutchman J. A. van 't Hoff[3], a shared Noble prize was given to W. S. Sharpless and R. Noyori for their work on chirally catalyzed hydrogenation reactions, and to K. B. Sharpless for his work on chirally catalyzed oxidation reactions. The main reason why chirality is so important in chemistry is the different biological activities of mirror image compounds, a fascinating example of which is the taste of carvone: while the D-form has a caraway taste, the L-form tastes minty.

A chiral molecule can be converted into its mirror image by a space inversion followed by a rotation through an angle π. The operator that performs a space inversion, thereby reflecting the spatial coordinates of every particle at the origin, $(\mathbf{r} \rightarrow -\mathbf{r})$, is called the parity operator, $\mathcal{P}$. If $\mathcal{P}$ commutes with the Hamiltonian of the system, $\hat{H}$, then the physics is the same regardless of whether it is described in a left- or right-handed coordinate system. This kind of symmetry is called parity. If, say, we have two chiral states, $|\mathrm{L}\rangle$ and $|\mathrm{R}\rangle$, and the Hamiltonian commutes with $\mathcal{P}$, then $|\mathrm{L}\rangle$ and $|\mathrm{R}\rangle$ are obviously not eigenstates of the Hamiltonian. The eigenstates are plus- and

[3]van 't Hoff proposed that carbon was tetraedrically surrounded. This concept explained the experiments on optical activity of Louis Pasteur. However, van 't Hoff received the Noble prize for another subject: the laws of chemical dynamics and osmotic pressure in solution.

minus-combinations of these handed states. Hund[16] attributed the presence of chiral molecules to the very long time required for an initially prepared handed state to change to the state of opposite handedness. This, however, does not explain why one can bottle the left- and right-handed forms of a chiral compound but not their coherent superposition[17]. An answer to this question might be the presence of parity-violating interactions[18].

In the 1950s it was discovered that parity is violated in nuclear physical processes that are governed by the weak interaction[19, 20]. In molecules, however, by far the the most important force is the electromagnetic force, and at first sight it is not clear how the parity violating weak force might affect molecular systems. A connection between these two forces was given in the 1960s by Glashow, Weinberg and Salam[21–23], with the unification of the weak and electromagnetic interaction within the electroweak model. The effects of the parity-violating weak interaction are, however, so small that up to now experimentalists have not been able to detect the effect in molecular systems. Recent calculations of parity-violation effects for the C-F stretching mode of chiral methyl fluorides indicate that the resolution of current precision optical spectroscopy has to be improved by about two or three orders of magnitude if the effect is to be detected[24]. This makes the search for the breakdown of mirror image symmetry one of the most challenging tasks for molecular spectroscopists.

Since the effect of the parity-violating weak interaction on molecules is so small, the use of perturbation theory seems to be the natural choice for calculating it. The question is then: what is the (effective) perturbation Hamiltonian needed? To answer this, one has to start from the standard model of physics. A detailed route from the current standard model of physics to the Hamiltonians used in parity-violation calculations can be found in a nice overview by Berger[25]. Here we will not go into detail, just give the operator. Within the four-component Dirac-Coulomb method[4], the operator commonly used for the calculation of parity-violation energies, E_{PV}, is the nuclear spin-independent $\mathcal{P}$-odd operator[26],

$$\hat{H}_p = \frac{G_F}{2\sqrt{2}} \sum_{i,n} Q_{W,n} \gamma_i^5 \varrho_n \left(\mathbf{r}_i\right), \tag{1.11}$$

where the summations run over the electrons i and the nuclei n. $G_F = 1.166\,37 \times 10^{-11}$ MeV^{-2} $= 2.222\,55^{-14}$ a.u. is the Fermi coupling constant, the pseudo-scalar γ^5 chirality operator is given by

$$\gamma^5 = \begin{pmatrix} \mathbf{0} & \mathbf{I} \\ \mathbf{I} & \mathbf{0} \end{pmatrix}, \tag{1.12}$$

[4]See section 1.2 for more information about four-component methods.

where $\mathbf{I}$ and $\mathbf{0}$ are the 2×2 unit and zero matrix, respectively. The normalized nucleon density[5] is ϱ_n and $Q_{W,n} = -N_n + Z_n\left(1 - 4\sin^2\theta_W\right)$ is the weak charge of nucleus n with N_n neutrons and Z_n protons. For the terms depending on the Weinberg mixing angle θ_W, we used the value $\sin^2\theta_W = 0.2319$. Note that $\hat{H}_p$ in this case is represented by a 4×4 matrix.

Using the Dirac-Coulomb formalism, where spin-orbit coupling is included in a variational manner, E_{PV} can simply be calculated as a first-order property. In a non-relativistic or scalar-relativistic framework, the equivalent of equation 1.11 is approximately given by[27]:

$$\hat{H}_p^{nr} \approx \frac{G_F}{4\sqrt{2}} \sum_{i,n} Q_{W,n} \left[\boldsymbol{\sigma}_i \cdot \mathbf{p}_i, \varrho_n\left(\mathbf{r}_i\right)\right]_+ , \tag{1.13}$$

where $[a, b]_+$ is the anticommutator of a and b, $\boldsymbol{\sigma}_i$ are the Pauli spin matrices (see section 1.2) and $\mathbf{p}_i$ is the electron momentum operator. Since this operator is purely imaginary, the expectation value for a non- or scalar-relativistic wavefunction is zero. This problem can be circumvented by using response theory, with the spin-orbit operator as the perturbation that mixes imaginary character into the wavefunction. The disadvantage of such an approach is clearly that E_{PV} has to be calculated as a second-order property, whereas in the Dirac-Coulomb formalism it can be calculated as a first-order property.

Within the Dirac-Coulomb formalism, this implies that E_{PV} can be calculated simply by taking the expectation value of $\hat{H}_p$, if we have an exact wavefunction or a wavefunction obtained using a variational method. If we have two molecular states, $|\Psi\rangle$ and $\mathcal{P}|\Psi\rangle$, related by parity inversion (i.e. they are each others mirror image), then,

$$E_{\mathrm{PV}} = \langle\Psi|\hat{H}_p|\Psi\rangle = -\langle\mathcal{P}\Psi|\hat{H}_p|\mathcal{P}\Psi\rangle. \tag{1.14}$$

The parity-violating operator lifts the energy of one enantiomer by E_{PV}, and lowers the energy of its mirror image by the same amount. The parity-violation energy difference between the two mirror images is thus

$$\Delta E_{\mathrm{PV}} = 2|E_{\mathrm{PV}}|. \tag{1.15}$$

Recently, calculations have been performed with the goal to find suitable candidates to measure the effect of parity-violation in experiment [24, 28–30]. In a later stage, theory will also be needed to analyze and interpret the results of such experiments.

[5] In the limiting case of a point nuclear charge this is a three-dimensional Dirac delta function.

1.2 Relativistic electronic structure theory

The special theory of relativity is based on two postulates:

1. The laws of physics are the same in all inertial frames.

2. The velocity of light in the vacuum c is a fundamental constant and thus the same in all intertial frames.

Incorporating the consequences of these postulates in the theory of quantum mechanics results in relativistic quantum mechanics. The difference between results obtained using a relativistic model and a non-relativistic model are called 'relativistic effects'. These effects are not real physical effects, but result from the use of different models in describing physical phenomena.

By now it is well established that we need to use a relativistic model in the quantitative description of the electronic structure of molecules containing heavy elements. If extremely high accuracy is demanded, relativistic effects might even play a role for molecules that contain only light elements. A distinction can be made between scalar relativistic effects and spin-orbit coupling (SOC) effects. Scalar relativistic effects arise because in the vicinity of the (heavy) nucleus electrons acquire high velocities, a substantial fraction of the velocity of light. SOC effects result from the coupling of spin degrees of freedom with orbital motion. SOC phenomena are of symmetry breaking nature.

In the next subsections some aspects of relativistic electronic structure theory are discussed. A more comprehensive overview of this topic can be found in the two books edited by Schwerdtfeger[31, 32].

1.2.1 The Dirac equation

The equation for a single particle (an electron in our case) in an external potential, $-\phi(\mathbf{r})$, that moves in accordance with quantum mechanics and special relativity is the Dirac equation[33]:

$$\hat{h}_D\psi = i\frac{\partial\psi}{\partial t}. \tag{1.16}$$

with[6]

$$\hat{h}_D = \beta c^2 + c\boldsymbol{\alpha}\cdot\mathbf{p} - \phi\left(\mathbf{r}\right) \tag{1.17}$$

[6]The vector potential, $\mathbf{A}$, has been left out, because it is not relevant for the following.

Where $\mathbf{p}$ is the momentum operator. In the standard representation, $\boldsymbol{\alpha}$ is given by

$$\alpha_i = \begin{pmatrix} \mathbf{0} & \sigma_i \\ \sigma_i & \mathbf{0} \end{pmatrix}, \tag{1.18}$$

with $\mathbf{0}$ a 2×2 zero matrix and σ_i, $i = x, y, z$, are the Pauli spin matrices

$$\sigma_x = \begin{pmatrix} 0 & 1 \\ 1 & 0 \end{pmatrix}, \quad \sigma_y = \begin{pmatrix} 0 & -i \\ i & 0 \end{pmatrix}, \quad \sigma_z = \begin{pmatrix} 1 & 0 \\ 0 & -1 \end{pmatrix}. \tag{1.19}$$

β is given by

$$\beta = \begin{pmatrix} \mathbf{I} & \mathbf{0} \\ \mathbf{0} & -\mathbf{I} \end{pmatrix}. \tag{1.20}$$

In the work described in this thesis we restrict ourselves to potentials that are time-independent. This means that we can use the time-independent Dirac equation[7]

$$\hat{h}_D \psi = E\psi. \tag{1.21}$$

Since the α and β matrices are 4×4 matrices, the solutions of this eigenvalue equation are four-component wavefunctions,

$$\psi = \begin{pmatrix} \psi^{\mathrm{L}\alpha} \\ \psi^{\mathrm{L}\beta} \\ \psi^{\mathrm{S}\alpha} \\ \psi^{\mathrm{S}\beta} \end{pmatrix}. \tag{1.22}$$

The components with a superscript L correspond to the 'Large' component, the ones with superscript S correspond to the 'Small' component.

In non-relativistic quantum chemistry, it is common to talk about 'orbitals', 1-component 1-electron wavefunctions. The solution of the Dirac equation is a four-component vector, it is common to use in this case the term 'spinor' instead of orbital.

If the Dirac equation is solved for a free particle, i.e. $\phi(\mathbf{r}) = 0$ for all $\mathbf{r}$, we get two kinds of solutions: solutions with eigenvalues less than $-mc^2$ and solutions with eigenvalues greater than $+mc^2$. Our main interest is in the positive energy solutions. For the positive energy solutions, the upper components (ψ^{L}) have a large amplitude and the lower components (ψ^{S}) have a small amplitude.

[7] From this point we will simply refer to this equation as 'the Dirac equation'.

In non-relativistic quantum mechanics, the variation principle is a very useful concept. In the Dirac theory the formulation of such a variational formalism is problematic because if the negative energy continuum is empty electrons will fall into it under emission of photons. Dirac resolved this dilemma in 1929 by postulating that the negative energy states are completely filled[34]. If an electron is excited from the negative energy continuum a 'hole' is left behind. The hole behaves as a particle with the same mass as an electron but with opposite charge. The negative energy states are therefore connected with *positrons*. The filling of the negative energy continuum implies that the 'vacuum' is infinitely charged and has an infinite energy. This awkward property can be solved by going one step further and using *normal ordered* operators, which means that the vacuum expectation value of the corresponding operator is subtracted from the operator. The effect is that, although filled, the charge and energy of the vacuum are zero.

In programs that employ the Dirac Hamiltonian one uses the empty Dirac approach, i.e. the negative continuum is not filled. In a four-component Hartree-Fock calculation, for example, the desired electronic state is an excited state to which one converges by using vector selection by implicitly projecting out negative energy states[35]. This is equivalent to employing a mini-max principle[36] where the energy is minimized with respect to positive energy parameters and maximized with respect to negative energy parameters.

1.2.2 Many-electron relativistic theory

In this thesis only calculations on systems containing more than one electron are considered. This means that the interaction between electrons has to be taken into account. The Hamiltonian for the complete electron-electron interaction can be obtained from quantum electrodynamics (QED)[37]. However, this interaction can not be written in closed form, and can only be obtained from time-dependent perturbation theory. For practical purposes approximations to the electron-electron interaction have to be made. Here we restrict ourselves to interactions in the lowest order. The interaction of one electron with another via the exchange of a photon with frequency $\omega_{\alpha\gamma}$ is[38]

$$\hat{v}_{ij,\alpha\gamma} = \frac{1}{r_{ij}} - \left(\frac{\boldsymbol{\alpha}_i \cdot \boldsymbol{\alpha}_j}{r_{ij}} \exp(i\omega_{\alpha\gamma} r_{ij}) + (\boldsymbol{\alpha}_i \cdot \nabla_i)(\boldsymbol{\alpha}_j \cdot \nabla_j) \frac{\exp(i\omega_{\alpha\gamma} r_{ij}) - 1}{\omega_{\alpha\gamma}^2 r_{ij}} \right), \quad (1.23)$$

in case the Coulomb gauge is used ($\nabla \cdot \mathbf{A} = 0$). It is a good approximation to let $\omega \to 0$, in which case the electron-electron interaction reduces to the

Coulomb-Breit interaction[39]

$$\hat{g}^{Coulomb-Breit}(i,j) = \frac{1}{r_{ij}} - \left(\frac{\boldsymbol{\alpha}_i \cdot \boldsymbol{\alpha}_j}{r_{ij}} + \frac{1}{2}(\boldsymbol{\alpha}_i \cdot \nabla_i)(\boldsymbol{\alpha}_j \cdot \nabla_j) r_{ij} \right). \quad (1.24)$$

The first term is the well known Coulomb interaction, which also appears in non-relativistic calculations. The term between brackets is the Breit interaction. The first term of the Breit interaction is called the Gaunt interaction since it was also derived by Gaunt in 1929[40]. The Gaunt interaction is a current-current interaction and contains spin-spin, orbit-orbit and spin-other-orbit contributions. The second term of the Breit interaction is called the gauge term and arises from the retardation of the interaction due to the finite speed of light. This term doesn't appear when one uses the Feynman gauge.

The Coulomb interaction is the lowest order interaction in perturbation theory. The Breit interaction comes in order c^{-2} in the perturbation expansion and is neglected in many four-component calculations[8]. All four-component results reported in the following have been performed using DIRAC[41]. In this program, only the non-relativistic Coulomb electron-electron interaction is implemented.

The final Hamiltonian that we will use for our relativistic calculations on molecules in the Born-Oppenheimer reference frame is the following

$$\hat{H}_{DC} = \sum_i \hat{h}_D(i) + \frac{1}{2} \sum_{i \neq j} \hat{g}^{Coulomb}(i,j) + \hat{V}_{NN}, \quad (1.25)$$

where we have a summation over one-electron Dirac Hamiltonians, the Coulomb electron-electron interaction, and the classical repulsion of nuclei, $\hat{V}_{NN}$. This Hamiltonian is called the Dirac-Coulomb Hamiltonian.

The bottleneck in quantum-chemical calculations is the calculation of the electron-electron interaction. It is common practice to expand molecular orbitals (MO) (or molecular spinors (MS)), ψ_I, as a linear combination of a set of trial functions, a basis set $\{\chi_\mu\}$,

$$\psi_I = \sum_\mu C_{\mu I} \chi_\mu \quad (1.26)$$

where $\{C_{\mu I}\}$ is a set of expansion coefficients that need to be determined. Due to this strategy one encounters the so called two-electron integrals

$$(\mu\nu|\kappa\rho) = \int\int \chi_\mu(\mathbf{r}_1)\chi_\nu(\mathbf{r}_1) \frac{1}{r_{12}} \chi_\kappa(\mathbf{r}_2)\chi_\rho(\mathbf{r}_2)\, d\mathbf{r}_1 d\mathbf{r}_2. \quad (1.27)$$

[8] In most four-component programs it's also not implemented.

In a four-component calculation the basis set used for the evaluation of the small component is different from the basis set for the large component (see section 1.4). The basis set for the large component is similar in size to that for a non-relativistic calculation. However, the basis set for the small component is about 2 to 3 times larger than the large component basis. In calculations where the Dirac-Coulomb Hamiltonian is employed, three different classes of two electron integrals appear: integrals over only the large component, (LL|LL); integrals where the basis set of one electron are of L type and the basis set for the other electron are of S type, (LL|SS) and (SS|LL); and a class of the integrals of (SS|SS) type. It is evident that the presence of such extra integrals over the small component makes four-component calculations much more expensive than non-relativistic calculations.

The situation for the four-component methodology gets even worse if we realize that, unless magnetic interactions are present, in non-relativistic calculations we only have to deal with real numbers, while in four-component calculations it can happen that we have to work with complex numbers, depending on the symmetry of the system under consideration. Another difference is that the non-relativistic Hamiltonian doesn't have an explicit dependence on spin, which means that orbitals can be split in a product of a spatial part and a spin part. As a consequence, the spin part can be integrated analytically, and the sixteen two-electron integrals can be reduced to one. In the Dirac-Coulomb Hamiltonian, spin and spatial degrees of freedom are coupled, the so called spin-orbit coupling (SOC), and we can not factorize the spin degrees of freedom out. Fortunately, some reduction in computational work can be gained by exploiting time-reversal symmetry, from which it can be shown that certain kinds of two-electron integrals are related. See reference [42] and [43] for more details.

The use of point group symmetry can reduce the computational costs of electronic structure calculations significantly. In non-relativistic theory we only have to consider the point group symmetry operations that work on the spatial coordinates of the molecule. The Schrödinger Hamiltonian is invariant under these operations. However, the Dirac-Coulomb Hamiltonian is not. Since the spin and spatial degrees are coupled, the symmetry operations that leave the Dirac-Coulomb Hamiltonian invariant are a product of spatial and spin operations. As a result the number of symmetry operations is doubled, and the groups are called double groups. Besides the irreducible representations (irreps) that are used in non-relativistic theory − the boson irreps − we also have irreps that describe the one-electron functions of the Dirac-Coulomb Hamiltonian: the fermion irreps. Unfortunately the number of fermion irreps is not the same as the number of boson irreps. An example is the symmetry group of water: C_{2v}. While C_{2v} has four different boson

irreps, it only has one fermion irrep. This means that fewer two-electron integrals are zero on symmetry grounds. More about double groups can be found in the literature, in [44], [45] and [46], for example.

Since there is quite a difference in the costs of a full Dirac-Coulomb calculation and a non-relativistic calculation, it is interesting to look for methods that take relativistic effects into account in an approximate but more efficient way than the full Dirac-Coulomb method. Approximations to Dirac-Coulomb calculations are discussed in the next section.

1.2.3 Approximate methods

One way to reduce the computational effort is to make approximations within the four-component framework. This has the advantage that the accuracy of approximations can easily be tested, and results can be kept close to those of the full four-component calculations. Following this route most computational time can be saved by approximating two-electron integrals over the small component. In most of the applications described in this thesis, we simply neglected the (SS|SS) integrals, since their contribution is often negligible. The effect of (SS|SS) integrals on the energy can approximately be accounted for using a simple Coulombic correction[47]. Due to the locality of the small component wavefunction around the nuclei it is physically well justified to make even more severe approximations, and neglect all two-electron integrals that have small component basis functions centered on different nuclei, the so called one-center approximation[48, 49]. More development in this direction might be expected in the near future, thereby extending the applicable range of four-component algorithms[50].

As mentioned above the coupling between spatial and spin degrees of freedom (SOC) is another factor making DC calculations way more expensive than non-relativistic calculations. However, spin-free relativistic effects, also called scalar-relativistic effects dominate the relativistic corrections to electronic structure in most closed shell systems. A reasonable approximation would seem to be to neglect the spin-dependent parts of the Hamiltonian. To this end the spin-dependent and spin-independent part of the Dirac equation have to be separated. Within a four-component framework, Dyall[51] achieved this using the so called modified Dirac operator, which was first introduced by Kutzelnigg[52]. At this point it is also worthwhile mentioning that SOC operators cannot be defined unambiguously, but depend on the method of separation of spin-free and spin-dependent terms, as has been demonstrated nicely by Visscher and van Lenthe[53].

Another strategy is to treat relativistic effects in a perturbative manner. One perturbative approach is the Direct Perturbation Theory (DPT) method

developed by Kutzelnigg[54, 55]. In this method the metric is changed, after which the resulting equation is expanded in c^{-2}.

An old, but often used perturbation method, is based on the elimination of the small component followed by expansion of the results in $(E-\hat{V})/mc^2$. To first order, this gives the so-called Breit-Pauli operator[56]. However, this operator contains singular terms restricting its use to first-order perturbation theory. Applications following this route show that it gives sufficiently accurate results for the first and second transition-metal row, but for the third row a treatment of relativistic effects to higher order is needed[57].

A method that can be used in variational calculations is the Douglas-Kroll-Hess (DKH) method[58–61]. In this method the Large and Small component are approximately decoupled by a sequence of unitary transformations. The unitary transformations contain external potential terms. The resulting operators are products of a square root expression of p^2, and the resolution of identity technique is used to evaluate them.

Another method that can be used in variational calculations is the zero order regular approximation (ZORA) method. Based on initial work of Chang, Pélissier, and Durand (CPD)[62] it has been developed further by van Lenthe *et al.* [63–66]. In the ZORA method, the Large and Small components are decoupled using a Foldy-Wouthuysen transformation[67]; the resulting equation is subsequently expanded in $E/(2mc^2-\hat{V})$. The equation to zeroth order is the ZORA equation. In effect, the ZORA equation is a Schrödinger equation with a modified kinetic energy operator. Because of the appearance of the potential, $\hat{V}$, in the denominator, it is mainly used in density functional theory because local potentials are used there. Due to the use of the non-local exchange potential in *ab initio* methods, one has to make use of the resolution of identity to be able to use ZORA[68]. The relation between the Dirac equation, the non-relativistic Lévy-Leblond equation[69], Dyall's spin-free relativistic equation and the ZORA and scalar-relativistic ZORA equation has been elegantly demonstrated by Visscher and Saue[70] using the quaternion modified Dirac equation.

Both DKH and ZORA are two-component methods if SOC is included. If only scalar-relativistic effects are taken into account, DKH and ZORA are both one-component methods, and both Hamiltonians are essentially as expensive to use as than their non-relativistic counterpart. It is surprising that, although both DKH and ZORA have been in use for more than ten years, nobody has ever made a systematic comparison of the performance of DKH and ZORA with DC as a reference. A comparison on the same footing between ZORA and DKH, but not DC, for spectroscopic properties of some diatomic molecules has been made by Hong *et al.* [71]. The conclusion was that the methods give almost the same results. In general it can be said

that both DKH and ZORA are methods that reproduce most of the relativistic effect, also if heavy elements are present, and are very cost effective alternatives to the DC Hamiltonian.

For most chemical properties only the valence electrons are of importance, and the electron density near the nucleus doesn't change much on molecule formation. This insight is used in the treatment of relativistic effects using the so called effective core potential (ECP) method[72]. In the ECP method the core electrons are not taken into account explicitly in the Hamiltonian, but their effect is modeled by a set of parameters whose values are based on relativistic atomic reference calculations. This method is the most economical way to treat relativistic effects since the number of electrons (of heavy elements) is drastically reduced and besides the extra parameters, which only affect the one-electron part of the Hamiltonian, the non-relativistic Hamiltonian can be used. The ECP method is a very useful method in geometry optimizations, the calculation of electric properties like dipole moments, polarizabilities, etc. However, for properties that are heavily determined by the shape of the wavefunction in the vicinity of the nucleus, like EFGs and NMR parameters, the use of ECPs is less suited.

Almost all results presented in this thesis are based on the DC Hamiltonian. One might wonder why one of the good, computationally more efficient, alternatives mentioned above is not used to take relativistic effects into account? If one of these more economical methods were used, a larger basis set could be adopted so that in the end the quality of calculations might be even higher at the same cost. For most applications presented in this work it can be said that we are seeking the highest quality of calculations possible. Approximations made in the relativistic description might be critical for the quality of the results. For example, for a core-valence property like the EFG, a high level description of relativistic effects is very important in obtaining accurate results. The basis sets we use are of high enough quality because the molecules studied are very small, with only a few atoms.

Another advantage of using the DC formalism, compared to approximate methods, is that the property operators stay simple. In the ZORA and DKH method, besides the transformation of the Hamiltonian, the property operator should also be transformed, resulting in complicated expressions for the property operators. Neglecting the transformation of the property operators results in the so called *picture change effect* [73]. This effect might be negligible for valence properties, like the dipole moment, but it can not be neglected for a property like the EFG[74].

As already mentioned in subsection 1.1.3, for the calculation of parity-violation in molecules, the DC formalism is very advantageous because SOC is included in a variational manner. For this property, it might be expected

that a high-level relativistic formalism is important anyway. For an overview of properties for which it is advantageous to work within the DC formalism, see the thesis of Jørn Thyssen[43].

A practical reason for why most calculations have been performed using the DC formalism is that almost all have been performed using the DIRAC program[41]. DIRAC is a molecular four-component program which, in addition to DC calculations, can also perform spin-free calculations. ZORA is implemented, but not as efficiently as it could be. Other relativistic methods are not implemented in DIRAC. Besides DIRAC, there are several other programs with which molecular four-component calculations can be performed (see references [75–80]).

1.3 Electron correlation

If more than two particles interact with each other, the equations that describe the behavior of these particles can not be solved exactly. Approximations are needed. In electronic structure theory, one of these methods is the Hartree-Fock (HF) method; this method is described in numerous textbooks (see, for example, references [81, 82]). In the HF method the wave-function is represented by a single Slater determinant. The HF method is variational with respect to the parameters that describe the wavefunction, the spinor coefficients. The spinors that describe the HF wavefunction are solutions of one electron equations in the average field of the other electrons. However, in reality electrons do not move in an average field, but their movement depends on the instantaneous position of the other electrons − their motion is correlated. Some methods that try to include the effects of electron correlation are described in the following subsections.

Even though HF neglects electron correlation, it works reasonably well for describing closed-shell ground-state wave functions at the molecular equilibrium geometry. Since HF is a relatively cheap method it is still quite popular.

There are many methods that account for electron correlation. For a good overview of the most important methods see references [82–84]. The difference between the exact solution of the Schrödinger equation and the Hartree-Fock equation is the correlation energy. One can also make a distinction between *static* and *dynamical* correlation, although this division is somewhat loosely defined. Static correlation is also known as near-degeneracy or nondynamical correlation and arises from the near-degeneracy of electronic configurations; it may be described by a few determinants. Dynamical correlation is associated with the instantaneous correlation between the electrons, arising from their mutual repulsion, and requires a large number of determi-

nants. Most of the results described in this thesis correspond to molecules that are in a state where static correlation is not important. This means that Hartree-Fock already provides a qualitatively correct description of the wavefunction. The methods we use to take correlation effects into account are especially well suited to representing dynamical correlation.

1.3.1 Møller-Plesset perturbation theory

Conceptually, one of the simplest methods to take electron correlation into account is many-body perturbation theory (MBPT) with the Møller-Plesset perturbation operator. In the theoretical chemistry community, these methods are denoted as MPn (with n the order of perturbation theory used). In the physics community they are often denoted as MBPT(n).

Møller and Plesset were the first to develop a perturbation theory in which the HF wavefunction is taken as zeroth-order solution to the exact wavefunction. The difference between the exact Hamiltonian and the HF Hamiltonian is considered as a small perturbation, which corrects the average-field approximation of HF such that the correlated movement of the electrons is explicitly included. In this thesis, only perturbation theory up to second-order, MP2, is used.

The MP2 correlation energy is given by

$$E_{\mathrm{MP2}}^{\mathrm{corr}} = \frac{1}{4} \sum_{IJAB} \tau_{IJ}^{AB} \langle AB||IJ\rangle, \tag{1.28}$$

where $\langle AB||IJ\rangle$ is an anti-symmetrized two-electron integral,

$$\begin{aligned} &\langle AB||IJ\rangle = \\ &\int\int \psi_A^\dagger(\mathbf{r}_1)\,\psi_B^\dagger(\mathbf{r}_2)\,\frac{1}{r_{12}}\left[\psi_I(\mathbf{r}_1)\,\psi_J(\mathbf{r}_2) - \psi_J(\mathbf{r}_1)\,\psi_I(\mathbf{r}_2)\right] d\mathbf{r}_1 d\mathbf{r}_2, \end{aligned} \tag{1.29}$$

and the MP2 excitation amplitudes, τ, are given by

$$\tau_{IJ}^{AB} = \frac{\langle IJ||AB\rangle}{(\epsilon_I + \epsilon_J - \epsilon_A - \epsilon_B)}, \tag{1.30}$$

where spinor eigenvalues are indicated by the Greek letter ϵ. I and J denote occupied spinors and A and B denote virtual spinors.

For closed shell molecules MP2 takes most effects of electron correlation into account and therefore works quite well. It is a relatively economical method for taking electron correlation effects into account, scaling as N^5, where N is a measure of the system size. Interesting developments to reduce the scaling, and thereby increasing the applicability of MP2, are the use of density fitting[85], local MP2[86, 87], or a combination of both techniques[88].

1.3.2 Coupled-cluster theory

If highly accurate calculations on closed-shell molecules have to be performed, the coupled-cluster method is often the best choice. The computational costs scale, however, steeply with system size, restricting the method to small to medium sized molecules. New developments using localized orbitals and density fitting will hopefully result in interesting applications on larger molecules in the near future[89, 90].

In coupled-cluster theory the wavefunction is written in the following exponential form

$$|\mathrm{CC}\rangle = \exp(\hat{T})|\mathrm{HF}\rangle, \tag{1.31}$$

with $\hat{T}$ the cluster operator

$$\hat{T} = \hat{T}_1 + \hat{T}_2 + ... \tag{1.32}$$

where $\hat{T}_1$ produces single excitations, $\hat{T}_2$ double excitations, etc. For closed-shell systems the excitation operators may be written in the form

$$\hat{T}_1 = \sum_{IA} t_I^A \hat{E}_{AI}, \tag{1.33}$$

$$\hat{T}_2 = \sum_{IJAB} t_{IJ}^{AB} \hat{E}_{AI}\hat{E}_{BJ}, \tag{1.34}$$

...

where $\hat{E}_{AI}$ is an excitation operator, exciting an electron from the occupied spinor I to the unoccupied spinor A. The amplitudes, t_I^A, t_{IJ}^{AB}, ... are the variables that have to be determined.

Rewriting the Schrödinger (or Dirac) equation in the form

$$\exp(-\hat{T})\hat{H}\exp(\hat{T})|\mathrm{HF}\rangle = E_{\mathrm{CC}}|\mathrm{HF}\rangle, \tag{1.35}$$

the coupled-cluster energy can be obtained by projection from the left by the HF reference state

$$E_{\mathrm{CC}} = \langle \mathrm{HF}|\exp(-\hat{T})\hat{H}\exp(\hat{T})|\mathrm{HF}\rangle. \tag{1.36}$$

Projection from the left by the manifold of excited determinants, $|\Phi\rangle$, gives the non-linear coupled-cluster equations,

$$\langle \Phi|\exp(-\hat{T})\hat{H}\exp(\hat{T})|\mathrm{HF}\rangle = 0, \tag{1.37}$$

that needs to be solved to obtain the amplitudes. In practice the non-linear coupled-cluster equations are solved in an iterative manner.

If we truncate the expansion of the cluster operator after the double excitations we denote the coupled-cluster model by CCSD; if we truncate after the triple excitations, CCSDT, etc. Since CCSDT scales as N^8 it is restricted to very small molecules, and finds application mainly in benchmarking of other methods[91]. A method that takes the effect of triple excitations into account in an approximate, but excellent, way is the CCSD(T) method[92]. In the CCSD(T) method, the CCSD equations, which scale as N^6, are first solved. Next the perturbative (T) term is calculated using the single and double amplitudes. Although it scales as N^7, it doesn't have to be calculated iteratively, giving it a small prefactor. For small to medium sized closed-shell molecules that are dominated by the HF configuration, CCSD(T) is often the best choice for obtaining high quality results.

1.3.3 Density functional theory

The methods described in the previous sections are called *ab initio* methods, since the models don't require empirical parameters from the outset. These methods are wavefunction based; the wavefunction, Ψ, is the central quantity. Another approach is density functional theory (DFT). In this approach the electron density, ρ is the central quantity. Since DFT has hardly been used in the research of this thesis, DFT will be discussed only briefly here.

In some chapters results of DFT are used for comparison. In chapter 8 a comparison between Hartree-Fock, MP2 and DFT is given for parity-violation calculations on CHFClBr. For good reviews of DFT see reference [84] and [93].

The ground state energy of a system can be found by solving the Kohn-Sham (KS) equations. These equations have a similar form to the HF equations, so a lot of techniques used in Hartree-Fock theory can be used in DFT and *vice versa*. In contrast to HF, with DFT, it is in principle possible to calculate exact energies. However, in the KS equations the so called exchange correlation energy functional $E_{\mathrm{XC}}[\rho]$ appears. $E_{\mathrm{XC}}[\rho]$ is not known, which means that approximate functionals have to be used. There are many flavors of approximations to $E_{\mathrm{XC}}[\rho]$ in use today. We will not mention all of them here, but refer instead to reference [84]. Worthy of mention are the so called local density approximation (LDA)[94] and generalized gradient approximations (GGA): BLYP[95, 96], PW86[97]. Another functional that is used in chapter 8 is a hybrid functional: B3LYP[98].

DFT offers many advantages. It is currently the most popular electronic structure method. Because it scales similarly to HF, it is much more economical than correlated *ab initio* methods. It is, however, generally, much more reliable than HF. Its favorable scaling with system size, and performance

that is good enough for most purposes, makes it the most suited method to research of real chemical problems. Another very import advantage of DFT (that it shares with HF) are the solutions of the KS equations themselves. The solutions are singly or doubly occupied orbitals (or spinors), which allow for easier interpretation of results than the correlated *ab initio* methods. The reason why, however, the main results in this thesis are based on coupled-cluster methods is that, even though DFT is able to give reliable results, it can not compete with the accuracy of coupled-cluster for the small closed shell molecules treated in this thesis. Achieving as high an accuracy as possible is one of the main goals of the research presented here.

1.4 Basis sets

As already mentioned in section 1.2.2, it is common in quantum chemistry to expand the unknown wavefunctions in a set of known functions: a basis set. This has the advantage that the equations that have to be solved are transformed to matrix equations, which, by using appropriate methods from linear algebra, can be solved efficiently by a computer.

To keep the computation time as short as possible we like to have sets that are small, i.e. a short expansion, and/or have forms that are computationally easy to handle. On the other hand the basis sets should be able to represent the true wavefunction as accurately as possible. The most widely used type of basis functions are the so called Gaussian type orbitals (GTO). In Cartesian form a GTO is given by

$$\chi_\mu = N_\mu x^{n_x} y^{n_y} z^{n_z} e^{-\alpha_\mu r^2} \tag{1.38}$$

where $n_x + n_y + n_z = l$, with l the angular momentum label, N_μ is a normalization factor, and α_μ an exponential factor.

There are two different approaches to expanding a four-component spinor. In one approach the large and small component of a four-component spinor are expanded in a basis of two-component spinors. In another the scalar components of the 4-spinor are expanded in a scalar basis. The second approach allows for the use of the same integral evaluation implementation as used in a non-relativistic methodology. In the following we restrict ourselves to the second approach, more details of the first can be found in references [77, 99].

The basis sets used for the small component are not the same as those

for the large component, because they differ in parity. We can write

$$\psi_I = \begin{pmatrix} \psi_I^{\mathrm{L}\alpha} \\ \psi_I^{\mathrm{L}\beta} \\ \psi_I^{\mathrm{S}\alpha} \\ \psi_I^{\mathrm{S}\beta} \end{pmatrix} = \begin{pmatrix} \sum_\mu C_{\mu I}^{\mathrm{L}\alpha} \chi_\mu^{\mathrm{L}} \\ \sum_\mu C_{\mu I}^{\mathrm{L}\beta} \chi_\mu^{\mathrm{L}} \\ \sum_\nu C_{\nu I}^{\mathrm{S}\alpha} \chi_\nu^{\mathrm{S}} \\ \sum_\nu C_{\nu I}^{\mathrm{S}\beta} \chi_\nu^{\mathrm{S}} \end{pmatrix} \tag{1.39}$$

with $\{\chi_\mu^{\mathrm{L}}\}$ and $\{\chi_\nu^{\mathrm{S}}\}$ the basis sets for the large and small component, respectively. However, in order to obtain the right non-relativistic limit, the small component basis has to be related to the large component basis: they are balanced. This requirement is called *kinetic balance*, and we must have

$$\{\chi_\mu^{\mathrm{S}}\} \supseteq \{(\boldsymbol{\sigma} \cdot \mathbf{p})\chi_\mu^{\mathrm{L}}\}. \tag{1.40}$$

Due to the $\boldsymbol{\sigma} \cdot \mathbf{p}$ operator, the small component set is larger than the large component set. For example, small component p-functions are generated from large component s-functions and large component d-functions. In the case of n_s large component s-functions and n_d large components d-functions in $n_s + n_d$ small component p-functions would result. However, the size of the small component basis set can be reduced by ensuring that the large component s-functions and d-functions have common exponents in the regions where they coincide. In practice this would usually mean that the exponents for the d-functions are a subset of the exponents of the s-functions, and we end up with n_s different small component p functions. If we use this methodology to reduce the size of the small component basis set, we are led to two sets of exponents: one describing the family of *s, d, g,* etc. symmetries, and one for *p, f, h,* etc. symmetries. This type of basis set is called a *dual family* basis[100].

It is evident that it matters what values for the exponents we chose in our GTO set, since we want to describe the wavefunction as accurately as possible with as few basis functions as possible. For non-relativistic electronic structure calculations a lot of different basis sets are available, especially for the first two rows of the periodic table. Most basis sets are generated by optimizing the exponents of the GTOs with respect to the energy, yielding energy optimized basis sets. Particularly worthy of mention are the correlation-consistent basis sets developed by Dunning and coworkers [101, 102], which allow for a systematic recovery of the correlation energy and with which extrapolation to the basis set limit might be employed if a hierarchy of these

sets is used [103–106]. The correlation-consistent basis sets have recently been extended by Peterson *et al.*[107] for the use in ECP calculations of heavier elements, namely the post-*d* group 16-18 elements. This means that in relativistic ECP calculations, systematic extrapolation to the basis set limit starts to be possible as well.

Unfortunately, for four-component calculations not so many basis sets are available. A lot of work in this field has still to be done. For light elements it is common to simply use non-relativistic basis sets, sometimes with adjusted contraction coefficients or leaving the basis set uncontracted. For the heavier elements the non-relativistic basis sets are not well suited, especially in describing the core region where the four-component wavefunction is much more compact than the non-relativistic wavefunction, which means that GTOs with higher exponents are needed.

In the research presented in this work our, goal was not to extend the correlation-consistent basis set for the use in four-component calculations, although this seems to be absolutely necessary in order to make the use of the DC Hamiltonian in quantum chemistry more widespread. We used a pragmatic approach to obtain basis sets of sufficient quality for calculation of the molecular properties we are interested in: we extended an initially energy optimized basis with extra functions, depending on the contribution made by the functions to the property of interest. Since we can not apply the variational principle to obtain suitable values for the exponents in this approach, we used a simple strategy to obtain them, we used so called *even-tempered* basis sets[108]. For even-tempered basis sets the ratio between subsequent exponents, i and $i-1$, is constant for a particular l

$$\alpha_i = \alpha\beta^{i-1}. \tag{1.41}$$

This means that for each l we only need to determine two parameters, an α and a number that determines the ratio between exponents, β. Since we make use of dual family sets, we only need to optimize two different βs. Although, in terms of the number of GTOs needed for a given accuracy, even-tempered sets are less economical than unconstrained basis sets, the size does not differ much. This relies on the empirical observation that the ratio between exponents of fully unconstrained, optimized basis sets is actually approximately constant. Another, qualitative, justification of the use of even-tempered basis sets is the fact that the overlap between two subsequent even-tempered GTOs is constant and determined only by the parameter β[82], giving rise to a well spread distribution of Gaussians. The disadvantage of having more basis functions is − in our view − however counterbalanced by the systematic and straightforward extension of an even-tempered basis

set. Examples of even-tempered basis sets that are suitable for accurate calculations on a particular property can be found in chapters 3, 4 and 5.

1.5 This thesis

This thesis is about the accurate calculation of first-order molecular properties, an important aspect of which is the incorporation of special relativity.

In chapter 2 some method development is presented. Formulas for the calculation of analytical first-order molecular properties at the Dirac-Coulomb MP2 level are described. To reduce computational costs, the formalism allows the use of inactive spinors. The implementation of this formalism in the DIRAC program is discussed.

The calculation of electric field gradients (EFG) is described in chapter 3 and 4. Calculating the EFG on a particular nucleus, combined with the experimental nuclear quadrupole coupling constant, allows for the determination of the nuclear quadrupole moment (NQM). So, by combining theoretical and experimental molecular data one can determine a property of the nucleus: its quadrupole moment. In chapter 3 this has been applied to obtain the NQM of ^{115}In using four diatomic molecules. In chapter 4 we apply the same strategy, using nine different diatomic molecules, to obtain the NQM of ^{127}I.

Chapter 5 and 6 treat the calculation of dipole moments. The dipole moment function of hydrogen iodide is tackled in chapter 5. Previous doubts about the quality of experimental numbers appear to be not well founded, and the gap between theory and experiment is closed. The importance of basis sets and the variational inclusion of spin-orbit coupling is stressed in this chapter. In the next chapter, one of the most well known molecules is treated: water. A gas phase water molecule still presents many challenges to theoreticians. Theoretical calculations can only be of significant complementary value to the analysis of the rotation-vibration spectrum of water if the quality of the calculations is of an extraordinarily high quality. Even for water, this requires the treatment of relativity. In this chapter the relativistic correction to the dipole moment surface of water is described. This will be used in the future to analyze high temperature spectra of water, which have several important applications.

In chapter 7 and 8 results of applications with the implementation described in chapter 2 will be shown. The method is applied to the calculation of parity-violation effects in chiral molecules. Since this effect is so small, experimentalist have not yet been able to detect it. The results presented in these chapters therefore have a predictive character. In chapter 7 parity-

violation energies of hydrogen peroxyde analogs are presented. Chapter 8 discusses the effect of parity-violation on the C-F stretching mode of CHFClBr.

Chapter 2

Analytical first-order molecular properties at the Dirac-Coulomb MP2 level: theory and implementation

The first implementation of analytical first-order one-electron molecular properties at the Dirac-Coulomb MP2 level of theory is described. The formalism presented allows the use of inactive spinors.

2.1 Introduction

In a non-relativistic framework, analytical expressions for gradients in second-order Møller-Plesset perturbation theory (MP2) have been known for over twenty years[109]. Since the mid-eighties several advances have been made for a more efficient calculation of MP2 gradients. Using the Z-vector method of Handy and Schaefer[110] only a single coupled perturbed Hartree-Fock (CPHF) equation has to be solved, instead of one for each perturbation. Another advance was the extension of the MP2 gradient formalism to allow for inactive occupied and virtual orbitals [111, 112]. This is especially important for molecules containing heavy elements that have many core electrons that are not very important for most molecular properties. Neglect of core correlation allows then for significant savings in computertime while hardly affecting the accuracy of the calculation. A very detailed derivation of the non-relativistic MP2 analytical gradient in the spin-orbital basis has recently been given by Aikens *et al.*[113]. To reduce disk storage requirements, direct and semi-direct algorithms emerged in the beginning of the

nineties[114–116]. A subsequent development of parallel algorithms in the mid-nineties[117, 118] made it possible to further reduce the computational time. Nevertheless, the N^5 scaling of the MP2 energy and gradient calculations, where N is the number of electrons correlated, limits also the parallel algorithms to relatively small systems. Calculations on large molecules are only possible if this computational scaling is reduced, *e.g.* by means of the approximations made in the resolution of identity MP2 (RI-MP2)[119] and local MP2 (LMP2)[120] methods.

Molecular properties can be significantly affected by relativity if the molecule contains one or more heavy elements. If one is interested in valence properties it is often possible to introduce a relativistic effective core potential (RECP) on the heavy elements to model the most important relativistic effects. For molecular geometries[121] and electric response properties[122] RECPs have shown to perform rather well. A limitation of the RECP method is, however, the use of the pseudo-orbitals that differ substantially from the true valence orbitals in the core region. This makes the method less suited for properties like NMR shieldings and nuclear quadrupole coupling constants (NQCCs), where the computed value is to a large extent determined by the shape of the wavefunction in the vicinity of the nucleus. RECPs can in general not be used for calculation of such properties on heavy centers, although they are still useful in the calculation of NMR shieldings for the light elements in systems containing heavy elements[123, 124]. In all-electron calculations one may include relativity by means of perturbation theory[125]. Calculating the relativistic effect on a specific property in this manner requires, however, the calculation of linear response functions that are one order higher than required by the property that one is interested in. More efficient algorithms may be formulated if relativity is included from the outset, *e.g.* by employing a variationally stable approximate relativistic Hamiltonian like the Douglas-Kroll-Hess (DKH)[60] Hamiltonian or the zeroth-order regular approximation (ZORA)[63]. Both of these methods require that the transformation, which transforms the original Dirac Hamiltonian to the approximate form, should also be applied to the operators that describe the molecular property of interest. Neglecting this transformation results in so-called picture change effects[73], which are usually small for valence properties, but are not negligible for core properties[74].

The most straightforward approach to take relativity into account is to start directly from the untransformed 4-component Dirac-Coulomb (DC) Hamiltonian. This is the route that we will follow in this research paper. We restrict the current discussion to first-order molecular properties for which the basis functions do not depend on the perturbation that is applied. Molecular properties where the basis functions are perturbation dependent, like the

molecular gradient used in structure optimizations, require additional terms and are left for future work. The 4-component approach based on the DC Hamiltonian requires use of complex 4-component molecular spinors (MS), instead of the real 1-component molecular orbitals (MO) found in ordinary electronic structure theory. The approach has the advantage that the operators remain relatively simple since picture change transformations are not necessary. Since our main focus will be on properties of systems with heavy elements, which have many electrons, we will allow for use of inactive spinors to increase the computational efficiency.

In previous applications we used the finite-field or finite-perturbation method to calculate first-order molecular properties, see for example references [126] and [127]. Although the calculation of first (and higher-)order properties using the finite-field method requires practically no extra programming, it has several disadvantages[2]. First of all the finite-field method is less efficient than analytical methods, because for each property of interest additional finite-field calculations have to be performed. For most first-order properties it is easy to find field strengths which, after numerical differentiation, give results that are numerically stable and give practically the same results as corresponding analytical values. There are, however, first-order properties for which it is very hard or even impossible to obtain a numerically stable result in the finite-field approach. An example of numerical instability by finite-field calculations was encountered by Thyssen *et al.*[128] who studied the parity-violating electroweak interaction in H_2O_2 and H_2S_2. Use of high exponent s and p functions to achieve basis set convergence turned out to be impossible since this lead to a too wide range of values of matrix elements over the perturbing operator. The resulting numerical noise made accurate parity-violation calculations by means of the finite-field method on the heavier element series H_2Se_2, H_2Te_2, and H_2Po_2 impossible. Relativistic correlated calculations of electroweak interactions have therefore so far been limited to H_2O_2 and H_2S_2 for which the problems were still manageable. With our analytical implementation of DC-MP2 first order molecular properties we can now extend such relativistic correlated calculations to the heavier analogs of this series, H_2Se_2 and H_2Te_2. We describe results of these calculations in chapter 7, but first we describe the theory and implementation to allow for such analytical property calculations in section 2.2 and 2.3, respectively.

2.2 Theory

The Dirac-Coulomb electronic Hamiltonian has the same generic form as the non-relativistic Hamiltonian

$$\hat{H}_0 = \sum_i \hat{h}(i) + \frac{1}{2}\sum_{i\neq j} \hat{g}(i,j) + \hat{V}_{NN}, \tag{2.1}$$

so that many non-relativistic electronic structure methods can be generalized to the relativistic domain. The main difference lies in the fact that the molecular Dirac equation has two kind of solutions: positive energy solutions, that describe bound state solutions for the electrons in the molecule, and negative energy solutions, from which electrons may be excited to form electron-positron pairs. In the no-pair approximation the latter type of excitation is neglected so that the negative energy states can be discarded after the Hartree-Fock (HF) Self Consistent Field procedure is completed. Molecular properties can also in the relativistic case be defined as energy derivatives of a complete Hamiltonian that depends on an external perturbation,

$$\hat{H} = \hat{H}_0 + \lambda \hat{P}. \tag{2.2}$$

If all wave function parameters were fully optimized one may employ the Hellmann-Feynman theorem and evaluate first-order properties as an expectation value. This is not the case for the MP2 approach so that we need to consider the so-called response contribution to the second order one-electron density matrix as well. Since we have practically the same overall structure as in non-relativistic theory we can make use of the extensive literature on MP2 gradient calculations. A new aspect is the dependence of the relaxation contribution to the density matrix on the negative energy solutions. That such a contribution should be accounted for can be easily understood by performing the following *gedanken-experiment*. Find the self-consistent solutions for a system in the absence of external fields and divide them into positive and negative energy solutions. Then switch on a constant external field, find again the solutions, and divide them in positive and negative solutions. In both cases well-defined sets of negative and positive solutions are found that can be expressed in terms of each other. The positive energy solutions in the perturbed case contain contributions from both the positive and the negative energy sets for the unperturbed solutions. Mimicking the addition of an external field, as is done in the series expansion around zero field strength in the analytical procedure, requires therefore mixing of the positive and negative energy solution blocks. We will see that the formulas that take this mixing into account are closely related to those used to describe the effects

of inactive spinors that play no role in the correlation calculation but are relaxed under the influence of the perturbation in the Hartree-Fock step.

For an extensive derivation of the non-relativistic analytical gradient for MP2 we refer to (*e.g.*) papers by Head-Gordon[129] and Gauss and Cremer[130]. What we will discuss in detail are the modifications necessary to take care of the negative energy spinors and the complex algebra resulting from the use of a complex Hamiltonian and spinors. In the present derivation and implementation equations were simplified using the fact that the basis functions are assumed not to depend on the perturbation that is applied. The Z-vector technique of Handy and Schaefer[110] is used, in the derivation, to avoid the calculation of a set of coupled-perturbed Hartree-Fock equations for each perturbation. The same final results can also be obtained by using the Lagrange multiplier technique of Helgaker and Jørgensen[131, 132] that considers the derivative of a variational energy functional. The simplifications that are explicitly invoked using the Handy-Schaefer technique appear then automatically.

In the implementation section we will include time-reversal symmetry in the theory and introduce Kramers pairs. The initial equations are, however, best discussed in a spinor basis, the relativistic equivalent of the spin-orbital formulation in nonrelativistic theory. We use the convention that spinors are indicated by uppercase letters. We will use *I, J, K* to denote active occupied canonical spinors, *A, B, C* for active virtual canonical spinors, *X, Y* for negative energy canonical spinors, *P, Q, R, S* refer to general spinors, while *V, W* denote any virtual or negative energy spinor. To make a distinction between inactive and active spinors we use the notation of Head-Gordon[129]: single primes denote inactive spinors (*e.g.*, *J'* is an inactive occupied spinor), double primes indicate the union of inactive and active spinors (*e.g.*, *A"* is any virtual spinor).

Greek indices, μ, ν, κ, λ are used for basis functions or atomic orbitals (AO). In an implementation it is convenient to choose real basis functions that describe either the large, L, or the small, S, components of the wave function, but this distinction is not relevant for most of the formulas presented in this paper. We therefore omit the additional component label to keep the notation simple.

The equations for an analytical first-order derivative of the MP2 correlation energy will be derived for the MP2 correlation energy within the no-pair approximation that is given by[133]:

$$E^{(2)} = \frac{1}{4} \sum_{IJAB} \tau_{IJ}^{AB} \langle AB||IJ\rangle, \tag{2.3}$$

where $\langle AB||IJ\rangle$ is an anti-symmetrized two-electron integral,

$$\langle AB||IJ\rangle = \int\int \psi_A^\dagger(\mathbf{r}_1)\,\psi_B^\dagger(\mathbf{r}_2)\,\frac{1}{r_{12}}\left[\psi_I(\mathbf{r}_1)\,\psi_J(\mathbf{r}_2) - \psi_J(\mathbf{r}_1)\,\psi_I(\mathbf{r}_2)\right] d\mathbf{r}_1 d\mathbf{r}_2 \tag{2.4}$$

and the MP2 excitation amplitudes, τ, are given by

$$\tau_{IJ}^{AB} = \frac{\langle IJ||AB\rangle}{(\epsilon_I + \epsilon_J - \epsilon_A - \epsilon_B)}, \tag{2.5}$$

where spinor eigenvalues are indicated by the Greek letter ϵ. Since the energy is not variationally determined it is not possible to formulate first order properties directly in terms of an expectation value of the wave function. It is, however, possible to define an effective *relaxed* density matrix $D_{PQ}^{(2)}$ that describes the first order response of the system to an arbitrary perturbation[134]. Taking the first order derivative of the correlation energy of the Hamiltonian defined in equation (2.2) gives an expression in terms of the effective density matrix and property matrix

$$\frac{dE^{(2)}}{d\lambda} = \sum_{PQ} D_{PQ}^{(2)} P_{QP}. \tag{2.6}$$

In MS basis the relaxed density matrix can be divided into a number of blocks due to the partioning of both the occupied and virtual electronic spinors into an inactive and an active part that defines four separate subspaces, while the class of negative energy states adds a fifth subspace that does not appear in nonrelativistic theory. The hermiticity of the matrix reduces the number of 25 possible combinations to 15 unique combinations, five more than in nonrelativistic theory. Fortunately some of the additional blocks turn out to be zero while others can be shown to be identical in structure to an existing block.

We start by considering the diagonal blocks of the second-order density matrix, $\mathbf{D}^{(2)}$, that describes the change of the density relative to the Hartree-Fock reference density. The elements in the negative energy, inactive occupied and inactive virtual diagonal blocks are all zero since the occupation of these spinors is not changed in the MP2 wave function. The non-zero blocks are the active occupied and active virtual blocks for which the expression in terms of wave function amplitudes reads:

$$D_{IJ}^{(2)} = -\frac{1}{2}\sum_{KAB}\left(\tau_{IK}^{AB}\right)^* \tau_{JK}^{AB}, \tag{2.7}$$

$$D^{(2)}_{AB} = \frac{1}{2}\sum_{IJC}\left(\tau^{AC}_{IJ}\right)^{*}\tau^{BC}_{IJ}. \tag{2.8}$$

For the off-diagonal elements that describe the first order response of the wave function to a perturbation, it is convenient to expand the coefficients of the perturbed spinors $C^{\lambda}_{\mu P}$ in terms of the coefficients of the unperturbed spinors $C_{\mu Q}$[135]:

$$C^{\lambda}_{\mu P} = \sum_{Q} C_{\mu Q} U^{\lambda}_{QP}. \tag{2.9}$$

We stress that index Q in equation (2.9) should run over all types of spinors, inactive occupied (OI), active occupied (OA), active virtuals (VA), inactive virtuals (VI) and negative energy (NE) spinors, since mixing between all these subspaces will occur when the perturbation is switched on. The mixing between positive and negative energy spinors serves to obtain full Hartree-Fock relaxation of the electronic spinors to the effect of the applied perturbation. Such effects may be of importance, in particular for derivatives of magnetic fields, and other operators that introduce a relatively strong coupling between the positive and negative energy spinors[136]. Such relaxation effects should not be confused with the contributions that arise when lifting the no-pair restriction as is done in atomic QED calculations[137, 138].

Using the spinor response matrix $\mathbf{U}^{\lambda}$ the first-order derivative of the no-pair MP2 correlation energy with respect to λ can be cast in the following form:

$$\begin{aligned}\frac{dE^{(2)}}{d\lambda} &= \sum_{I"J"} D^{(2)}_{I"J"} P_{J"I"} + \sum_{A"B"} D^{(2)}_{B"A"} P_{A"B"} \\ &+ \frac{1}{2}\sum_{VI"}\left(L^{*}_{VI"}U^{\lambda}_{VI"} + L_{VI"}U^{\lambda *}_{VI"}\right) \\ &+ \frac{1}{2}\sum_{AX}\left(L^{*}_{AX}U^{\lambda}_{AX} + L_{AX}U^{\lambda *}_{AX}\right). \end{aligned} \tag{2.10}$$

Just as in non-relativistic theory the spinor response elements U^{λ}_{IJ} and U^{λ}_{AB} are zero when the basis set is not perturbation dependent. This eliminates all terms concerning the derivative of the AO-overlap matrix that should otherwise be taken into account as well. The active-active diagonal blocks of the second order density matrices $D^{(2)}_{I"J"}$ and $D^{(2)}_{A"B"}$ were defined above. The two active-inactive off-diagonal blocks are

$$D^{(2)}_{I'J} = D^{(2)*}_{JI'} = \frac{1}{2}\frac{L_{I'J}}{(\epsilon_J - \epsilon'_I)} = \frac{1}{2}\frac{(L1)_{I'J}}{(\epsilon_J - \epsilon'_I)} \tag{2.11}$$

and

$$D^{(2)}_{BA'} = D^{(2)*}_{A'B} = \frac{1}{2}\frac{L_{BA'}}{(\epsilon'_A - \epsilon_B)} = \frac{1}{2}\frac{(L2)_{BA'}}{(\epsilon'_A - \epsilon_B)} \tag{2.12}$$

with the $L1$ and $L2$ matrices defined in equations (2.14) and (2.15) below.

The last two summations of (2.10), containing $\mathbf{U}^\lambda$ matrix terms, describe the relaxation of the Hartree-Fock spinors to the applied perturbation. $\mathbf{L}$ in equation (2.10) is the MP2 Lagrangian:

$$L_{PQ} = (L1)_{PQ} + (L2)_{PQ} + (L3)_{PQ}\,, \tag{2.13}$$

where the individual terms are given by

$$(L1)_{PI} = \sum_{JBC} \langle PJ||BC\rangle \tau^{BC*}_{IJ} \text{ for } P \notin \text{OA} \tag{2.14}$$

$$(L2)_{AQ} = -\sum_{JKB} \langle JK||QB\rangle \tau^{AB*}_{JK} \text{ for } Q \notin \text{VA} \tag{2.15}$$

and

$$(L3)_{VI"} = 2\sum_{J"K"} \langle J"V||K"I"\rangle D^{(2)}_{K"J"} + 2\sum_{B"C"} \langle C"V||B"I"\rangle D^{(2)}_{B"C"} \tag{2.16}$$

Matrix elements that are not listed, *e.g.* $(L2)_{A'I}$, are zero. The elements of the Lagrangian can be computed in an one step procedure if transformed two-electron integrals are available. With the Lagrangian available one may then subsequently solve the Coupled-Perturbed Hartree-Fock (CPHF) equations for the response matrix, $\mathbf{U}^\lambda$, and compute the energy derivative via equation (2.10).

In deriving the CPHF equations one should take into account that both the wave function and Hamiltonian are complex and that the DC-HF procedure should be regarded as a minmax procedure that minimizes the energy with respect to rotations amongst positive energy spinors while maximizing the energy with respect to positive-negative energy rotations[139]. The CPHF equations for the DC Hamiltonian are given by Saue and Jensen[140]:

$$\begin{pmatrix} \mathbf{A} & \mathbf{B} \\ \mathbf{B}^* & \mathbf{A}^* \end{pmatrix} \begin{pmatrix} \mathbf{U}^\lambda \\ \mathbf{U}^{\lambda *} \end{pmatrix} = \begin{pmatrix} \mathbf{P} \\ \mathbf{P}^* \end{pmatrix}, \tag{2.17}$$

where the precise form of **A** and **B** blocks of the Hessian is given below. The structure of this equation depends on the symmetry of the perturbation operator. We are interested in first order properties that are described by hermitian property operators. For these properties it is possible to rewrite the equation in terms of $\mathbf{U}^\lambda$ only, i.e. to eliminate the lower part. This is discussed in detail by Saue and Jensen[140] who also consider the case of a general time-dependent perturbation of frequency ω.

In equation (2.10) only the response matrices $U^\lambda_{VI"}$ and U^λ_{AX} occur explicitly. Response matrices that concern rotations within the same class of spinors can be chosen zero since such rotations do not affect the MP2 energy. Likewise we may ignore rotations between negative energy and inactive virtual spinors and put $U^\lambda_{A'X}$ to zero. The different rotations are coupled via the $A_{PQ,RS}$ and $B_{PQ,RS}$ elements in the Hessian. There are three special cases for **A** and **B** depending on the type of spinors that the indices P, Q, R and S refer to. We list them below.

Case 1 : P and R correspond to virtual or NE spinors, V and W respectively, and Q and S correspond to the occupied spinors, $I"$ and $J"$ respectively. The elements of **A** and **B** are

$$A_{VI",WJ"} = (\epsilon_V - \epsilon_{I"})\,\delta_{VW}\delta_{I"J"} + \langle VJ"||I"W\rangle \tag{2.18}$$

and

$$B_{VI",WJ"} = \langle VW||I"J"\rangle. \tag{2.19}$$

These blocks of the Hessian are also found in a non-relativistic derivation where V and W do only run over the virtual spinors. The other two blocks are needed to determine the rotations between the negative energy spinors and the active virtual spinors. This is only important in correlated calculations where such rotations affect the perturbed correlation energy, these rotation matrices need not be determined in uncorrelated relativistic CPHF calculations.

Case 2 : P corresponds to a VA spinor, A, and index Q to a NE spinor, X, R and S are the same as in Case 1. The matrix elements of the Hessian are

$$A_{AX,WJ"} = \langle AJ"||XW\rangle \tag{2.20}$$

and

$$B_{AX,WJ"} = \langle AW||XJ"\rangle \tag{2.21}$$

Case 3: The diagonal elements of the Hessian for the NE-VA rotations,

$$A_{AX,BY} = (\epsilon_A - \epsilon_X)\,\delta_{AB}\delta_{XY} \tag{2.22}$$

and

$$B_{AX,BY} = 0 \ . \tag{2.23}$$

All other possible combinations of P, Q, R and S elements of $\mathbf{A}$ and $\mathbf{B}$ are zero or irrelevant.

This formulation is not yet in the desired effective density matrix form. Moreover, we see that the matrix $\mathbf{U}^{\lambda}$ depends on the specific perturbation that is to be applied. To avoid this dependence and shift the dependence on the perturbation to the property matrix we need to introduce the Z-vector method developed by Handy and Schaefer[110]. This Z-vector, $\mathbf{Z}$, is defined by

$$\begin{pmatrix} \mathbf{A} & \mathbf{B} \\ \mathbf{B}^* & \mathbf{A}^* \end{pmatrix} \begin{pmatrix} \mathbf{Z} \\ \mathbf{Z}^* \end{pmatrix} = \begin{pmatrix} \mathbf{L} \\ \mathbf{L}^* \end{pmatrix} . \tag{2.24}$$

This equation has the same structure as the original CPHF equation, but since the Lagrangian $\mathbf{L}$, equation (2.13), does not depend on the perturbation it needs to be solved only once. The desired energy derivative with respect to a specific property operator is then determined via

$$\begin{pmatrix} \mathbf{L} \\ \mathbf{L}^* \end{pmatrix}^{\dagger} \begin{pmatrix} \mathbf{U}^{\lambda} \\ \mathbf{U}^{\lambda *} \end{pmatrix} = \begin{pmatrix} \mathbf{Z} \\ \mathbf{Z}^* \end{pmatrix}^{\dagger} \begin{pmatrix} \mathbf{A} & \mathbf{B} \\ \mathbf{B}^* & \mathbf{A}^* \end{pmatrix} \begin{pmatrix} \mathbf{U}^{\lambda} \\ \mathbf{U}^{\lambda *} \end{pmatrix} = \begin{pmatrix} \mathbf{Z} \\ \mathbf{Z}^* \end{pmatrix}^{\dagger} \begin{pmatrix} \mathbf{P} \\ \mathbf{P}^* \end{pmatrix} , \tag{2.25}$$

that is obtained by using equations (2.24) and (2.17). Comparing equation (2.25) with equations (2.6) and (2.10) shows that the off-diagonal blocks of the effective density matrix are given by Z-vectors elements: $D^{(2)}_{VI"} = \frac{1}{2} Z^*_{VI"}$ and $D^{(2)}_{AX} = \frac{1}{2} Z^*_{AX}$.

Because the upper and lower part of equation (2.24) are each others complex conjugate, we only need to solve the upper part of the Z-vector equations. The block structure of the $\mathbf{A}$ and $\mathbf{B}$ matrices may be used to further reduce the work. We take the upper part of equation (2.24), and use the definitions for $\mathbf{A}$ and $\mathbf{B}$, the V - O and NE - O blocks of $\mathbf{Z}$ to obtain

$$\begin{aligned} &(\epsilon_V - \epsilon_{I"}) \, Z_{VI"} \\ &+ \sum_{WJ"} \left(\langle VJ" || I"W \rangle Z_{WJ"} + \langle VW || I"J" \rangle Z^*_{WJ"} \right) = L_{VI"} . \end{aligned} \tag{2.26}$$

This coupled set of equations are 4-component CPHF equations with a modified right hand side and it can thus be solved in an iterative manner using

effective Fock matrices constructed in AO basis with the linear response algorithm described by Saue and Jensen[140].

For the VA - NE block, we need to solve

$$\begin{aligned}&(\epsilon_A - \epsilon_X)\, Z_{AX} \\ &+ \sum_{VJ"} \left(\langle AJ"||XV\rangle Z_{VJ"} + \langle AV||XJ"\rangle Z^*_{VJ"}\right) = L_{AX},\end{aligned} \tag{2.27}$$

and we see, after rewriting this equation into

$$\begin{aligned}&Z_{AX} = \\ &\frac{1}{(\epsilon_A - \epsilon_X)} \left(L_{AX} - \sum_{VJ"} \left(\langle AJ"||XV\rangle Z_{VJ"} + \langle AV||XJ"\rangle Z^*_{VJ"}\right) \right),\end{aligned} \tag{2.28}$$

that we can obtain the VA - NE elements in an one step procedure after the virtual - OA and NE - OA elements of $\mathbf{Z}$ are determined.

2.3 Implementation and computational considerations

All non-zero elements of the effective density matrices were given in the preceding section. The diagonal blocks that depend only on the amplitudes can be computed in molecular spinor basis at a similar cost to an MP2 energy evaluation. The off-diagonal blocks require formation of the Lagrangian and solution of the CPHF equations. This is best done in a mixed AO-MO representation to avoid the formation of integrals that have one or more labels that belong to the large inactive or NE blocks of spinors. Switching to AO representation means that we need to consider in more detail the AO basis and structure of the MO–coefficients. We employ the DIRAC program[41] that utilizes quaternion algebra[46] in combination with real basis functions over either the large or the small component of the wave function.

2.3.1 Time reversal symmetry

In the absence of magnetic fields, the states of a single fermion are doubly degenerate[141]. Pairs of states with the same energy are related by time-reversal and will give the same spatial density upon integration over the spin degrees of freedom. These so-called Kramers pairs can be used as a relativistic equivalent of spatial orbitals. In analogy to the reformulation of spinorbital formulations to orbital formulations we may also write all formulas in terms

of Kramers pairs instead of in terms of individual spinors. This reduces the dimension of the function space by a factor of two in cases where we may sum over the partners. In that case it will suffice to use a lowercase label that runs over all Kramers pairs. Spinors will also be indexed by lowercase indices that run over the Kramers pairs and a bar is used to distinguish between the two paired spinors that share the same index, *e.g.* spinor q has a Kramers partner $\bar{q}$.

A hermitian and time-symmetric matrix constructed over Kramers pairs can be simplified by use of the quaternion unitary transformation matrix:

$$\mathbf{U} = \frac{1}{\sqrt{2}} \begin{pmatrix} \mathbf{I} & \check{\jmath}\mathbf{I} \\ \check{\jmath}\mathbf{I} & \mathbf{I} \end{pmatrix}, \tag{2.29}$$

where $\mathbf{I}$ is a 2×2 unit matrix. The transformation with $\mathbf{U}$ will blockdiagonalize the closed shell or restricted open shell HF equations and can also be used for the Lagrangian and effective density matrix. Below we will first discuss the density matrix dependent part of the Lagrangian, $\mathbf{L}3$, equation (2.16), followed by the amplitude dependent parts $\mathbf{L}1$ and $\mathbf{L}2$, equations (2.14) and (2.15) respectively. Applying the quaternion unitary transformation to the Lagrangian results in:

$${}^{Q}L_{pq} = L_{pq} + L_{p\bar{q}}\check{\jmath} = Re(L_{pq}) + Im(L_{pq})\check{\imath} + Re(L_{p\bar{q}})\check{\jmath} + Im(L_{p\bar{q}})\check{k}. \tag{2.30}$$

We evaluate $\mathbf{L}3$ in AO basis, similar to the algorithm of Frisch *et al.*[114] for the non-relativistic case, to avoid the formation of two electron integrals with inactive spinors (OI, VI and NE spinors). In AO-basis this part of the Lagrangian can be formed at the same cost as a Fock matrix via

$${}^{Q}\left(L3\right)_{\mu\nu} = 2\sum_{\kappa\rho}\left[(\mu\nu|\kappa\rho) - (\mu\rho|\kappa\nu)\right]{}^{Q}D^{(2)}_{\rho\kappa}, \tag{2.31}$$

with ${}^{Q}D^{(2)}_{\rho\kappa}$ the second-order density matrix transformed to AO basis,

$${}^{Q}D^{(2)}_{\rho\kappa} = \sum_{rs}{}^{Q}C_{\rho r}\,{}^{Q}D^{(2)}_{rs}\,{}^{Q}C^{*}_{\kappa s}, \tag{2.32}$$

where rs corresponds to all occupied-occupied and virtual-virtual pairs.

The formation of $\mathbf{L}1$ and $\mathbf{L}2$ is time consuming since the index p in the anti-symmetrized two electron integrals of $\mathbf{L}1$ can be an OI, any virtual or a NE spinor, and the index q appearing in the anti-symmetrized two electron integrals of $\mathbf{L}2$ runs over any occupied, VI and NE spinors. We first apply a three-quarter transformation of the two-electron integrals and contract these transformed integrals on the fly with the MP2 amplitudes. The resulting

Lagrangian is then in mixed AO-MS basis and may be transformed via a relatively cheap two-index transformation to either AO or MO basis. A similar strategy has been applied by Head-Gordon for **L**2 in his semi-direct non-relativistic algorithm[129].

A complication is that the transformed two electron integrals from the index transforming part of DIRAC are transformed to the compact double quaternion format defined in reference [50] that defines all integrals with Kramers pair labels. Amplitudes are, however, more easily defined in terms of complex integrals over spinors[142]. We therefore decided to rewrite the amplitudes in a double quaternion format so that an efficient contraction with the three quarter transformed two electron integrals is possible.

The definition of the amplitudes in double quaternion format is not trivial due to the anti-symmetry relations that the amplitudes fulfill. For two-electron integrals we have a clear distinction between the quaternion labels that belong to the first and second electron and this may be utilized to define relations to the complex spinor notation form. For amplitudes and anti-symmetrized quantities in general, labels cannot be unambiguously assigned to an electron. In order to resolve this problem we start from the formulas written in spinor form and insert the appropriate definitions for the integrals wherever possible. Starting point is the equation for **L**1 as given in equation (2.14):

$$(L1)_{PI} = \sum_{JBC} \langle PJ||BC\rangle \tau_{IJ}^{BC*} = 2 \sum_{JBC} (PB|JC)\, \tau_{BCIJ}, \tag{2.33}$$

that is rewritten in terms of non-antisymmetrized two electron integrals. For ease of notation in the following we write τ_{IJ}^{BC*} from now on as τ_{BCIJ}. After the introduction of quaternion notation this equation may in the end be written in a more compact form in terms of three quarter transformed two electron integrals ${}^{Q}\mathbf{G}$. To this end we first start from equation (2.33), write the fully transformed integrals in terms of half-transformed integrals and switch to Kramers pair notation for the indices J and C

$$\begin{aligned}(L1)_{PI} &= 2 \sum_{B} \sum_{\mu\nu} \sum_{\sigma}^{\alpha,\beta} \sum_{jc} C_{\mu P}^{\sigma *} C_{\nu B}^{\sigma} \\ &\cdot \left[(\mu\nu|jc)\, \tau_{BcIj} + (\mu\nu|\bar{j}\bar{c})\, \tau_{B\bar{c}I\bar{j}} + (\mu\nu|j\bar{c})\, \tau_{B\bar{c}Ij} + (\mu\nu|\bar{j}c)\, \tau_{BcI\bar{j}} \right],\end{aligned} \tag{2.34}$$

where α and β indicate the two components of the large and small component bispinors. Quaternion notation can be introduced in equation (2.34) by

converting the half-transformed integrals to quaternion notation, using,

$$\begin{aligned}
(\mu\nu|jc) &= (\mu\nu|jc)^0 + (\mu\nu|jc)^1 \, i \\
(\mu\nu|j\bar{c}) &= (\mu\nu|j\bar{c})^2 + (\mu\nu|j\bar{c})^3 \, i \\
(\mu\nu|\bar{j}\bar{c}) &= (\mu\nu|jc)^* \\
(\mu\nu|\bar{j}c) &= -\left(\mu\nu|j\bar{c}\right)^* .
\end{aligned} \tag{2.35}$$

and gives

$$\begin{aligned}
(L1)_{PI} =& 2 \sum_{B} \sum_{\mu\nu} \sum_{\sigma}^{\alpha,\beta} \sum_{jc} C^{\sigma *}_{\mu P} C^{\sigma}_{\nu B} \\
& \cdot \Big\{ (\mu\nu|jc)^0 \left[\tau_{BcIj} + \tau_{B\bar{c}I\bar{j}} \right] + (\mu\nu|jc)^1 \left[\tau_{BcIj} - \tau_{B\bar{c}I\bar{j}} \right] \\
& + (\mu\nu|jc)^2 \left[\tau_{B\bar{c}Ij} - \tau_{BcI\bar{j}} \right] + (\mu\nu|jc)^3 \left[\tau_{B\bar{c}Ij} + \tau_{BcI\bar{j}} \right] \Big\},
\end{aligned} \tag{2.36}$$

where superscript 0 corresponds to the real quaternion unit and the superscript 1, 2 and 3 to the imaginary quaternion units $\check{\imath}$, $\check{\jmath}$ and $\check{k}$ respectively.

In the next step we also write the summation over B as two sums over the Kramers partners b and $\bar{b}$, write out the summation over α and β, and convert the coefficient matrix of the spinor with label b to quaternion format[143]

$$\begin{aligned}
& (L1)_{PI} = \\
& 2 \sum_{b} \sum_{\mu\nu} \sum_{jc} \Big\{ C^{\alpha *}_{\mu P} \left(C^{0}_{\nu b} + i C^{1}_{\nu b} \right) + C^{\beta *}_{\mu P} \left(-C^{2}_{\nu b} + i C^{3}_{\nu b} \right) \Big\} \\
& \cdot \Big\{ (\mu\nu|jc)^0 \left[\tau_{bcIj} + \tau_{b\bar{c}I\bar{j}} \right] + (\mu\nu|jc)^1 \left[\tau_{bcIj} - \tau_{b\bar{c}I\bar{j}} \right] \\
& + (\mu\nu|jc)^2 \left[\tau_{b\bar{c}Ij} - \tau_{bcI\bar{j}} \right] + (\mu\nu|jc)^3 \left[\tau_{b\bar{c}Ij} + \tau_{bcI\bar{j}} \right] \Big\} \\
& + \\
& 2 \sum_{b} \sum_{\mu\nu} \sum_{jc} \Big\{ C^{\alpha *}_{\mu P} \left(C^{2}_{\nu b} + i C^{3}_{\nu b} \right) + C^{\beta *}_{\mu P} \left(C^{0}_{\nu b} - i C^{1}_{\nu b} \right) \Big\} \\
& \cdot \Big\{ (\mu\nu|jc)^0 \left[\tau_{\bar{b}cIj} + \tau_{\bar{b}\bar{c}I\bar{j}} \right] + (\mu\nu|jc)^1 \left[\tau_{\bar{b}cIj} - \tau_{\bar{b}\bar{c}I\bar{j}} \right] \\
& + (\mu\nu|jc)^2 \left[\tau_{\bar{b}\bar{c}Ij} - \tau_{\bar{b}cI\bar{j}} \right] + (\mu\nu|jc)^3 \left[\tau_{\bar{b}\bar{c}Ij} + \tau_{\bar{b}cI\bar{j}} \right] \Big\}.
\end{aligned} \tag{2.37}$$

We now have all summations in terms of Kramers' pairs or AO functions but still have one complex matrix (the leftmost coefficient matrix) and have indices P and I refering to spinors and not Kramers' pairs. Since we do not sum over P and I we take a special case in order to list the expression in

terms of Kramers' pair indices. We take $(L1)_{pi}$:

$$
\begin{aligned}
&(L1)_{pi} = \\
&2\sum_{b}\sum_{\mu\nu}\sum_{jc}\Big\{\left(C^{0}_{\mu p} - iC^{1}_{\mu p}\right)\left(C^{0}_{\nu b} + iC^{1}_{\nu b}\right) + \left(-C^{2}_{\mu p} - iC^{3}_{\mu p}\right)\left(-C^{2}_{\nu b} + iC^{3}_{\nu b}\right)\Big\} \\
&\cdot\Big\{(\mu\nu|jc)^{0}\left[\tau_{bcij} + \tau_{b\bar{c}i\bar{j}}\right] + (\mu\nu|jc)^{1}\left[\tau_{bcij} - \tau_{b\bar{c}i\bar{j}}\right] \\
&+ (\mu\nu|jc)^{2}\left[\tau_{b\bar{c}ij} - \tau_{bci\bar{j}}\right] + (\mu\nu|jc)^{3}\left[\tau_{b\bar{c}ij} + \tau_{bci\bar{j}}\right]\Big\} \\
&+ \\
&2\sum_{b}\sum_{\mu\nu}\sum_{jc}\Big\{\left(C^{0}_{\mu p} - iC^{1}_{\mu p}\right)\left(C^{2}_{\nu b} + iC^{3}_{\nu b}\right) + \left(-C^{2}_{\mu p} - iC^{3}_{\mu p}\right)\left(C^{0}_{\nu b} - iC^{1}_{\nu b}\right)\Big\} \\
&\cdot\Big\{(\mu\nu|jc)^{0}\left[\tau_{\bar{b}cij} + \tau_{\bar{b}\bar{c}i\bar{j}}\right] + (\mu\nu|jc)^{1}\left[\tau_{\bar{b}cij} - \tau_{\bar{b}\bar{c}i\bar{j}}\right] \\
&+ (\mu\nu|jc)^{2}\left[\tau_{\bar{b}\bar{c}ij} - \tau_{\bar{b}ci\bar{j}}\right] + (\mu\nu|jc)^{3}\left[\tau_{\bar{b}\bar{c}ij} + \tau_{\bar{b}ci\bar{j}}\right]\Big\}.
\end{aligned}
\tag{2.38}
$$

From which follows the definition of the three quarter transformed two electron integrals ${}^{Q}\mathbf{G}$

$$
G^{\Lambda_{34},\Lambda_2}_{jc\mu b} = \sum_{\nu} C^{\Lambda_2}_{\nu b}\,(\mu\nu|jc)^{\Lambda_{34}}\,; \quad (\Lambda_2, \Lambda_{34} = 0,1,2,3)\,. \tag{2.39}
$$

Writing the Lagrangian now in mixed AO − MS basis

$$
{}^{Q}\mathbf{L}1^{(\mathrm{AO-MS})} = \left({}^{Q}\mathbf{G}\right)^{T}\left({}^{Q}\mathbf{T}\right). \tag{2.40}
$$

Requiring this form uniquely defines the amplitudes in double quaternion

format, ${}^{Q}\mathbf{T}$:

$$
\begin{aligned}
T^{00}_{jcbi} &= \tfrac{1}{2} Re\left(\tau_{bcij} + \tau_{b\bar{c}i\bar{j}}\right) & T^{01}_{jcbi} &= \frac{1}{2} Im\left(\tau_{bcij} + \tau_{b\bar{c}i\bar{j}}\right) \\
T^{10}_{jcbi} &= -\tfrac{1}{2} Im\left(\tau_{bcij} - \tau_{b\bar{c}i\bar{j}}\right) & T^{11}_{jcbi} &= \frac{1}{2} Re\left(\tau_{bcij} - \tau_{b\bar{c}i\bar{j}}\right) \\
T^{20}_{jcbi} &= \tfrac{1}{2} Re\left(\tau_{b\bar{c}ij} - \tau_{bci\bar{j}}\right) & T^{21}_{jcbi} &= \frac{1}{2} Im\left(\tau_{b\bar{c}ij} - \tau_{bci\bar{j}}\right) \\
T^{30}_{jcbi} &= -\tfrac{1}{2} Im\left(\tau_{b\bar{c}ij} + \tau_{bci\bar{j}}\right) & T^{31}_{jcbi} &= \frac{1}{2} Re\left(\tau_{b\bar{c}ij} + \tau_{bci\bar{j}}\right) \\
T^{02}_{jcbi} &= -\tfrac{1}{2} Re\left(\tau_{\bar{b}cij} + \tau_{\bar{b}c\bar{i}\bar{j}}\right) & T^{03}_{jcbi} &= \frac{1}{2} Im\left(\tau_{\bar{b}cij} + \tau_{\bar{b}c\bar{i}\bar{j}}\right) \\
T^{12}_{jcbi} &= \tfrac{1}{2} Im\left(\tau_{\bar{b}cij} - \tau_{\bar{b}c\bar{i}\bar{j}}\right) & T^{13}_{jcbi} &= \frac{1}{2} Re\left(\tau_{\bar{b}cij} - \tau_{\bar{b}c\bar{i}\bar{j}}\right) \\
T^{22}_{jcbi} &= -\tfrac{1}{2} Re\left(\tau_{\bar{b}\bar{c}ij} - \tau_{\bar{b}\bar{c}i\bar{j}}\right) & T^{23}_{jcbi} &= \frac{1}{2} Im\left(\tau_{\bar{b}\bar{c}ij} - \tau_{\bar{b}\bar{c}i\bar{j}}\right) \\
T^{32}_{jcbi} &= \tfrac{1}{2} Im\left(\tau_{\bar{b}\bar{c}ij} + \tau_{\bar{b}\bar{c}i\bar{j}}\right) & T^{33}_{jcbi} &= \frac{1}{2} Re\left(\tau_{\bar{b}\bar{c}ij} + \tau_{\bar{b}\bar{c}i\bar{j}}\right).
\end{aligned}
\tag{2.41}
$$

The individual components of the quaternion $(L1)_{\mu i}$ are obtained from (omitting the summations over bjc and explicit subscripts on $G^{\Lambda_{34},\Lambda_2}_{jc\mu b}$ and $T^{\Lambda_{34},\Lambda_T}_{jcbi}$)

$$
\begin{aligned}
(L1)^0_{\mu i} &= +G^{00}T^{00} + G^{10}T^{10} + G^{20}T^{20} + G^{30}T^{30} - G^{01}T^{01} \\
&\quad -G^{11}T^{11} - G^{21}T^{21} - G^{31}T^{31} - G^{02}T^{02} - G^{12}T^{12} \\
&\quad -G^{22}T^{22} - G^{32}T^{32} - G^{03}T^{03} - G^{13}T^{13} - G^{23}T^{23} \\
&\quad -G^{33}T^{33} \\
(L1)^1_{\mu i} &= +G^{01}T^{00} + G^{11}T^{10} + G^{21}T^{20} + G^{31}T^{30} + G^{00}T^{01} \\
&\quad +G^{10}T^{11} + G^{20}T^{21} + G^{30}T^{31} - G^{03}T^{02} - G^{13}T^{12} \\
&\quad -G^{23}T^{22} - G^{33}T^{32} - G^{02}T^{03} - G^{12}T^{13} - G^{22}T^{23} \\
&\quad -G^{32}T^{33} \\
(L1)^2_{\mu i} &= +G^{02}T^{00} + G^{12}T^{10} + G^{22}T^{20} + G^{32}T^{30} + Gi^{03}T^{01} \\
&\quad +G^{13}T^{11} + G^{23}T^{21} + G^{33}T^{31} - G^{00}T^{02} - G^{10}T^{12} \\
&\quad -G^{20}T^{22} - G^{30}T^{32} - G^{01}T^{03} - G^{11}T^{13} - G^{21}T^{23} \\
&\quad -G^{31}T^{33} \\
(L1)^3_{\mu i} &= +G^{03}T^{00} + G^{13}T^{10} + G^{23}T^{20} + G^{33}T^{30} - G^{02}T^{01} \\
&\quad -G^{12}T^{11} - G^{22}T^{21} - G^{32}T^{31} - G^{01}T^{02} - G^{11}T^{12} \\
&\quad -G^{21}T^{22} - G^{31}T^{32} - G^{00}T^{03} - G^{10}T^{13} - G^{20}T^{23} \\
&\quad -G^{30}T^{33},
\end{aligned}
\tag{2.42}
$$

where the signs appearing in equation (2.43) follow the quaternion multiplication rules for the second quaternion units of ${}^{Q}\mathbf{G}$ and ${}^{Q}\mathbf{T}$. From this AO-MS Lagrangian one may also obtain the MS-MS Lagrangian for which we write explicitly the real part.

$$
(L1)^0_{pi} = 4\sum_{\mu}\left(C^0_{\mu p}\,(L1)^0_{\mu i} + C^1_{\mu p}\,(L1)^1_{\mu i} + C^2_{\mu p}\,(L1)^2_{\mu i} + C^3_{\mu p}\,(L1)^3_{\mu i}\right). \tag{2.43}
$$

The full Lagrangian can be written in a compact manner as

$${}^{Q}\mathbf{L}1 = 4\left({}^{Q}\mathbf{C}\right)^{\dagger}\left({}^{Q}\mathbf{L1}^{(\mathrm{AO-MS})}\right)\ . \tag{2.44}$$

In the multiplication with the spinor coefficient matrix, ${}^{Q}\mathbf{C}$, we need to sum over the active virtual and the inactive spinors. This last step is fast since it scales as N^3, while the transformation itself scales as N^5.

The evaluation of the $\mathbf{L}2$ can be written in a similar fashion as $\mathbf{L}1$

$${}^{Q}\mathbf{L}2^{(\mathrm{AO-MS})} = \left({}^{Q}\mathbf{G}\right)^{T}\left({}^{Q}\mathbf{T}\right)^{*}, \tag{2.45}$$

and the last transformation step becomes:

$$ {}^{Q}\mathbf{L}2 = -4\left({}^{Q}\mathbf{L}2^{(\mathrm{AO-MS})}\right)^{\dagger}\left({}^{Q}\mathbf{C}\right). \tag{2.46} $$

The advantage of the quaternion formulation is that the extensive library of quaternion linear algebra routines that is available in DIRAC can be utilized.

2.3.2 Point group symmetry

In the previous section the inclusion of time reversal symmetry in the theory has been discussed. In this section we combine time reversal symmetry with spatial symmetry to employ the full symmetry of the molecular system.We write the 4-component complex wave function in terms of the individual components $\psi^T = \left(\psi^{L\alpha}, \psi^{L\beta}, \psi^{S\alpha}, \psi^{S\beta}\right)$. These functions are expanded in real scalar basis functions (AO-basis) that are adapted to boson irreducible representations (irreps) of the molecular point group. This procedure puts all the phase information on the MO-coefficients and makes it possible to use a non-relativistic integrals evaluation implementation to compute the primitive integrals. It can be shown [46] that the symmetry content of the wave function is given by

$$ \begin{aligned} \Gamma_L &= \left[\begin{array}{c} (\Gamma_\phi, \Gamma_\phi \otimes \Gamma_{R_z}) \\ \left(\Gamma_\phi \otimes \Gamma_{R_y}, \Gamma_\phi \otimes \Gamma_{R_x}\right) \end{array} \right], \\ \Gamma_S &= \left[\begin{array}{c} (\Gamma_\phi \otimes \Gamma_{xyz}, \Gamma_\phi \otimes \Gamma_z) \\ (\Gamma_\phi \otimes \Gamma_y, \Gamma_\phi \otimes \Gamma_x) \end{array} \right] = \Gamma_L \otimes \Gamma_{xyz}. \end{aligned} \tag{2.47} $$

For example: if the real part of $\psi^{L\alpha}$ transforms as the totally symmetric irrep Γ_0, the imaginary part of $\psi^{L\alpha}$ transforms as the rotation Γ_{R_z} and so on. Reformulation of the Dirac equation in terms of quaternion algebra gives two-component quaternion spinors

$$ {}^{Q}\psi^T = \left(\psi^{L\alpha} - \psi^{L\beta *}\check{\jmath}, \psi^{S\alpha} - \psi^{S\beta *}\check{\jmath}\right), \tag{2.48} $$

Comparing equations (2.47) and (2.48) we see that each boson irrep can be associated with a quaternion unit. It is convenient to classify a certain point group as *real, complex* , or *quaternion.* Without symmetry or with only inversion symmetry, pointgroups C_1 and C_i, large component basis functions may contribute to all four positions (real $L\alpha$, imaginary $L\alpha$, real $L\beta$ and imaginary $L\beta$) in ${}^{Q}\psi$ which means that the corresponding spinor coefficients are quaternion. However, basis functions that transform according to the

irreps of the *complex groups* C_s, C_2 and C_{2h} can contribute only to two positions so that the spinor coefficients are complex. In the *real groups* D_2, C_{2v} and D_{2h} only one specific position in the quaternion spinor remains so that these expansion coefficents are real. It is thus possible to combine time reversal and spatial symmetry by multiplying each symmetry adapted scalar basis function with the appropriate quaternion phase factor. This is done automatically by the quaternion multiplication routines of DIRAC so that quaternion matrices are made real or complex for point groups where this is possible. What it in effect means is that consideration of spatial symmetry leads in some cases to reduction of the algebra, i.e. a reduction from quaternion to complex or real algebra, thus reducing the computational effort. The current implementation of this scheme, as described in reference [46], is limited to D_{2h} since the integral generation module does not permit use of higher point group symmetry.

The reduction of algebra in case of the construction of the amplitude dependent part of the Lagrangian will be shown by a specific example, namely the case of C_{2v} symmetry. The point group C_{2v} has four boson irreps, A_1, A_2, B_1 and B_2. A_1 is associated with the real quaternion unit, A_2 with $\check{\imath}$, B_1 with $\check{\jmath}$ and B_2 with $\check{k}$. The phase shift that makes the MS coefficients real is applied so that equation (2.43) becomes

$$\begin{aligned}(L1)_{pi} = 4\sum_{\mu}\big(&C_{\mu p}^{\Gamma_{A_1}}\,(L1)_{\mu i}^{\Gamma_{A_1}} + C_{\mu p}^{\Gamma_{A_2}}\,(L1)_{\mu i}^{\Gamma_{A_2}} + \\ &C_{\mu p}^{\Gamma_{B_1}}\,(L1)_{\mu i}^{\Gamma_{B_1}} + C_{\mu p}^{\Gamma_{B_2}}\,(L1)_{\mu i}^{\Gamma_{B_2}}\big),\end{aligned} \tag{2.49}$$

where we omitted the subscript 0 for $(L1)_{pi}$ because it is now redundant with all imaginary coeffients being zero. The superscript on the MS coefficients and the AO-MS Lagrangian now indicates the boson irrep and we see that the identification with irrep labels replaces the identification with quaternion units.

We now consider the expression that defines the Lagrangian in the mixed AO-MS basis. Since only the real parts of amplitudes with an even number of barred indices have value non-zero in case of real groups, we see from the definition, equation (2.42), that only T^{00}, T^{11}, T^{22} and T^{33} remain. In terms of boson irreps we can indicate these T's by $T^{\Gamma_{A_1}}$, $T^{\Gamma_{A_2}}$, $T^{\Gamma_{B_1}}$ and $T^{\Gamma_{B_2}}$ respectively. The contraction to form the Lagrangian in mixed AO-MS basis

is then written as

$$\begin{aligned}
(L1)^{\Gamma_{A_1}}_{\mu i} &= +G^{(\Gamma_{A_1},\Gamma_{A_1})}T^{\Gamma_{A_1}} - G^{(\Gamma_{A_2},\Gamma_{A_2})}T^{\Gamma_{A_2}} \\
&\quad -G^{(\Gamma_{B_1},\Gamma_{B_1})}T^{\Gamma_{B_1}} - G^{(\Gamma_{B_2},\Gamma_{B_2})}T^{\Gamma_{B_2}} \\
(L1)^{\Gamma_{A_2}}_{\mu i} &= +G^{(\Gamma_{A_1},\Gamma_{A_2})}T^{\Gamma_{A_1}} + G^{(\Gamma_{A_2},\Gamma_{A_1})}T^{\Gamma_{A_2}} \\
&\quad -G^{(\Gamma_{B_1},\Gamma_{B_2})}T^{\Gamma_{B_1}} - G^{(\Gamma_{B_2},\Gamma_{B_1})}T^{\Gamma_{B_2}} \\
(L1)^{\Gamma_{B_1}}_{\mu i} &= +G^{(\Gamma_{A_1},\Gamma_{B_1})}T^{\Gamma_{A_1}} + G^{(\Gamma_{A_2},\Gamma_{B_2})}T^{\Gamma_{A_2}} \\
&\quad -G^{(\Gamma_{B_1},\Gamma_{A_1})}T^{\Gamma_{B_1}} - G^{(\Gamma_{B_2},\Gamma_{A_2})}T^{\Gamma_{B_2}} \\
(L1)^{\Gamma_{B_2}}_{\mu i} &= +G^{(\Gamma_{A_1},\Gamma_{B_2})}T^{\Gamma_{A_1}} - G^{(\Gamma_{A_2},\Gamma_{B_1})}T^{\Gamma_{A_2}} \\
&\quad -G^{(\Gamma_{B_1},\Gamma_{A_2})}T^{\Gamma_{B_1}} - G^{(\Gamma_{B_2},\Gamma_{A_1})}T^{\Gamma_{B_2}}, \qquad (2.50)
\end{aligned}$$

where the first symmetry label of G corresponds to the first quaternion unit and the second label to the second quaternion unit of the G defined in equation (2.39). The three-quarter transformed two-electron integrals, G, are automatically real since they are defined in terms of real primitive and real MS coefficients. We see that due to the quaternion phase shifts we need no quaternion algebra at all in the case of *real groups* and have reduced the complexity of the algorithm to real algebra and the computational work associated with the matrix multiplications by a factor of sixteen.

So far, we have largely neglected the division of the AO-basis into large, L, and small, S, component basis functions in the formulas. In the Dirac-Coulomb (DC) formalism only the blocks of the (LL|LL), (LL|SS), (SS|LL) and (SS|SS) two-electron integrals are needed. The kinetic balance condition dictates that the gradient of each large component basis function is contained in the small component basis set. Since we use real scalar one-component basis function the size of the small component basis set is approximately $2-3$ times larger than that of the large component basis set. The bottleneck in the current program becomes therefore the index transformation of two-electron integrals that involve the small component of the wave function. Although the (SS|SS) type of two-electron integrals can often be neglected in actual applications, this is not the case for the (LL|SS) and (SS|LL) type of integrals. In the case of DC-HF calculations it has been shown that significant computational savings are possible by applying a one-center approximation[48, 49] without losing much accuracy. In this approximation all multi-center electron-repulsion integrals over the small-component are removed. Generalization of this one-center approximation in 4-index transformations has been outlined in reference [50], but is not yet implemented in DIRAC. In a recent research paper Abe *et al.*[144] show an alternative approach in which four-component spinors are expanded in

a two-component basis set. This makes the index transformation more efficient since the size of the small component basis is then the same as the size of the large component basis. Such restricted kinetic balance schemes should give the most efficient approach in calculations on small molecules where integral approximation schemes based on the local nature of the small component and/or the neglect of spin-orbit coupling (SOC) terms[70] are not appropriate.

The MP2 amplitudes and the corresponding energy in the DIRAC program are calculated in the RELCCSD[142] module for the calculation of MP2 and coupled-cluster energies. Since RELCCSD uses transformed MS integrals that are stored on disk the current implementation of the MP2 first order molecular properties is not optimal. It requires two separate index transformations, one to compute the MP2 amplitudes and diagonal blocks of the effective density matrix, and another to obtain the amplitude dependent parts $\mathbf{L}1$ and $\mathbf{L}2$ of the Lagrangian. In this second index transformation of the AO two-electron integrals, we transform only three of the four indices and contract them 'on the fly' with the amplitudes. More efficient algorithms have been reported in non-relativistic quantum chemistry, like the semi-direct algorithm of Head-Gordon[129], where all these quantities are calculated in the same index transformation. Since we plan to extend the current code to the calculation of analytical first order coupled-cluster properties that necessitates a two-step procedure anyway, we have not made such a dedicated implementation for MP2 calculations.

2.4 Conclusions

We have presented a formulation and implementation of analytical first-order one-electron molecular properties at the Dirac-Coulomb MP2 level of theory. The formalism allows the use of inactive spinors, which is especially advantageous for systems containing heavy elements, since for most properties it is sufficient to only correlate valence and subvalence electrons. Even though we work in the no-pair formalism, negative energy spinors enter the equations due to the full Hartree-Fock relaxation of the active spinors to the effect of the applied perturbation. Time reversal symmetry is exploited by use of quaternion algebra. To reduce computational costs further point group symmetry up to D_{2h} is used. The bottleneck in the program is the transformation over two-electron integrals that involve the small component. This bottleneck might be overcome in the future by use of an one-center approximation as has already been applied successfully in Dirac-Coulomb HF theory.

2.5 Acknowledgements

JNPvS and LV thank the Netherlands Organization for Scientific Research (NWO) for financial support through the 'Jonge Chemici' program. Computer time provided by the Dutch National Computing Facilities (NCF) and travel support from the EU COST action D23, WG DIRAC and the Danish Natural Science Research Council grant no. 21-02-0467 are also gratefully acknowledged.

Chapter 3

The nuclear quadrupole moment of ^{115}In from molecular data

The nuclear quadrupole moment of ^{115}In has been determined by combining the experimental nuclear quadrupole coupling constants and electric field gradients, calculated at the four-component CCSD(T) level of theory, of four indium halides. Our recommended value for the nuclear quadrupole moment of ^{115}In is 770(8) millibarn. A basis set study at the Dirac-Coulomb Hartree-Fock level shows a slow convergence of the electric field gradient with respect to higher angular momentum functions.

3.1 Introduction

In the 'year-2001'[7] set of nuclear quadrupole moments (NQM), 26 new values are tabulated, as compared to the 'year-1992'[145] set. Eleven of these were solely determined via the molecular method and seven of these were determined in combination with atomic or solid state methods. The molecular method combines very accurately measured nuclear quadrupole coupling constants (NQCC) from microwave spectra, with a quantum chemical calculation of the electric field gradient (EFG) at the nucleus of interest. It has shown capable of producing accurate NQMs at relatively little expense. Since the rather inaccurate NQM of ^{115}In is not updated in the 'year-2001' set it is interesting to apply the molecular method to this isotope as well.

The standard value, 810 mb, for ^{115}In[7] was obtained by Belfrage *et al.*[146] from the observed hyperfine structure of the $5p$ ^{2}P, $7p$ ^{2}P and $8p$ ^{2}P states of the ^{115}In atom in combination with empirically derived values

for $\langle r^{-3} \rangle$ of these states[147]. The inaccuracy of these results is about 7%. Leiberich *et al.*[148] noted that this value is probably too high as it leads to inconsistencies between the experimental and calculated NQCCs in metallic indium. They derive a lower value of 760 mb taking the X-ray data and calculations on the muonic atom that were reported by Lee *et al.*[149] The accuracy of this NQM should be about 6%. Recently, van Lenthe and Baerends[150] computed NQCCs using the ZORA-4 DFT method for a range of compounds including the indium halides treated in this study. They also suggest a lower value of 740(30) mb for the NQM of ^{115}In.

The NQCC, $\nu_Q(X)$, in a linear molecule is given by[151]:

$$\nu_Q(X) = eq(X)\,Q(X)\,. \tag{3.1}$$

Inversion of this relation gives the NQM, Q (in barns), expressed in terms of the $\nu_Q(X)$ (in MHz) and the EFG, $q(X)$, (in atomic units):

$$Q(X) = \frac{\nu_Q(X)}{234.9647 q(X)}. \tag{3.2}$$

NQCCs for the indium halides tabulated to four digits accuracy or more are available from the book by Lucken.[152] Since these are already to first order corrected for vibrational effects it suffices to compute the EFG at the equilibrium geometry. Errors due to higher order vibrational effects should be small since the first order corrections are already small, ranging in the vibrational ground state from 0.46% for InF to 0.07% for InI.

Accurate calculation of EFGs requires large basis sets to describe the core and valence polarization. Halkier *et al.*[153] studied EFGs at the HF and CCSD level of theory for several light diatomic molecules and found that the EFG converges very slowly with standard basis set sequences, much slower than electric dipole and quadrupole moments. To make things worse, qualitative good basis sets for heavy elements are rare. For these reasons we optimized dedicated basis sets for indium at the Dirac-Coulomb Hartree-Fock (DC-HF) level of theory.

Apart from a large basis set one also needs to take relativistic effects and electron correlation effects into account to obtain an accurate description of the EFG. We do so by treating relativity at the Dirac-Coulomb (DC) level of theory, while using the CCSD(T) method to describe electron correlation.

3.2 Methods and computational details

We started by performing an extensive basis set study for In at the DC-HF level of theory. The two-step procedure to determine the optimal basis set

necessary for accurate calculation of EFGs is comparable to the strategy used in earlier work[126] on the EFGs of HBr and HI. In the first step we focus on the energy of the indium atom in its ground state, while in the second step we consider the EFG of the smallest of the four indium halides, InF.

We used so-called dual family basis sets[100] where the large component $(l+2)$-exponents are a subset of the large component (l)-exponents. The exponents in these sets were constrained by the even-tempered prescription[108] to limit the number of variable parameters. For the In atom this means that only four variables, α_s and β_s for $l = 0$, 2, 4 and α_p and β_p for $l = 1$, 3, 5 had to be varied, what can readily be done with a modified[154] version of GRASP[155]. In this energy optimization step we used a $23s17p12d$ basis set as starting point. When the optimal parameters were found, we performed three new calculations, in which the basis set was extended with one tight s, p or d-function, respectively, followed by reoptimization of α_s, β_s, α_p and β_p. The set that gave the largest energy lowering formed the starting point for new extensions. The procedure was repeated until the energy lowering upon extending the basis set became less than 10 mE_h.

In the second step, the α and β parameters were fixed and the convergence of the EFG as a function of basis set extension was studied. To allow for polarization in the molecule we first added three f-functions, centered around the exponent closest to the one of the f-function in the cc-VDZ basis of Dyall[156] (1.562 709 4). Next we systematically extended the basis to converge the EFG on In. Beginning with s-functions we added diffuse functions until the change in EFG became less than 0.001 a.u., after which we added additional tight functions until the same convergence was reached. The same procedure was repeated, with the extended basis, for higher angular momentum functions until the EFG with respect to g-functions was converged.

The results of this optimization are described in section 3.3.1. The differences between the strategy applied here and the one of reference [126] are that in the old procedure all exponents were a subset of the s-exponents and that in the study of the convergence of the EFG, several functions with different l value were added simultaneously. In this new study, we add one function of one particular l value at a time and also include g functions that were not considered previously.

For the correlated calculations we used a similar strategy as proposed by Kellö and Sadlej[9, 157] in the context of Douglas-Kroll EFG calculations. The valence and subvalence electrons are correlated at the CCSD(T) level of theory, while the electron correlation contribution due to the deeper lying shells is computed at the MP2 level of theory. This means that at the CCSD(T) level for InF 28 electrons are correlated, for InCl 36 electrons

are correlated and for InBr and InI 46 electrons are correlated. We thereby found that virtual spinors with spinor energies higher than 13 a.u. could be neglected (see section 3.3.2). All correlation contributions to the EFG are calculated using the finite field method, in which the correlation energy is differentiated with respect to the perturbation strength. The perturbation strength for these calculations was taken equal to $\pm 0.000\,01$ a.u. The total EFG of a method is the finite field correlation contribution plus the analytical HF (expectation) value. This mixed analytical/finite field scheme was introduced in reference [158], where an almost perfectly linear dependence of the correlation energy to the applied field strength was found.

All calculations of the electric field gradient were performed at the experimental equilibrium bond distances: R_e(InF)=3.752 a.u.[159], R_e(InCl) =4.538 a.u.[160], R_e(InBr)=4.806 a.u.[161] and R_e(InI)=5.204 a.u.[162]. In all our calculations we used fully uncontracted basis sets. The fluorine, chlorine and bromine basis sets were the same as used by Pernpointner and Visscher[158], except for chlorine where an extra diffuse p (0.0419) is added. For iodine we used the cc-pVTZ basis from Visscher and Dyall[163] augmented by one diffuse s (0.024 57), one tight p (250 937.594 414 2) and one diffuse p (0.040), the resulting iodine basis is a $22s18p12d1f$ set. All these basis sets can be considered as of approximately triple zeta quality, the ones for the lighter atoms being close to the original cc-pVTZ basis sets of Dunning and co-workers[101, 102, 164]. The electric field gradient calculations were performed using the DIRAC[41] electronic structure code using the standard Gaussian charge distribution for the nucleus[165]. In order to study the importance of scalar relativistic and spin-orbit coupling (SOC) contributions we not only performed relativistic DC calculations but also non-relativistic (NR) and scalar relativistic calculations. The non-relativistic (NR) calculations are based on the Lévy-Leblond Hamiltonian[69], the scalar relativistic calculations are based on the spin-free (SF) Dirac equation introduced by Dyall[51]. In all DC and SF EFG calculations we neglected the (SS|SS) type of integrals, since earlier studies have shown that these are negligible for the EFG[166]. As a check we performed one DC-HF calculation with (SS|SS) integrals included for InF and found a difference in the EFG on In of only 0.02%.

3.3 Results and discussion

3.3.1 Convergence of the electric field gradient in the Hartree-Fock calculations

For the indium atom the result of the optimization is a $25s19p12d$ even-tempered basis which gives an energy of $-5880.410\,40\ E_\mathrm{h}$, 21 m$E_\mathrm{h}$ above the DC-HF limit as calculated with GRASP[155] .The β_s for the s and d functions was 2.272 and the β_p of the p functions was 2.234. The highest s, p and d-exponents after the energy optimization were 20 702 066.70, 120 828.7227 and 2483.704 644 respectively.

The convergence of the EFG and the energy of InF by extending this basis is given in Table 3.1. The first g function that we used in the convergence study had exponent 0.677 07, which is comparable to the most diffuse f. The convergence of the EFG on In is very slow for the f and g functions, and we see that especially many tight functions are needed. The final basis, for which the EFG on In is converged within 0.001 a.u., is a $25s23p15d9f8g$ basis. The highest s, p, d, f and g exponents were 20 702 066.70, 1 347 862.219 141 1, 12 823.109 75, 434.534 442 5 and 41.007 795 7 respectively. To analyze the cause of this slow convergence we studied the individual spinor contributions to the EFG on In in InF. In Table 3.2 we list partial sums of spinor contributions and the differences in these partial sums upon adding 6 f functions to the $25s23p15d3f$ basis and adding 8 g functions to the resulting $25s23p15d9f$ basis. The main difference to the EFG on In upon extending the basis with f functions arises from the $2p$ spinors. When the basis is subsequently extended with g functions the main differences arise from the $3p$ and $3d$ spinors. This dependence can be understood by realizing that the EFG operator connects functions that differ by two units of angular momentum. It thereby weights the small admixture of the f-character in the closed p shell and similarly the small admixture of g-character in the closed d shell that occurs due to the molecule formation. Surprising is that this effect is so large that it needs to be taken into account to reach the desired accuracy. As could be expected, since we have no occupied f-shell in In, the addition of h-functions is not necessary. Adding a h-function to the $25s23p15d9f8g$ basis, with the h exponent comparable to the most diffuse g exponent, gave a difference of the EFG of only 0.0009 a.u.

We also did a minor study on the stability of the EFG on In for extending the fluorine basis. We hereby used the mentioned cc-pVTZ, the aug-cc-pVTZ, aug-cc-pVQZ and the aug-cc-pV5Z basis sets. The difference between the cc-pVTZ and aug-cc-pVQZ is -0.011 a.u., the difference between the aug-cc-pVQZ and aug-cc-pV5Z basis is -0.001 a.u. This means that with the

Table 3.1: Electric field gradients at the indium and fluorine nuclei in InF in atomic units using different basis sets for indium. The fluorine basis is the cc-pVTZ basis with two additional p functions (see Ref. [158]). The convergence (Δq^{In}) of the EFG at indium is also given. All calculations were performed at the DC-HF level of theory. diff. means diffuse.

Basis set		q^{In}	Δq^{In}	q^{F}
25s19p12d	(b1):	-4.4336		0.5438
25s19p12d3f	(b2): (b1+3 diff. f)	-4.4704	-0.0367	0.5348
26s19p12d3f	(b3): (b2+diff. s)	-4.4705	-0.0002	0.5362
	(b4): (b2+tight s)	-4.4703	0.0000	0.5348
25s20p12d3f	(b5): (b2+diff. p)	-4.4688	0.0015	0.5350
	(b6): (b5+diff. p)	-4.4688	0.0001	0.5350
	(b7): (b5+tight p)	-4.4723	-0.0034	0.5350
	(b8): (b7+tight p)	-4.4741	-0.0018	0.5350
	(b9): (b8+tight p)	-4.4756	-0.0015	0.5350
	(b10): (b9+tight p)	-4.4761	-0.0005	0.5350
25s23p13d3f	(b11): (b9+diff. d)	-4.4813	-0.0057	0.5287
	(b12): (b11+diff. d)	-4.4814	0.0000	0.5288
	(b13): (b11+tight d)	-4.4828	-0.0015	0.5287
	(b14): (b13+tight d)	-4.4847	-0.0019	0.5287
	(b15): (b14+tight d)	-4.4850	-0.0003	0.5287
25s23p15d4f	(b16): (b14+diff. f)	-4.4850	0.0000	0.5139
	(b17): (b14+tight f)	-4.4809	0.0037	0.5288
	(b18): (b17+tight f)	-4.4798	0.0012	0.5287
	(b19): (b18+tight f)	-4.4750	0.0048	0.5287
	(b20): (b19+tight f)	-4.4659	0.0091	0.5287
	(b21): (b20+tight f)	-4.4625	0.0034	0.5287
	(b22): (b21+tight f)	-4.4604	0.0021	0.5287
	(b23): (b22+tight f)	-4.4604	0.0000	0.5287
25s23p15d9f1g	(b24): (b22+diff. g)	-4.4396	0.0208	0.5289
	(b25): (b24+diff. g)	-4.4405	-0.0009	0.5288
	(b26): (b25+diff. g)	-4.4419	-0.0014	0.5280
	(b27): (b26+diff. g)	-4.4421	-0.0002	0.5281
	(b28): (b26+tight g)	-4.4340	0.0079	0.5284
	(b29): (b28+tight g)	-4.4319	0.0021	0.5285
	(b30): (b29+tight g)	-4.4285	0.0034	0.5285
	(b31): (b30+tight g)	-4.4238	0.0047	0.5285
	(b32): (b31+tight g)	-4.4211	0.0027	0.5285
25s23p15d9f9g	(b33): (b32+tight g)	-4.4202	0.0008	0.5285

Table 3.2: Spinor contributions to the EFG (in atomic units) at indium in InF for the $25s23p15d3f$ basis. Partial (Part.) sums of spinor contributions are also given, as well as differences in these partial sums between the different indium basis sets. The contribution of the F $1s_{1/2}$ spinor is added to the partial sum of the In $3p$ shell because its energy is just between the $3p_{1/2}$ and the $3p_{3/2}$ indium. All calculations have been performed at the DC-HF level of theory.

	$25s23p15d3f$	$25s23p15d3f$	$25s23p15d9f$	$25s23p15d9f8g$
Spinor	q_i	Part. sum q_i	Part. sum Δq_i	Part. sum Δq_i
$1s_{1/2}$	0.0086	0.0086	-0.0002	-0.0003
$2s_{1/2}$	0.0129	0.0129	-0.0002	-0.0006
$2p_{1/2}$	0.4598			
$2p_{3/2}$	3206.8787			
$2p_{3/2}$	-3207.4583	-0.1198	0.0187	0.0061
$3s_{1/2}$	0.0052	0.0052	0.0000	-0.0004
$3p_{1/2}$	1.7863			
F$1s_{1/2}$	-0.0757			
$3p_{3/2}$	595.4546			
$3p_{3/2}$	-597.4780	-0.3129	0.0082	0.0175
$3d_{3/2}$	92.7105			
$3d_{3/2}$	-92.1772			
$3d_{5/2}$	123.4478			
$3d_{5/2}$	-25.1868			
$3d_{5/2}$	-98.8341	-0.0399	0.0001	0.0171
$4s_{1/2}$	-0.0006	-0.0006	0.0000	0.0003
$4p_{1/2}$	3.3431			
$4p_{3/2}$	97.2239			
$4p_{3/2}$	-101.2474	-0.6804	-0.0024	-0.0005
F$2s_{1/2}$	-0.4570	-0.4570	-0.0001	-0.0002
$4d_{3/2}$	11.0968			
$4d_{3/2}$	-9.7183			
$4d_{5/2}$	13.2589			
$4d_{5/2}$	-3.6756			
$4d_{5/2}$	-10.5747	0.3871	-0.0002	0.0078
$5s - F2p$	-1.4601	-1.4601	-0.0005	-0.0027
F$2p$	-0.0246			
F$2p$	-0.0338	-0.0585	-0.0003	-0.0006
$5sp - F2p$	-2.1102	-2.1102	-0.0008	-0.0020
Total	-4.8255	-4.8255	0.0222	0.0414

$25s23p15d9f8g$ basis for In and the aug-cc-pV5Z for F, the EFG on In should be converged to almost 0.001 a.u. at the DC-HF level.

When doing correlated calculations, we have to compromise between basis set size and computational feasibility. For l =0, l =1 and l =2, we took those exponents from the HF EFG convergence study which made the EFG converge within about 0.01 a.u. For f and g we only took the most important functions, that could be chosen such that the EFG deviates less than 0.01 a.u. from the benchmark HF value. The final In basis which we used for the correlated calculations became then a $25s19p13d4f2g$ basis where the selected f exponents were 87.035 571 1, 3.491 740 3, 1.562 709 4 and 0.699 382 1 and the selected g exponents were 7.942 788 8 and 1.538 436 6. In Table 3.3 results for the four indium halides are presented. The deviation between these benchmark results and the results with the basis that we used for the correlated calculations are less than 0.01 a.u. and is used to correct the correlated EFG values calculated in the smaller basis.

3.3.2 Convergence of the electric field gradient in the correlated calculations

The uncontracted basis sets that we use generates many highlying virtual spinors that are unimportant for the correlation of valence and subvalence shells. To achieve better computational efficiency these virtuals are eliminated by applying an energy treshold for inclusion in the correlation calculation. To study the effect of truncating the active virtual space in this manner we varied this treshold in the spin-free formalism. Raising the virtual spinor threshold from 13 to 100 a.u. gave a change in the calculated EFG at the CCSD(T) level for InF, InBr and InI of 0.06% and for InCl of 0.21%. In the all-electron calculations at the MP2 level, which we use to estimate the effect of core correlation, the effect of higher virtuals should be more important because we then also consider core correlation. In these calculations we did therefore take all the virtual spinors into account. These all electron results can be compared to the smaller MP2 calculation (with the same active space as in the coupled-cluster calculations) to provide an estimate of the joint contribution of core correlation and the effect of higher lying virtual spinors on the valence spinors. Because of the small effect of the virtual spinors with energies between 13 and 100 a.u. on the valence correlation, and because the all-electron MP2 calculations will also give a good estimate of this effect, we conclude that it is justified to put the energy treshold at 13 a.u. in the coupled-cluster calculations. The correction obtained by comparing the full active space DC-MP2 and the small active space DC-MP2 calculations gives

changes in the EFG ranging from 0.04% for InI to 0.36% for InCl and is included in the CC values of Table 3.3.

The SOC effect on the EFG can be calculated by comparing the Dirac-Coulomb and the spin-free calculations. By comparing the DC-HF with the NR-HF calculations we see that relativistic effects are indeed very important. The relativistic contribution to the EFG ranges from -0.435 a.u. (9.83%) for InF to 0.300 a.u. (7.97%) for InI. The main contribution to the relativistic effects comes from scalar relativistic effects. For the benchmark basis the SOC contributions range from -0.019 a.u. (0.47%) for InBr to -0.015 a.u. (0.41%) for InI at the HF level. If we compare the CCSD(T) calculations using the SF formalism and the DC formalism, including the contribution of the all-electron MP2 calculations we see that the SOC effect ranges from -0.021 a.u. (0.53%) for InCl to -0.013 a.u. (0.40%) for InI, so the electron correlation effects do not affect the magnitude of SOC effects much in this case. The total relativistic contribution and the correlation contributions are of roughly the same magnitude but of opposite sign so that we see a fortuitous agreement between the NR-HF and the DC-CCSD(T) values. A similar cancellation was found for the EFG at Ag in AgCl by Pernpointner *et al.*[167].

3.3.3 Nuclear quadrupole moment of In

The resulting nuclear quadrupole moments of In extracted by the different methods from the four indium halides are presented in Table 3.4. At the HF level we see a mean absolute deviation of 3.7 and 3.8 mb for the DC and spin-free formalisms respectively and 8.4 mb at the non-relativistic level (for the small basis). At the correlated level the deviations between the NQMs of ^{115}In derived from the different molecules become smaller. At the DC level the mean absolute deviation in going from MP2 to CCSD(T) becomes smaller, from 3.6 to 1.0 mb. The small spread in NQM values for ^{115}In determined at the CCSD(T) level from the different indium halides gives already an indication of the quality of these calculations. In addition we also did some additional calculations to check the convergence of the calculated NQM.

As mentioned, the basis set that we used for the correlated calculations gave an EFG on In in the indium halide molecules that was converged within 0.01 a.u. at the DC-HF level. To check that this basis is also good enough for the correlated calculations we extended the basis with one diffuse p and one diffuse d, with exponents 0.028 058 5 and 0.057 715 5 respectively and performed a spin-free MP2 calculation for InF. The change in the EFG of InF was only 0.0007 a.u., so about 0.02%, again a negligibly small effect.

Table 3.3: EFG values at the indium nucleus (in atomic units) in different indium halides, calculated using different methods. The 'benchmark' values are calculated using the $25s23p15d9f8g$ basis for indium and the aug-cc-pV5Z basis for the halides, except for iodine where an aug-cc-pVTZ basis is used. All other values are calculated using the $25s19p13d4f2g$ basis for indium and the extended cc-pVTZ basis for the halides. NR means nonrelativistic, SF spin-free and DC Dirac-Coulomb.

Method	InF	InCl	InBr	InI
NR-HF	-3.990	-3.671	-3.553	-3.462
SF-HF	-4.409	-4.051	-3.898	-3.750
SF-HF_benchmark	-4.414	-4.054	-3.896	-3.739
SF-MP2	0.413	0.460	0.450	0.435
SF-MP2c[a]	0.408	0.453	0.443	0.438
SF-CCSDc[b]	0.330	0.337	0.320	0.310
SF-CCSD(T)c[b]	0.424	0.424	0.406	0.397
DC-HF	-4.425	-4.067	-3.910	-3.762
DC-HF_benchmark	-4.432	-4.074	-3.914	-3.754
DC-MP2	0.416	0.462	0.452	0.439
DC-MP2c[a]	0.404	0.449	0.441	0.438
DC-CCSDc[b]	0.326	0.347	0.318	0.309
DC-CCSD(T)c[b]	0.420	0.422	0.405	0.400
DFT ZORA-4[c]	-4.144	-3.783	-3.637	-3.475

[a]The MP2 contribution to the EFG due to all electrons and all virtual spinors.

[b]Corrected for the contribution due to the core electrons and higher lying virtuals estimated from the difference between the MP2c and MP2 results.

[c]Reference [150].

So far our focus with respect to basis sets has mainly been on InF that has the shortest bond distance of the four halides. To see whether enough diffuse functions are present in the basis we also performed some additional calculations on InI using the same diffuse functions as mentioned for InF. At the spin-free correlated level we find that the effect on the EFG value is indeed larger than in InF, although still very small. At the MP2 level a lowering of 0.0055 a.u. (0.l7%) is seen, at the CCSD(T) level 0.0038 a.u. (0.11%), giving rise to a slightly higher NQM.

Besides the spread in NQM values that is determined by comparing values from different molecules there is also a possibility of a systematic error that does not contribute to the spread. This error is difficult to estimate. Given the calculations that we performed, we believe the error in the basis set is negligible, in any case far below 1%. The vibrational correction error is

Table 3.4: NQMs of ^{115}In (in mb) derived using different methods and from different indium halides. The 'benchmark' values are calculated using the $25s23p15d9f8g$ basis for indium and the aug-cc-pV5Z basis for the halides, except for iodine where an aug-cc-pVTZ basis is used. The correlation contributions are calculated using the $25s19p13d4f2g$ basis for indium and the extended cc-pVTZ basis for the halides. NR means nonrelativistic, SF spin-free, and DC Dirac-Coulomb. At the correlated level the NQMs are corrected for the contribution due to core correlation and higher lying virtuals.

Method	InF	InCl	InBr	InI	Average
NR-HF	775.7	764.7	760.2	746.7	761.8 ± 8.4
SF-HF	701.8	693.0	692.9	689.5	694.3 ± 3.8
SF-HF_benchmark	701.1	692.4	693.4	691.6	694.6 ± 3.3
SF-MP2	772.6	779.4	782.3	783.2	779.4 ± 3.4
SF-CCSD	757.8	755.2	755.5	754.1	755.6 ± 1.6
SF-CCSD(T)	775.6	773.3	774.0	773.8	774.2 ± 1.0
DC-HF	699.4	690.2	690.9	687.2	691.9 ± 3.7
DC-HF_benchmark	698.3	689.1	690.1	688.7	691.6 ± 3.3
DC-MP2	768.3	774.6	777.6	779.7	775.1 ± 3.6
DC-CCSD	753.7	750.7	751.1	750.6	751.5 ± 1.1
DC-CCSD(T)	771.4	768.8	769.6	770.8	770.2 ± 1.0
DFT ZORA-4[a]	746.8	742.1	742.8	744.0	743.3 ± 1.5

[a]Reference [150].

also expected to be very small. This leaves possible errors in the electron correlation contribution as the largest source of uncertainty. From their ample experience with the calculation of electric field gradients of small molecules at the Douglas-Kroll CCSD(T) level of theory, Kellö and Sadlej[9, 168, 169] believe that an inaccuracy of 1% to the total EFG, due to the neglect of higher order electron correlation effects, should be an upper limit. We also take this estimate for our CCSD(T) calculations which makes our recommended value for the NQM of ^{115}In 770(8) mb. This value for the NQM of ^{115}In is in better agreement with the value favoured by Leiberich *et al.*[148] (760(50) mb) than with the standard value form Belfrage *et al.*[146] (810(60) mb), although it falls in both error bars. Our value for the NQM of ^{115}In indicates also that the value determined by van Lenthe and Baerends[150], using ZORA-4 and the Becke-Perdew functional, is too low, even though the spread in their values is of comparable size as ours.

The NQMs of other indium isotopes can be deduced by combining the measured B factors of atomic states and the NQM of ^{115}In. Eberz *et al.*[170]

tabulate the B factors for the $^2P_{3/2}$ states of the In isotopes 104-127. Here we only give the NQM of ^{113}In because it is, besides ^{115}In, the only stable isotope (with a natural abundance of about 4%). Using the ratio[171] $Q(^{113}\text{In})/Q(^{115}\text{In})$=0.986 362(15) we obtain a new value for $Q(^{113}\text{In})$ of 759(8) mb.

3.4 Conclusions

A new value for the nuclear quadrupole moment for ^{115}In has been determined by combining experimental nuclear quadrupole couplings constants with four-component CCSD(T) electric field gradient calculations of four indium halides. Our recommended value for the nuclear quadrupole moment of ^{115}In is 770(8) mb. Relativistic effects are shown to be almost as important as electron correlation effects, both about 10%, but since they are of opposite sign they almost cancel each other. A basis set study at the Dirac-Coulomb Hartee-Fock level showed that multiple tight f and g functions are needed to converge the electric field gradient for InF within 0.001 a.u.

3.5 Acknowledgements

We thank the Netherlands Organization for Scientific Research (NWO) for financial support through the 'Jonge Chemici' programme. We thank Dr. E. van Lenthe and Dr. M. Pernpointner for useful discussions.

Chapter 4

Molecular relativistic electric field gradient calculations suggest revision of the value of the nuclear quadrupole moment of ^{127}I

Relativistic *ab initio* methods are used to compute the electric field gradient at the iodine nucleus in nine different closed shell diatomic molecules. Combining these theoretical electric field gradients with experimental nuclear quadrupole coupling constants gives a consistent value of the nuclear quadrupole moment of ^{127}I of -696(12) millibarn. We argue that this value is more precise than the current standard value of the nuclear quadrupole moment of ^{127}I and recommend adjusting the reference value accordingly. The precision of this determination is still determined by technical limitations in the theoretical work, in particular the neglect of the two-electron Gaunt interaction in the Hamiltonian and correlation contributions beyond those described at the CCSD(T) level of theory, but the errors are reduced relative to the theoretical work that underlies the current standard value of this nuclear quadrupole moment. As a secondary study we also considered the calculation of the small electric field gradient at the gold nucleus in the AuI molecule and conclude that this computation remains a challenge for theoreticians.

4.1 Introduction

Of the various ways to determine the electric quadrupole moment of a nucleus[7] one of the most successful has proven to be the molecular method where nuclear quadrupole coupling constants (NQCC) obtained from microwave spectra are combined with quantum chemical calculations of the electric field gradient (EFG) at the nucleus of interest. The accuracy of this procedure is determined by that of the quantum chemical method for which one needs careful calculation of both relativistic and electron correlation effects.

The important nuclear quadrupole moment (NQM) of ^{127}I has been subject of many previous studies[126, 150, 169, 172–174] and was recently revised in the 2001 compilation of nuclear quadrupole moments[7, 175] where the value suggested by Bieroń *et al.*[169], -710(10) mb, was adopted. This reference value is the average of two atomic values (using the measured hyperfine interaction constant B) and a 'molecular' value derived from the NQCC observed in HI. These three values show a spread of 12 mb and the authors indicate that the molecular value of -705(7) mb that is based on a Douglas-Kroll-Hess CCSD(T) calculation might be the closest to the truth. They also present a historical overview of literature values of the NQM of iodine where one can see that the atomic and molecular values show a fairly good convergence.

In the present work we chose to use multiple molecular NQCCs to determine the NQM of ^{127}I. This provides for a more systematic way of estimating error bars on the derived NQM than is possible in a study on a single molecule. We chose the series of eight molecules: HI, IF, ICl, IBr, I2, CuI, AgI and TlI that were used in the comprehensive ZORA-4 DFT study of van Lenthe and Baerends[150]. To this series we added AuI since the NQM of this molecule was also recently measured[176].

The spread of the NQMs calculated from different molecular NQCCs gives an indication of the quality of the theoretical method and it is interesting to see how well different quantum chemical methods perform. Using ZORA-4 DFT van Lenthe and Baerends found a consistent value of the NQM of ^{127}I of -690(30) mb upon excluding the CuI and AgI results that were not in line with the other values. The poor performance of the DFT method for coinage metals halides was also observed in CuCl by Schwerdtfeger *et al.*[177] who related this to the problem that the currently available density functionals have in reproducing the dipole moment of these molecules. *Ab initio* methods like MP2, CCSD and CCSD(T) give accurate results for these lighter coinage metal halides and it is interesting to investigate whether this trend persists in the iodides.

4.2 Theory

The NQM $Q(X)$ (in barns, b) of nucleus X in a linear molecule can be calculated from[178]:

$$Q\left(X\right) = \frac{\nu_Q^X}{234.9647 q^X}, \tag{4.1}$$

with ν_Q^X the observed NQCC in MHz and q^X the EFG at this nucleus in atomic units. We usually compute only the value of q^X at R_e since vibrationally corrected NQCCs, $\nu_Q^{X,0}$, are either directly available from the literature [152, 172, 179, 180] or assessable via a first order fit [152, 176, 181]:

$$\nu_Q^X\left(\upsilon\right) = \nu_Q^{X,0} + \left(\upsilon + \frac{1}{2}\right)\nu_Q^{X,1}, \tag{4.2}$$

of the observed couplings $\nu_Q^X\left(\upsilon\right)$. The exception is CuI for which the experiment only provides the NQCC in the vibrational ground state[182]. This means that we calculate the EFG for this specific state via[183]

$$q^X\left(\upsilon\right) = q^{X,0} + \left(\upsilon + \frac{1}{2}\right)q^{X,1}, \tag{4.3}$$

which involves the computation of $q^{X,0} = q^X\left(R_\mathrm{e}\right)$ and the first and second derivative with respect to the reduced distance $\xi = \left(R - R_\mathrm{e}\right)/R_\mathrm{e}$

$$q^{X,1} = \frac{B_\mathrm{e}}{\omega_\mathrm{e}}\left[3\left(1 + \frac{\alpha_\mathrm{e}\omega_\mathrm{e}}{6B_\mathrm{e}^2}\right)\left(\frac{\partial q^X}{\partial \xi}\right)_{\xi=0} + \left(\frac{\partial^2 q^X}{\partial \xi^2}\right)_{\xi=0}\right]. \tag{4.4}$$

The spectroscopic constants B_e, ω_e and α_e can be taken from experiment[184]. An overview of other experimental data that was used, equilibrium geometries and NQCCs, is given in Table 4.1.

4.3 Methods and computational details

Since relativistic effects strongly influence the computed EFGs[185] we treat relativity with the four-component relativistic Dirac-Coulomb (DC) Hamiltonian. In order to analyze these relativistic effects we also performed non-relativistic (NR) and scalar relativistic calculations. This could easily be done with the relativistic electronic structure code DIRAC[41] that besides performing the DC calculations also allows transformations[70] to the non-relativistic (NR) Lévy-Leblond[69] or scalar relativistic spin-free (SF) Dirac

Table 4.1: References to the equilibrium geometries and vibrationally corrected NQCCs.

X	R_e (a.u.)	$\nu_Q^{X,0}$ (MHz)
H	3.040 95[a]	−1807.81[b]
F	3.609 38[a]	−3440.7482[c]
Cl	4.386 05[a]	−2928.91[d]
Br	4.665 73[a]	−2753.8[e]
I	5.038 01[a]	−2453.530[f]
Cu	4.418 18[a]	−938.07[g]
Ag	4.809 35[a]	−1060.85[d]
Au	4.669 71[h]	−1706.4[h]
Tl	5.317 69[a]	−438.123[d]

[a]Reference [184].

[b]Reference [179].

[c]Reference [180].

[d]Reference [152].

[e]NQCC vibrationally corrected using NQCCs from reference[181].

[f]Reference [172].

[g]Reference [182]. The NQCC could not be vibrationally corrected. The EFG is calculated for the vibrational ground state.

[h]NQCC vibrationally corrected using NQCCs from reference [176].

equations[51]. In all cases we describe the nucleus by an isotropic Gaussian charge distribution[165] and model its quadrupole moment separately[158].

For efficiency reasons we omitted the evaluation of the Coulomb (SS|SS) and Gaunt (SL|SL) types of two-electron integrals in most of the relativistic calculations. Of these two classes the most important are the Gaunt integrals that appear in the Dirac-Coulomb-Breit formalism. The contribution to molecular properties due to this relativistic two-electron operator was recently investigated by Pernpointner[186] in a study of the EFG on Tl in TlH. He found that inclusion of Gaunt integrals makes the EFG less negative by 0.6%. This is in line with earlier work by one of us [126] on HF, HCl and HBr where the effect on the EFG on the halogen atom was 0.03%, 0.19% and 0.29% respectively. We estimate that an effect of the order of 0.5% on the EFG in iodine compounds is therefore likely. Since Gaunt-type integrals are not available in the present DIRAC implementation, and because the MOLFDIR program package[75] that was used in the earlier work is not suited for calculations with the large basis sets that we use here, we had unfortunately to disregard this significant contribution. The smaller (SS|SS)

integral contribution, that forms part of the Dirac-Coulomb Hamiltonian, was included in cases where it gave a significant ($> 0.1\%$) contribution. This was only so for the 6^{th} row compounds AuI and TlI where we computed and added it at the Hartree-Fock level of theory.

Systematic studies of basis set convergence of the EFG on a nucleus in light molecules by Halkier *et al.*[153] show that use of a sufficiently large all-electron basis set is mandatory. Since a suitable basis set for iodine was not available we developed a new basis set using almost the same procedure as in our previous studies [126, 127]. The main difference, compared to this earlier work, is that in the present work the EFG calculations are performed for a wider range of diatomic molecules. This puts more emphasis on the flexibility of the basis set and made us revise the molecular verification procedure slightly by studying the convergence of two rather than one molecular EFG.

The first step in the basis set development consists of energy optimization of an even-tempered[108] dual-family[100] set at the Dirac-Coulomb Hartree-Fock (DC-HF) level of theory. This optimization is rather straightforward since only four parameters α_s and β_s for $l = 0,\ 2$ and α_p and β_p for $l = 1$ need to be determined. The optimal values of these weakly coupled parameters are readily found using a special[154] version of the GRASP[155] program. After satisfactory convergence of the atomic HF energy we keep the α and β parameters fixed and look at the convergence of the molecular EFG as function of basis set extension. As criteria we take the EFG on I in two molecules with different polarity, H^+I^- and F^-I^+, to ensure that the iodine basis set will be flexible enough for all molecules that we study.

All calculations are performed using fully uncontracted basis sets. The newly developed iodine basis set is discussed in more detail in the results section while the size and origin of the basis sets used for the ligands is displayed in Table 4.2. For convenience we also give a short description here.

For hydrogen we use the same basis set as described previously by Visscher *et al.*[126] which is the Sadlej[190] set extended with extra tight p and d functions. The fluorine, chlorine and bromine basis sets are the cc-pVTZ Dunning[101, 102, 164] sets extended with extra tight and diffuse functions as described in reference[127, 158]. For copper and silver we used the basis sets of Pernpointner *et al.*[187]. The gold basis is the PJHN[191] basis set extended with the two g exponents listed by Hess and Kaldor[188]. The thallium basis set is the $24s22p16d10f2g$ basis used by Fægri and Visscher[189] for the determination of spectroscopic constants of TlH.

Electron correlation is as important as relativity in the calculation of EFGs. We use a combination of MP2 and CCSD(T) calculations to compute both the important (sub)valence as well as core-valence and core-core corre-

Table 4.2: The basis sets that were used for the ligands (X) in the diatomic molecules.

X	basis set
H	$11s6p3d$[a]
F	$11s7p2d1f$[b]
Cl	$16s11p2d1f$[b]
Br	$21s15p9d1f$[b]
Cu	$20s15p11d3f$[c]
Ag	$21s17p14d3f$[c]
Au	$21s17p11d7f2g$[d]
Tl	$24s22p16d10f2g$[e]

[a]Reference [126].
[b]Reference [127].
[c]Reference [187].
[d]Reference [188].
[e]Reference [189].

lation effects. In the CCSD(T) calculations we chose the active space such that all valence and subvalence electrons are correlated. This corresponds to inclusion of the $4s$, $4p$, $4d$, $5s$ and $5p$ spinors of iodine and all other spinors that are in this energy range (above -10.7 a.u.). To reduce computational efforts we thereby deleted the highest virtuals with energies above 20 a.u. that are of little importance for valence and subvalence correlation. The effect of this removal of high-energy virtuals and the effect of electron correlation due to deeper lying shells was, however, calculated at the MP2 level of theory and used to correct the CCSD(T) values. This two-step strategy to calculate the electron correlation effects to the EFG was initially proposed by Kellö and Sadlej[9, 157] and works quite well if core contributions are small.

The full active space (all electrons correlated, no virtuals deleted) DC-MP2 calculations for all molecules were done with the integral direct MP2 module of DIRAC[192] while the other MP2 calculations as well as all the coupled-cluster calculations were performed with the RELCCSD[142] module of DIRAC. Because this module does not have an analytic gradient implementation we calculated the EFG correlation contribution via the finite field method. The perturbation strength used in these calculations was set to $\pm 0.000\,01$ a.u. The total EFG is obtained by adding the finite field correlation contribution to the HF expectation value[158].

Experimental bond distances were taken from Radzig and Smirnov[184] with the exception of AuI where the recent value of Reynard, Evans and

Gerry[176] was used. For CuI, where the derivatives of q^{X} are needed for the vibrational term $q^{X,1}$ of equation 4.4, we used a quartic fit to the q^{X} values calculated at R_{e}, $R_{\mathrm{e}} \pm 0.025$ a.u. and $R_{\mathrm{e}} \pm 0.050$ a.u. These derivatives are determined at the DC-MP2 level of theory since the accuracy of that method is sufficient to describe the small vibrational correction.

4.4 Results and discussion

4.4.1 Basis set development

The atomic energy optimization for iodine lead to a $26s19p13d$ even-tempered basis set which gives a DC-HF energy of $-7115.771\,52\ E_{\mathrm{h}}$ that is 23 mE_{h} above the DC-HF limit calculated by GRASP[155]. Analysis of the spinor coefficients shows that this basis has triple zeta character. The defining parameters are the ratio between the s (and d) exponents $\beta_s = 2.2385$, the ratio between p exponents $\beta_p = 2.2345$ and the highest s, p and d-exponents of 2.53×10^7, 1.90×10^5 and 7.99×10^3 respectively.

The EFG convergence study was started with this basis augmented by two f functions with exponents 1.10 and 0.493. The first g function that was added had exponent 0.226, which is comparable to the most diffuse f function. We then systematically added functions until the EFG on I in both HI and IF converged within 0.025%. This point was reached for a $26s24p15d11f8g$ basis (called the benchmark basis in the following) for which the highest s, p, d, f and g functions are 2.53×10^7, 4.74×10^6, 7.99×10^3, 6.84×10^2 and 6.35×10^1 respectively. The slow convergence of the EFG with respect to tight f and g functions was analyzed in our earlier convergence study of InF[127] and found to be due to the core contribution that requires many tight functions to stabilize. We should, however, note that the difference between the benchmark set and the start set is for both molecules only about 0.5%. While this difference is too high for the benchmark purpose that we have in this work, it also indicates that smaller sets may be used in ordinary production runs.

Using large uncontracted sets to reach the Hartree-Fock limit is feasible with the direct SCF implementation of DIRAC. This is, however, not the case for correlated calculations because coupled-cluster calculations with the benchmark basis require an extraordinary amount of memory, even when the virtual space is truncated by an energy threshold. We therefore modified the benchmark basis using the following criteria:

1. Only functions that made a contribution of more or equal than 0.25% to the EFG of iodine in HI and IF in the EFG HF convergence study

are included.

2. If two functions together made a contribution of more or equal than 0.25% in the EFG HF convergence study we take the basis function that gives the largest contribution.

3. Since correlated calculations are especially sensitive to basis set completeness with respect to diffuse functions we also calculate this contribution at the SF-MP2 level of theory. We thereby use the same criterion: include the function if it changes the EFG on HI, IF or IBr by more than 0.25%.

These criteria led to a $26s20p15d5f2g$ basis (the correlation basis) that was used in the correlation calculations. It consists of the same *s*- and *d*-functions as the benchmark basis but differs in the *p* basis by deletion of the four tightest exponents. The five *f* functions that were selected are those with exponents 137.0, 12.3, 1.10, 0.493 and 0.220, the selected *g* exponents are 0.505 and 0.226. Of the diffuse functions that we tested in step 3 we found that only the addition of a diffuse *d*-function (exponent 0.045) had a significant effect on the EFG (0.27% in IBr).

4.4.2 Selection of the active space in the CCSD(T) calculations

Possible errors due to truncation of the virtual space were tested at the SF-MP2 level for HI, IF, CuI and TlI as a representative sample for the molecules that we study. Increasing the virtual spinor energy threshold from 20 to 100 a.u. gives a change in the EFG on iodine of 0.06%, 0.03%, 0.29% and 0.04% respectively. To verify that these estimates are also reliable at higher levels of theory we performed the same calculation also at the SF-CCSD(T) level for the CuI molecule. The two methods agree well: upon increasing the threshold from 20 to 100 a.u. the MP2 method gives a change in EFG of 0.018 a.u. whereas CCSD(T) gives 0.021 a.u. This demonstrates that the small effect of high lying virtuals on the valence correlation is well described by the more economical MP2 method.

4.4.3 Relativistic effects on the electric field gradient

The strong influence of relativistic effects on the EFG at the iodine nucleus is apparent from the comparison between the HF values at the NR and the DC level in Table 4.3. For the larger EFGs found in HI and the interhalogens the effect runs from 17% (HI, IBr) to 13% in IF. The smaller EFGs of the

coinage metal iodines show much larger relativistic effects that increase from 27% in CuI to 65% in AuI. This is consistent with previous findings in atomic calculations[185] and other calculations on coinage metal chlorides[187]. The relativistic effects for the heaviest molecule, TlI, is smaller again at 29%. In all molecules, relativistic effects make the absolute value of the EFG larger which can be explained by the fact that the dominating contribution comes from a hole in the $5p$ shell for which the expectation value of $\langle r^{-3} \rangle$ increases due to relativity[185].

This qualitative picture of an EFG being increased by the relativistic contraction of the $5p$ shell does not consider spin-orbit coupling (SOC) effects. In TlI we see by comparing the DC-HF and SF-HF calculations that SOC alone makes the EFG on iodine in the TlI molecule almost 13% larger. SOC effects are for this molecule thus almost as large as scalar relativistic effects. The SOC effects in the interhalogens are smaller but still significant ranging from 2.6% for IF to 1.5% for IBr and make the EFG smaller in this case. For the other molecules SOC hardly influences the EFG: the effects range from 0.6% for AuI to only 0.20% in HI.

The importance of SOC effects on the EFG at iodine in TlI was already reported by van Lenthe and Baerends[150] who found an effect of 20% using the ZORA-4 formalism. Interesting is that, expressed in absolute terms the SOC contribution is 0.546 a.u. at the ZORA-4 DFT level while it is below 0.4 a.u. when calculated as difference between DC and SF calculations: HF gives then 0.356 a.u. while CCSD(T) gives 0.376 a.u. No systematic trend with respect to this difference in the ZORA and 4-component Hamiltonians can be identified, for the smaller SOC contributions in the other molecules the ZORA-4 DFT value is sometimes below the DC-HF value or has even a different sign. This is probably a manifestation of the fact that there is no unique spin-free Dirac equation[53] and hence also no unique SOC operator. It is somewhat surprising, however, that this difference is so large because the effect on the energy of different choices of SOC operators is rather small[53].

As already mentioned in the section 4.2 the contribution of the (SS|SS) type of two-electron integrals was only accounted for in the AuI and TlI calculations. This is done by calculating the effect of the (SS|SS) integrals at the DC-HF and SF-HF level in the correlation basis and then adding this as a correction to the benchmark DC and SF HF values respectively. In both molecules the effect was about 0.1%. For HI, I2 and AgI we also calculated the (SS|SS) contribution but found it to be negligibly small at 0.03%, 0.03% and 0.05% respectively. Since this is also expected for the other light diatomics, CuI, IF, ICl and IBr, we did not explicitly calculate the effect of (SS|SS) integrals there.

Table 4.3: EFG values at the iodine nucleus (in atomic units) in different diatomic molecules.[a]

Method	HI	IF	ICl	IBr	I_2	CuI	AgI	AuI	TlI
NR-HF	9.6943	20.1016	16.8166	15.6120	13.5955	2.8185	2.8297	2.7586	1.9671
SF-HF	11.6674	23.8669	20.0068	18.5731	16.2785	3.8433	4.5368	7.9301	2.4246
SF-HF_benchmark	11.6419	23.8033	19.9130	18.5059	16.1860	3.8316	4.5299	7.9207	2.4193
DC-HF	11.6309	23.2333	19.5971	18.2826	15.9931	3.8490	4.5420	7.9686	2.7765
DC-HF_benchmark	11.6189	23.1997	19.5328	18.2394	15.9239	3.8418	4.5404	7.9683	2.7732
DC-MP2	-0.7774	-2.1569	-1.7152	-1.5163	-0.8511	2.1322	2.1502	3.3476	-0.2654
DC-MP2c[b]	-0.6804	-1.9856	-1.5669	-1.3675	-0.7266	2.2020	2.2209	3.4927	-0.2362
DC-CCSDc[c]	-0.3445	-1.6796	-1.3554	-0.9148	-0.6444	1.6231	1.7538	2.3325	-0.0511
DC-CCSD(T)c[c]	-0.5182	-2.2282	-1.7787	-1.5660	-0.9415	1.9508	1.9809	2.5812	-0.1330
DFT ZORA-4[d]	11.3369	20.8850	17.8874	16.8696	15.0871	7.4942	7.8458		2.7491

[a]The 'benchmark' values are calculated using the $26s24p15d11f8g$ basis for iodine. All other calculations are performed using the $26s20p15d5f2g$ basis. NR means nonrelativistic, SF spin-free and DC Dirac-Coulomb.

[b]The MP2 correlation contribution to the EFG due to all electrons and all virtual spinors.

[c]Corrections for the contribution due to the core electrons and higher lying virtuals estimated from the difference between MP2c and MP2 results.

[d]Reference [150].

4.4.4 Nuclear quadrupole moment of ^{127}I

Given the final values of the EFGs in the nine molecules considered we may now study the consistency of the derived NQMs of ^{127}I. In Table 4.4 we see a clear convergence of the DC values through the hierarchy of wave-functions HF, MP2, CCSD and CCSD(T). The mean absolute deviation goes from 147.2 mb, 21.1 mb, 15.4 mb to 5.4 mb, whereas the difference between the lowest and highest determined NQM decreases from 408 mb at the HF level to 18.6 mb at the CCSD(T) level.

Looking at these deviations from the average value we see that the EFGs in the coinage metal iodines are clearly the most challenging to calculate. The HF method performs very poorly and underestimates the EFGs by roughly 50%. Going to MP2 gives a dramatic improvement but the deviation from the average values still indicates that also this method overestimates the EFGs by roughly 5%. CCSD and especially CCSD(T) perform well and give NQMs close to the average CCSD(T) value. We conclude that the applied *ab initio* methods are able to represent the EFG on iodine in the coinage metal iodines and that the discrepancy found in the corresponding DFT calculations is indeed due to the difficulties that contemporary density functionals have in describing such transition metal molecules[150, 177].

TlI also presents a difficult case. In this case HF gives an NQM at iodine in TlI close to the average CCSD(T) value, but it is now the MP2 method that overestimates the correlation contribution significantly. The problem persists to some extent to the CCSD(T) level since the NQM from TlI shows the largest deviation, 9.8 mb, from the average. One reason for this relatively large deviation might be the magnitude of the EFG in TlI, since this NQM is derived from the smallest NQCC of the molecules that were studied. Since this value of the NQCC is still larger than the EFG in other systems to which the molecular method could be successfully applied[158, 194] it is, however, more likely that the combination of a large core with substantial core correlation effects and large SOC effects is responsible for the relatively low accuracy of the electronic structure calculation.

Looking closer at the results of the HI molecule obtained by Bieroń *et al.*[169] in their reference study we find a substantial difference between our DC-CCSD(T) NQM value and their DKH-CCSD(T) value. We find a NQM for ^{127}I of -693.1 mb which differs almost 2% from the value of -705 mb that they report. Because the HI molecule is often used as benchmark system we would like to find out what is causing this discrepancy. Analyzing the differences between the two methods made us identify four possible causes. The most prominent one is at first sight the difference in Hamiltonians: we use the fully relativistic DC Hamiltonian whereas Bieroń *et al.*[169] apply

Table 4.4: NQMs of ^{127}I (in mb) computed from the molecular NQCCs.[a]

Method	HI	IF	ICl	IBr	I_2	CuI	AgI	AuI	TlI	average	MAD
NR-HF	-793.7	-728.5	-741.3	-750.7	-768.1	-1416.5	-1595.6	-2632.6	-947.9	-1152.8	485.9
SF-HF	-659.4	-613.6	-623.1	-631.0	-641.5	-1038.8	-995.2	-915.8	-769.8	-765.3	146.3
SF-HF_benchmark	-660.9	-615.2	-626.0	-633.3	-645.2	-1042.0	-996.7	-914.6	-771.4	-767.2	145.7
DC-HF	-661.5	-630.3	-636.1	-641.0	-653.0	-1037.3	-994.0	-911.4	-671.6	-759.6	147.5
DC-HF_benchmark	-662.2	-631.2	-638.2	-642.6	-655.8	-1039.2	-994.4	-911.4	-672.4	-760.8	147.2
DC-MP2	-703.4	-690.3	-693.8	-694.6	-687.2	-659.1	-667.8	-633.0	-735.0	-684.9	21.1
DC-CCSD	-682.4	-680.5	-685.8	-676.5	-683.5	-728.7	-717.3	-705.0	-685.0	-693.9	15.4
DC-CCSD(T)	-693.1	-698.3	-702.1	-702.9	-697.0	-687.6	-692.3	-688.4	-706.2	-696.4	5.4
DFT ZORA-4 (BP)[b]	-678.7	-701.2	-696.9	-694.7	-692.2	-532.7	-575.5		-678.3	-656.3	51.1
DFT DKH (PW)[c]	-711.6		-712.4	-707.4							
DFT (BPE)[d]					-689.0						
DKH-CCSD(T)[e]	-705.6										

[a]The 'benckmark' values are calculated using the $26s24p15d11f8g$ basis for iodine. The correlation contributions are calculated using the $26s20p15d5f2g$ basis for iodine. NR means norrelativistic, SF spin-free and DC Dirac-Coulomb. At the correlated level the NQMs are corrected for the contribution due to the core correlation and higher lying virtuals. The NQMs from the literature are calculated using the EFGs from the corresponding articles and the vibrationally corrected NQCCs. MAD means mean absolute deviation.

[b]Reference [150].

[c]Reference [193].

[d]Reference [172].

[e]Reference [169].

the scalar relativistic Douglas-Kroll-Hess (DKH)[58, 60] Hamiltonian. Other differences are the nuclear model, the difference in basis set, and the difference in the number of electrons correlated at the CCSD(T) level. All of these can be examined via explicit calculation and we decided to perform these calculations to locate the most important cause of the observed discrepancy.

Computing the EFG with a point nucleus model instead of a finite nucleus model gives a negligible effect on the EFG of 0.002%. Choosing a smaller active space (correlating 18 instead of 26 electrons) at the CCSD(T) level like Bieroń *et al.* did makes the NQM 1.6 mb less negative. This is significant and indicates that MP2 treatment of the subvalence $4s$ and $4p$ electrons does gives rise to an error but it is not the chief cause of the discrepancy. More important is the fact that the basis sets used by Bieroń *et al.*, a contracted $[23s18p15d2f/23s18p9d2f]$ set for iodine and a contracted $[11s7p2d/7s4p2d]$ set for hydrogen, are smaller than the ones that we used. We verified this hypothesis by uncontracting their set and applying the resulting basis in a DC-HF and DC-CCSD(T) calculation. We then found that while at the DC-HF level the calculated NQM is almost the same as calculated with the benchmark basis, -660.6 compared to -662.2 mb, the deviation at the correlated level is substantial. Using Bieroń's basis in a correlated calculation (correlating 18 electrons at the DC-CCSD(T) level) gives a value of -709.6 mb which is indeed close to their DK-CCSD(T) value but almost 20 mb larger than the one obtained with our $26s20p15d5f2g$ correlation basis (-691.7 mb). The large influence of the basis set on the correlation contribution to the EFG is a manifestation of the slow convergence of the correlation energy with respect to basis set size and we think that the additional tight f and g functions are important in this respect. We have not explicitly performed calculations using the scalar relativistic DKH formalism to further test the effect of the different formalisms to describe relativistic effects but we conclude that given the good agreement of the methods when the same basis is used, and the earlier observation that SOC effects are small for HI, this difference plays only a minor role. The most important factor is the smaller basis set that Bieroń *et al.* used which appears to be not fully converged at the correlated level.

Given the larger basis set and correlating space that we use we thus conclude that the 'molecular' value of Bieroń *et al.*, -705 mb, is too high. Taking also the other eight molecular values into account we find an average value of the NQM of -696(5) mb. This makes the deviation from Bieroń's 'atomic' values, -711.1 mb and -717.1 mb, even higher although they already mention that the lower molecular value may be closer to the true value. The consistency of the derived molecular NQMs from the nine different molecules give us reason to believe that our even lower value is still more accurate.

Finally we investigate sources of possible systematic errors in the applied

strategy that may not manifest themselves directly in the observed mean absolute deviation. Looking at the NQCCs that are used we conclude that higher order vibrational effects are negligible since the first order vibrational effects, that we corrected for, are already small at a maximum of 1% for HI. Concerning the Hamiltonian that we used in the EFG calculation: we already discussed the influence of the choice of nuclear model and the neglect of the Breit interaction. The influence of the nuclear model is negligible while we estimate the effect of the Gaunt interaction in HI to be of the order of 0.5% on basis of the results in the series HF, HCl and HBr. The magnitude and the direction of this effect can of course be different for the other molecules and this might make the net effect on the average smaller. Since we have no direct evidence for such cancellations we allow for 0.5% uncertainty in our NQM value due to neglected Breit interactions.

Turning to the basis sets that were used in the calculations we should keep in mind that, even with the large sets that we applied and the satisfactory convergence with basis set size at the HF level of theory, the question of saturation at the correlated level is not fully answered. Explicit convergence studies at the CCSD(T) level of theory would be helpful but these are not feasible with the current implementation and available computer hardware. Remaining systematic errors due to possible insaturation are therefore hard to exclude. Another source of error that arises from the treatment of core electrons and high energy virtuals at the MP2 level of theory instead of CCSD(T) can, however, be estimated via the formula

$$\begin{aligned} \Delta q^{\text{CCSD(T) core}} &= \frac{\left(q^{\text{CCSD(T) valence corr.}} - q^{\text{MP2 valence corr.}}\right)}{q^{\text{MP2 valence corr.}}} \\ &\times \left(q^{\text{MP2 all electron corr.}} - q^{\text{MP2 valence corr.}}\right), \end{aligned} \tag{4.5}$$

where $q^{\text{CCSD(T) valence corr.}}$ stands for the correlation contribution to the EFG of the valence and subvalence electrons at the CCSD(T) level, $q^{\text{MP2 valence corr.}}$ for the corresponding MP2 contribution and $q^{\text{MP2 all electron corr.}}$ is the MP2 correlation contribution of all electrons. Using this estimate we find that the error in treating the effect of the core electrons and high energy virtuals at the MP2 level is 1 mb in the calculated NQM for all molecules, except for TlI where it amounts to 3 mb. This error is therefore quite small and is taken into account by adding 1 mb to the error bar.

Looking at errors due to the correlation method we find that higher order correlation effects beyond CCSD(T) are hard to estimate. In many applications it is observed that CCSD(T) is significantly more accurate than CCSD but quantitative studies beyond this level of theory are rare. Halkier *et al.*[195] compared EFGs in BF and HF calculated using full configuration-interaction (FCI) with CCSD and CCSD(T) values and concluded that the

difference between FCI and CCSD(T) is smaller than the difference between CCSD(T) and CCSD. For the molecules that we studied the average absolute difference between the CCSD(T) and CCSD EFGs is of the order of 3% and this gives reason to believe that the estimate of 1% used by Bieroń *et al.*[169] for the CCSD(T) error in HI is applicable to our series as well.

Summing up the various sources of errors that we discussed above we arrive at an error bar for the derived NQM of 12 mb. This error bar is more than twice as large as the observed mean absolute deviation of the calculated NQMs from the different molecules and we are therefore reasonably confident that it also includes systematic errors that are made in our applied method. We therefore recommend a new value of the NQM of ^{127}I of -696(12) mb.

Coming to the earlier DFT work that is also shown in Table 4.4 we conclude they show good overall agreement with our CCSD(T) results. The chief problem in DFT is in the description of the coinage metal compounds: if these are excluded the ZORA-4 Hamiltonian with the Becke-Perdew functional[95, 97] as applied by van Lenthe and Baerends[150] gives an NQM that deviates only 1% percent from the average CCSD(T) value. This deviation is smaller than observed in our previous work on indium[127] where a difference of about 4% between such *ab initio* and DFT results was found. Using the Perdew-Wang exchange[97] and Perdew correlation[196] functional together with the Douglas-Kroll-Hess Hamiltonian, Malkin *et al.*[193] report systematically lower values of the derived NQM for HI, ICl and IBr, with an average of -710 mb. The value of -689 mb derived from the I_2 molecule by Haas and Petrilli[172], who used the Perdew-Burke-Ernzerhof functional[197] does agree quite well with our results.

4.4.5 Electric field gradient at Au in AuI

Because analytical evaluation of first order molecular properties at the correlated level is not implemented in the DIRAC program we would need to perform additional finite field calculations to obtain the EFG on the ligand atoms. In that case one should of course also investigate more closely the completeness of the basis set on these atoms with respect to the tight functions that are important for the EFG. Since this was not the primary purpose of the current study we did not perform such additional calculations. For the EFG on Au in the AuI molecule we, however, made an exception because this EFG is of more interest than the others. The measurement of the NQCC is relatively recent[176] and due to the small EFG it presents a challenging case for electronic structure calculations.

Similar molecules, the coinage metal chlorides, were studied in 1999 by Pernpointner *et al.*[187] at the DKH-CCSD(T) level of theory. For CuCl and

AgCl they found very good agreement with experiment for the NQCC on the metal as well as for the NQCC on the chlorine atom while for AuCl the experimental NQCCs were not known at that time. A year later Evans and Gerry[198] measured those NQCCs and reported that the NQCC on chlorine was in good agreement with the predicted value of Pernpointner *et al.* The measured NQCC on Au was, however, quite different. The theoretical DKH-CCSD(T) value is 75.43 MHz while experiment gives only 10.01 MHz. In this case there is little reason to believe that a too inaccurate value of the NQM is the cause of the discrepancy because this value is rather precisely determined[199]. Clearly the problem is in the size of the small EFG which is a very difficult task even for an accurate method as DKH-CCSD(T). Since the (vibrationally corrected) NQCC of Au in AuI is almost an order of magnitude larger than that of AuCl, 78 MHz compared to 10 MHz, it would be interesting to see whether this case might be easier for *ab initio* calculation. We tackled this problem using the same computational methods as applied in the calculation of the EFG of iodine on AuI, but reduced the basis sets on iodine and expanded the one on gold. For iodine we now employed the same basis set[163] as in the calculation of the EFG on indium in InI[127]. For gold we constructed an adequate basis by taking the basis set as used by Pernpointner *et al.*[187] in AuCl and augmenting it by three g functions, with exponents 4.506, 0.948 and 0.394, which results in a $23s20p14d10f3g$ basis. As usual both basis sets were used in uncontracted form.

The results of calculations on the NQCC of Au in AuI are given in Table 4.5. It is apparent that the applied *ab initio* methods are also in this molecule not able to reproduce the experimental NQCC correctly. HF is completely off and gives even the wrong sign for the EFG. MP2 gives the correct sign but at a value that is more than twice too large. CCSD improves substantially by giving a value that deviates only 10% from the experimental number but this is an accidental cancellation of errors since going to CCSD(T) makes the deviation increase again to 85%. Because the basis set on gold is not much larger than the iodine EFG basis, while gold has 26 electrons more, one may expect improvement by enlarging this basis set. Since the EFG at Au was not our main interest in this study we have not performed a convergence study. Interesting to note is, however, that both the relative and the absolute difference between CCSD and CCSD(T) values is large. The large relative difference of 41% is of course partly explained by the small value of the EFG but the large absolute difference between the CCSD and CCSD(T) values of 0.47 a.u. suggests that higher order correlation effects may also be important. Given both the accurate measurement of the NQCC and the availability of a reliable NQM makes this a suitable molecule to benchmark methods upon and further work would be interesting.

Table 4.5: NQCC at the gold nucleus in AuI.

Method[a]	NQCC (MHz)[b]
NR-HF	-350.8
SF-HF	-281.3
DC-HF	-292.4
DC-MP2	186.4
DC-MP2c[c]	197.3
DC-CCSDc[d]	85.5
DC-CCSD(T)c[d]	145.4
Experimental[e]	78.3

[a]NR means non-relativistic, SF spin-free and DC Dirac-Coulomb.

[b]The *ab initio* NQCCs are calculated using the corresponding EFGs and the NQM of ^{197}Au, reference [199].

[c]The MP2 value due to all electrons and all virtual spinors.

[d]Correction for the contribution due to the core electrons and higher lying virtuals estimated from the difference between the MP2c and MP2 results.

[e]Reference [176].

4.5 Conclusions

Combining electric field gradients from Dirac-Coulomb CCSD(T) calculations with experimental nuclear quadrupole coupling constants for a series of molecules we derived a consistent value of the nuclear quadrupole moment of ^{127}I. Systematic reduction of the mean absolute deviation was observed upon going through the hierarchy HF−MP2−CCSD−CCSD(T). The previous molecular determination of the nuclear quadrupole moment of ^{127}I was shown to suffer from basis set insaturation errors. We propose a new value for the NQM of ^{127}I as -696(12) mb for which the error bar is chiefly determined by errors due to the neglect of higher order correlation effects (1%) and neglect of two-electron relativistic effects (0.5%). Other sources of errors were also investigated but proven to play a minor role. As a secondary study we also briefly investigated the NQCC of the gold nucleus in AuI. The computation of a reliable EFG is difficult because even the Dirac-Coulomb CCSD(T) method gives a value that deviates by 85% from the experimental value. Improvement may come from the use of larger basis sets but it might also be possible that one needs to include higher order correlation effects or (and) the Breit interaction to obtain a satisfactory result.

4.6 Acknowledgements

The authors gratefully thank the Netherlands Organization for Scientific Research (NWO) for financial support through the 'Jonge Chemici' program. Computer time provided by the National Computing Facilities (NCF) is gratefully acknowledged. This research is part of the COST-D9 (PAMALOF) and COST-D26 (HAMEC) activities of the European Union. We thank Ephraim Eliav and Trond Saue for useful discussions.

Chapter 5

Theoretical and experimental evaluation of the radial function for electric dipole moment of hydrogen iodide

From relativistic quantum-chemical calculations of the molecular electronic structure of hydrogen iodide HI in electronic state $X^1\Sigma^+$ or 0^+ using the Dirac-Coulomb CCSD(T) method, we have evaluated the electric dipole moment μ at 17 values of internuclear distance R . On this basis we have calculated the pure vibrational expectation value in the vibrational ground state and matrix elements of $\mu(R)$ for transitions from that ground state to the first seven vibrationally excited states within the electronic ground state. For comparison with these results, we have undertaken a reanalysis of all existing data of intensities of vibration-rotational transitions in infrared spectra, combined with an experimental value of the expectation value of $\mu(R)$ in the ground state from the Stark effect, to generate a radial function for electric dipole moment. Agreement between calculated and experimental values of vibrational matrix elements of electric dipole moment is satisfactory, resolving outstanding questions about experimental and computational accuracy in the literature. We predict matrix elements for intensities of vibration-rotational bands $6-0$ and $7-0$, not yet measured.

5.1 Introduction

The objective of our present work is to re-examine the theoretical dipole moment of HI using quantum-chemical methods at the state of the art, ex-

pecting that there is room for improvement of the theoretical results reported by Iliaš *et al.*[200]. In particular we investigate whether their suspicion of experimental data is well founded. For the purpose of such an examination, it is essential that also all secondary experimental data be subjected to critical analysis. We therefore generated also a new potential-energy curve and a new radial function for electric dipole moment directly from experimental data according to well developed methods[201].

Many researchers have undertaken calculations on the electric dipole moment of the hydrogen iodide molecule, either only at the equilibrium internuclear distance R_e or as a function of distance R[122, 125, 200, 202–211]. After non-relativistic calculations in the 1970s [202, 203], the first relativistic calculations appeared in the 1980s [204–206], in the 1990s the latter calculations, combined with sophisticated methods to describe electron correlation, yielded results in reasonable agreement with experiment[207–209]. Of previous publications on the dipole moment of HI, only some recent, and − for our purpose − relevant ones are summarised below.

Alekseyev *et al.*[210] employed a scalar relativistic effective core potential (RECP) in their multi-reference configuration-interaction (MR-CI) calculation of the dipole-moment function of HI. After inclusion of a spin-orbit coupling (SOC) contribution −0.009 a.u., their result, 0.176 a.u., coincided with the experimental value for the dipole moment at R_e[212]. This agreement should, however, be considered fortuitous because their basis set contained only one *f* function and no higher angular-momentum functions, and was hence too small to prevent significant basis-set truncation errors. The RECP treatment of relativistic effects on the dipole moment was proven to be reliable by Norman *et al.*[122] who performed non-relativistic (NR), RECP, Douglas-Kroll-Hess (DKH) and Dirac-Coulomb (DC) Hartree-Fock (HF) calculations of static response properties, at R_e, of hydrogen halides.

Maroulis[209] performed NR-CCSD(T) calculations with a larger basis and supplemented these with a relativistic correction −0.040 a.u. taken from the work of Kellö and Sadlej[125]. On a basis of a discrepancy 9 per cent between his computed $\mu(R_e) = 0.191$ a.u and the experimental value, Maroulis suggested that new measurements of dipole moment be performed. Iliaš *et al.*[200] reported an extensive study of correlation and relativistic effects on the dipole moment and dipole polarizability; they included relativistic effects by means of the DKH Hamiltonian using also the CCSD(T) method to account for electron correlation. Through estimation of the omitted small effect of SOC by configuration-interaction calculations, they reported a value 0.154 ± 0.03 a.u. that deviated significantly from Maroulis's value and from the experimental value; they concluded also that the experimental values of the dipole moment and its first derivative with distance were inaccurate.

The dependence of the dipole moment on internuclear distance is not observed directly but derived from infrared absorption spectra. Experimental measurements of spectral intensities of lines in infrared bands of a diatomic species in absorption yield data from which a radial function for the electric dipole moment is deduced. Although there is no measurement of intensity in the pure rotational band of HI, a measurement by van Dijk and Dymanus[212] of the Stark effect on the first transition in that band yielded an expectation value $\langle 0|\mu(R)|0\rangle = 0.4477 \pm 0.0005$ D $= 0.1761 \pm 0.0002$ a.u. that underlies the value of μ at R_e questioned by Maroulis and by Iliaš *et al.* Ameer and Benesch[213], Niay *et al.*[214], Riris *et al.*[215] and Bulanin *et al.*[216] measured intensities of lines of HI in the fundamental vibration-rotational band with increasing precision in that chronological order. Benesch[217], Meyer *et al.*[218] and Bulanin *et al.*[219] measured intensities of lines of HI in band $\upsilon' = 2 \leftarrow \upsilon = 0$. Meyer *et al.*[218] and Riris *et al.*[215] published measurements of intensities in band $\upsilon' = 3 \leftarrow \upsilon = 0$, and Niay *et al.*[220] reported that their own measurements verified those of Meyer *et al.*[218] as presented in Haeuslers thesis[221]. For bands $\upsilon' = 4, 5 \leftarrow \upsilon = 0$, Niay *et al.*[220] reported the only known data. Many authors have reported measurements of frequency type for both HI and DI, from the pure rotational bands to the sixth overtone $\upsilon' = 7 \leftarrow \upsilon = 0$.

5.2 Methods and computational details

The most important factors determining the quality of theoretical calculations on molecules containing only light elements are the treatment of electron correlation and the basis set[222]. For molecules containing heavy elements, such as iodine in this case, relativity becomes an important factor as well[223]. In the following paragraphs we describe how we treat these aspects in our calculations.

For hydrogen we used the same basis set as for the calculation of the electric field gradient in HI[126, 224] which is the Sadlej basis[190] extended with additional tight p and d functions. For iodine we generated a new basis: we applied a strategy similar to that in previous work on electric field gradients [126, 127, 224], according to which we extend the basis set until the value of the property studied converges within a certain criterion. Specifically, for iodine we began with the same optimised atomic Dirac-Coulomb Hartree-Fock (DC-HF) basis as in our previous calculations on iodine compounds [224], which is a $26s19p13d$ even-tempered dual-family basis set augmented with two f functions. Beginning at $l = 0$ we added individual functions on the small exponent side of the range until the DC-HF dipole moment of

HI altered less than 0.001 au. At that point we began to add functions on the large exponent side. This process of successively adding diffuse-like and tight-like functions was repeated for values of l up to four. For correlated calculations the requirements of a basis set are more severe than for uncorrelated calculations [82]. To ensure that our basis set is sufficient to describe the dipole moment of HI at the correlated level, we tested the convergence of the dipole moment also at the spin-free Dirac-Coulomb (SFDC) CCSD level. We specifically investigated the convergence of the dipole moment by adding complete diffuse *spdfgh* shells to the iodine basis. The results of this study of the influence of the basis set on the computed dipole moment are reported in section 5.3.

To describe the effect of electron correlation we applied the CCSD(T) method. For reasons of computational efficiency we used spinors in the energy range only between −15 hartree and +50 hartree in the correlated calculations. Contributions from core spinors and from virtual spinors with higher energies are negligible (less than 0.0002 a.u.), as was verified in several test calculations at the DC-MP2 and SFDC-CCSD levels of theory, respectively.

The DC Hamiltonian includes all relativistic effects which makes direct comparison with earlier calculations difficult. To assess the relative importance of scalar and SOC effects we therefore also performed non-relativistic calculations using the Lévy-Leblond Hamiltonian[69] and scalar relativistic calculations using the SFDC formalism of Dyall[51].

In all calculations of electronic structure we used the DIRAC program[41] and conformed to our customary procedure of neglecting the numerous two-electron integrals that involve only the small component, S, of the wave function[47]. Test calculations show that this omission gives an error less than 0.000 01 a.u. in this case. To calculate the dipole moments we added the HF expectation value and the finite-field correlation contributions computed using field strengths +0.0005 and −0.0005 a.u. We calculated 17 dipole moments in a range $R/10^{-10}$ m = [1.2, 1.9] and fitted these to a polynomial in $x = (R - R_e)/R_e$.

Although the basis set was optimised for our main interest the dipole moment, we expect this basis to be adequate also for spectral parameters. We obtained spectral parameters with the CCSD(T) method, with the same active space as for calculations of the dipole moment. Two-electron integrals of type (SS|SS) were again neglected. We calculated 19 energy points in a range $R/10^{-10}$ m = [0.8, 2.5] and corrected all these points for basis-set superposition errors. The minimum of each curve was obtained with a cubic fit, using five points about the minimum, spaced 1 pm from each other. Other spectral parameters were obtained on fitting energies of vibration-rotational states $E(v, J)$, obtained through use of the LEVEL program[225],

to the expression

$$\begin{aligned} E(v,J) &= -D_{\mathrm{e}} + \omega_{\mathrm{e}}\left(v+\frac{1}{2}\right) - \omega_{\mathrm{e}}x_{\mathrm{e}}\left(v+\frac{1}{2}\right)^2 \\ &+ \omega_{\mathrm{e}}y_{\mathrm{e}}\left(v+\frac{1}{2}\right)^3 + B_v J(J+1), \end{aligned} \tag{5.1}$$

with

$$B_v = B_{\mathrm{e}} - \alpha_{\mathrm{e}}\left(v+\frac{1}{2}\right). \tag{5.2}$$

5.3 Results

5.3.1 Function for the dipole moment from quantum-chemical calculations

In this section we compare the effects of basis set, electron correlation and relativity on the dipole-moment function. To allow a fair study of the effect of one parameter on the dipole-moment function, we tried to eliminate errors in other parameters as much as possible to avoid interference and cancellation of errors. For example, when seeking the effect of relativity on the dipole moment, we used the CCSD(T) method to describe electron correlation and applied our best basis set.

Table 5.1 presents results of our study of the basis set: the upper part shows the variation of dipole moment at the DC-HF level on extending the basis set as described in the preceding section; the lower part shows the analogous variation at the SFDC-CCSD level (at the HF level only the additions of the basis functions that contribute sufficiently to be retained in the set are shown). At the DC-HF level, few basis functions are required to make the dipole moment converge. Evident are the additions of a diffuse p function, which has exponent 0.0441, that contributes −0.0257 a.u., and of two diffuse d functions, which have exponents 0.2255 and 0.1007, with contributions −0.0086 a.u. and −0.0115 a.u. respectively. Addition of the first diffuse shell for the correlated calculations is important: the SFDC-CCSD value is altered by 0.0221 a.u. Addition of an i function and of a tight shell of *spdfgh* functions is unimportant. The final basis set for which the SFDC-CCSD dipole moment alters less than 0.001 a.u. with respect to the next basis is a $28s22p17d5f3g2h$ basis. Applying this basis set in the correlated DC calculations, we obtained an accurate theoretical dipole-moment function of HI.

Table 5.1: Convergence of dipole moment μ at R_e on systematic extension of the iodine basis set[a]; the upper part corresponds to Dirac-Coulomb Hartree-Fock values, the lower part to spin-free CCSD values. For the Hartree-Fock values only the relevant values are shown.

Basis I		μ/a.u.	$\Delta\mu$/a.u.
	DC-HF		
$26s19p13d$	(b1):	-0.1699	
$26s19p13d2f$	(b2): (b1+2 diff. *f*)	-0.1664	0.0035
$26s20p13d2f$	(b3): (b2+diff. *p*)	-0.1921	-0.0257
$26s20p14d2f$	(b4): (b3+diff. *d*)	-0.1955	-0.0086
$26s20p15d2f$	(b5): (b4+diff. *d*)	-0.2000	-0.0115
$26s20p15d2f1g$	(b6): (b5+tight *g*)	-0.1988	0.0012
	SFDC-CCSD		
$26s20p15d2f1g$	(b7): (b6)	-0.1648	
$26s20p15d3f1g$	(b8): (b7+tight *f*)	-0.1633	0.0015
$26s20p15d4f1g$	(b9): (b8+tight *f*)	-0.1627	0.0006
$27s21p16d4f2g1h$	(b10): (b8+diff. *spdfgh*)	-0.1853	-0.0220
$28s22p17d5f3g2h$	(b11): (b10+diff. *spdfgh*)	-0.1880	-0.0027
$29s23p18d6f4g3h$	(b12): (b11+diff. *spdfgh*)	-0.1880	0.0000
$28s22p17d5f3g2h1i$	(b13): (b11+diff. *i*)	-0.1879	0.0001
$29s23p18d6f4g3h$	(b14): (b11+tight *spdfgh*)	-0.1880	-0.0001

[a]The basis set for hydrogen is Sadlej's basis set[190] plus extra tight p and d functions[126] resulting in an $11s6p3d$ set; this basis is large enough to fulfil the desired criteria.

Fig. 5.1 shows the dipole moments as a function of R for some basis sets listed in Table 5.1. Both the magnitude of the dipole moment near R_e and the dependence of the dipole moment on distance alter significantly on proceeding from small to large basis sets, underlining the importance of employing large basis sets in the calculation.

In Fig. 5.2 we present curves for $\mu(R)$ for electron-correlation methods MP2, CCSD and CCSD(T). We performed these calculations using the DC Hamiltonian and a $28s22p17d5f3g2h$ basis. This plot demonstrates that the perturbative MP2 approach fails even for small displacements from R_e, as noted by Maroulis[209].

Fig. 5.3 shows curves for $\mu(R)$ calculated using various Hamiltonians; the NR results are calculated using the Lévy-Leblond Hamiltonian and the SFDC results using the spin-free Hamiltonian of Dyall, whereas the DC results are the full Dirac-Coulomb results, all at the CCSD(T) level. The new

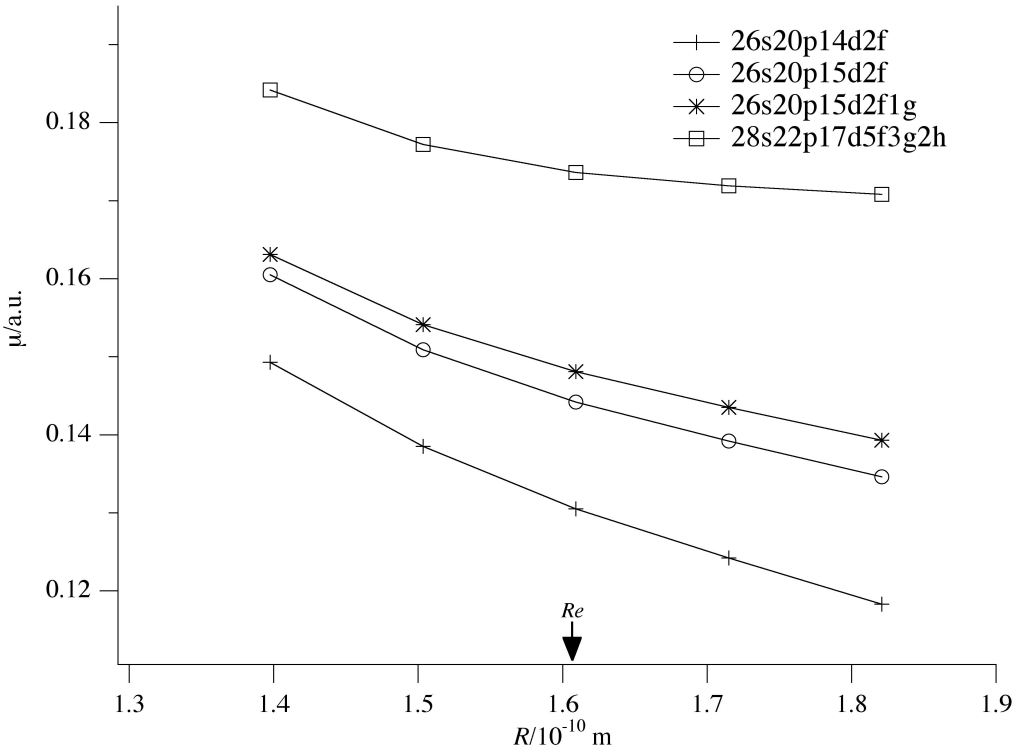

Figure 5.1: DC-CCSD(T) dipole moment μ *versus* internuclear distance in a region $R/10^{-10}$ m = [1.4, 1.8] using various basis sets for iodine. The position of R_e is indicated with an arrow.

experimental curve is explained in the subsection on analysis of spectral data and in the discussion.

A fit of the DC-CCSD(T) points of calculated dipole moment to a polynomial in x for comparison with previous results yielded this formula

$$\begin{aligned}
\mu\,(x)\,/\mathrm{a.u.} &= (0.173\,566\,7 \pm 0.000\,005\,3) - (0.037\,12 \pm 0.000\,08)x \\
&+ (0.2258 \pm 0.0005)x^2 - (0.8068 \pm 0.0053)x^3 \\
&- (0.0440 \pm 0.0132)x^4 + (0.369 \pm 0.103)x^5 \\
&+ (0.863 \pm 0.116)x^6 + (0.124 \pm 0.743)x^7 \\
&- (11.18 \pm 0.46)x^8 + (16.76 \pm 2.15)x^9 \\
&+ (11.9 \pm 0.7)x^{10} - (24.0 \pm 2.1)x^{11}
\end{aligned} \tag{5.3}$$

in which the uncertainties specified as single standard deviations represent only the error of fitting to that polynomial. An essentially exact fit of the

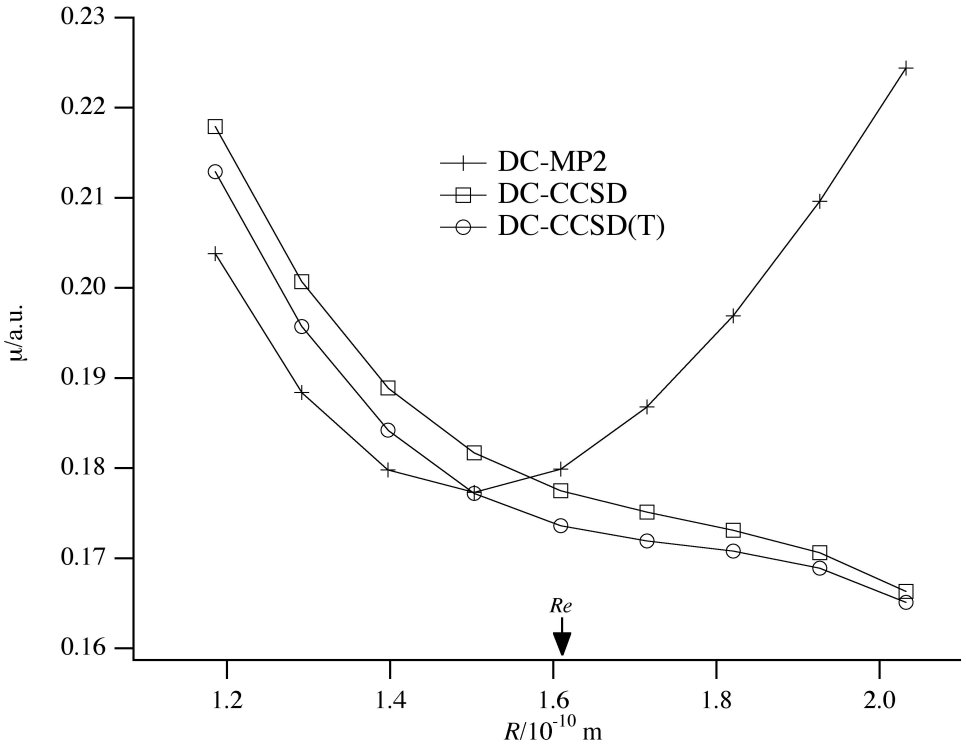

Figure 5.2: Dipole moment μ *versus* internuclear distance in a region $R/10^{-10}$ m = [1.2, 2.0] using various correlated methods. The position of R_e is indicated with an arrow.

17 computed points, within the last digit of each computed value, required a polynomial of degree 11. The terms beyond x^7 have little statistical or physical significance and reflect merely the constraint to an exact fit; these terms are not further used.

An analogous fit of computed energies to provide a potential-energy curve was impracticable because the computed points are not spaced sufficiently densely for this purpose. As the study of the dipole-moment function was our main interest, we therefore chose to combine the computed dipole-moment function with a function for potential energy derived from experimental data. With the above theoretical function for electric dipole moment, this function, according to the coefficients presented in Table 5.5, produced theoretical estimates of matrix elements of electric dipole moment for vibrational transitions presented in Table 5.2.

Table 5.2: Pure vibrational matrix elements of electric dipole moment from theoretical calculations and from fits of intensities of individual lines in vibration-rotational bands of HI, Herman-Wallis coefficients $C_0^{v'}$ and $D_0^{v'}$, and sources of intensity data.

Band	$< v' \lvert\mu(R)\rvert v >$/C m	$C_0^{v'}$	$D_0^{v'}$	ref.
$0-0$	1.4731×10^{-30} [a]			
	$(1.4934 \pm 0.0017) \times 10^{-30}$ [b]			
$1-0$	-1.6672×10^{-32} [a]	0.1323[c]	0.0035[c]	
	$(-1.358 \pm 0.011) \times 10^{-32}$ [d]	$0.131\,91 \pm 0.000\,01$[d]	$0.004\,42 \pm 0.000\,01$[d]	[216]
$2-0$	7.1788×10^{-33} [a]	0.0317[c]	0.00025[c]	
	$(6.582 \pm 0.033) \times 10^{-33}$ [d]	$0.030\,99 \pm 0.000\,01$[d]	$-0.000\,244 \pm 0.000\,001$[d]	[219]
$3-0$	-4.0211×10^{-33} [a]	0.0116[c]	0.000 023[c]	
	$(-4.085 \pm 0.42) \times 10^{-33}$ [d]	0.0088 ± 0.0015[d]	$-0.001\,56 \pm 0.000\,14$[d]	[215, 218]
$4-0$	1.4325×10^{-33} [a]	0.0163[c]	0.000 066[c]	
	$(1.332 \pm 0.156) \times 10^{-33}$ [d]	0.0213 ± 0.0008[d]	0.0020 ± 0.0001[d]	[220]
$5-0$	-4.7745×10^{-34} [a]	0.0169[c]	0.000 24[c]	
	$(-4.521 \pm 0.052) \times 10^{-34}$ [d]	0.0143 ± 0.0013[d]	0.0027 ± 0.0002[d]	[220]
$6-0$	1.6896×10^{-34} [a]			
$7-0$	-6.2495×10^{-35} [a]			

[a] From theoretical calculations.

[b] From the Stark effect, reference [212].

[c] Calculated with $\mu(x)$ from experiment.

[d] From direct fitting of experimental data in the specified references.

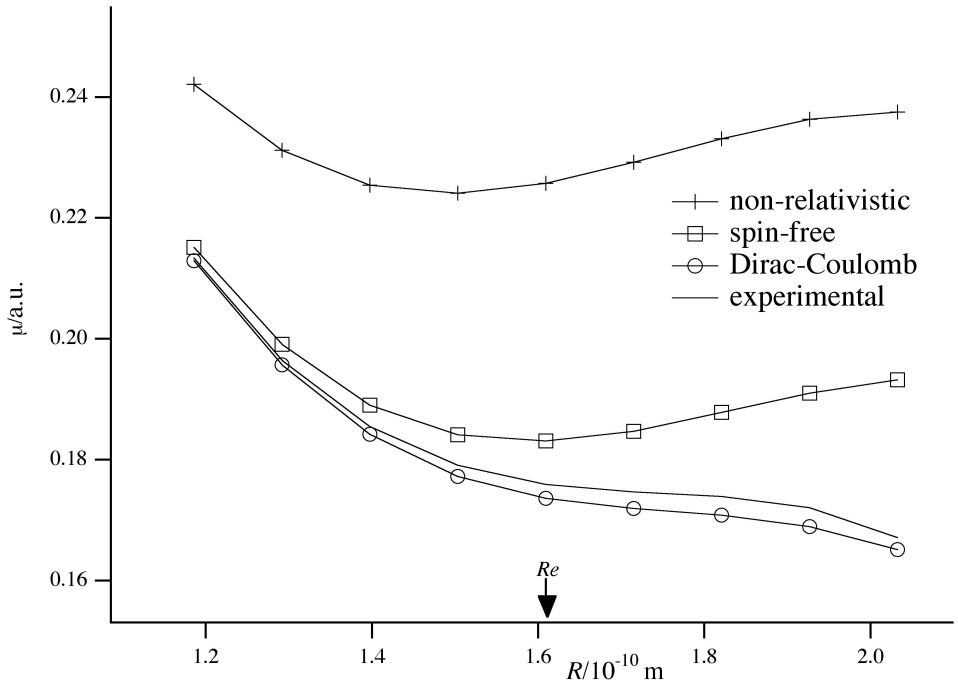

Figure 5.3: Dipole moment μ *versus* internuclear distance in a region $R/10^{-10}$ m = [1.2, 2.0] calculated using various Hamiltonians; experimental values correspond to the new dipole moment function, equation 5.7. The position of R_e is indicated with an arrow.

5.3.2 Spectral parameters from quantum-chemical computations

For transitions involving only the lower vibrational states it is possible to calculate spectral parameters with reasonable accuracy. We have done so at the CCSD(T) level of theory using the Lévy-Leblond, spin-free and Dirac-Coulomb Hamiltonians, and also using the SFDC-CCSD(T) energies augmented with HF SOC contributions; the results for these parameters are collected in Table 5.3. The experimental equilibrium binding energy, D_e, combines a value of the spectral dissociation energy D_0 from the literature [226] with a zero-point vibrational energy from our analysis of frequency data.

Table 5.3: Spectral parameters from CCSD(T) calculations compared with those from experiment; NR signifies non-relativistic, SFDC spin-free, SOC spin-orbit coupling and DC Dirac-Coulomb.

	NR	SFDC	SFDC+SOC correction[a]	DC	Feller *et al.*[b]	experiment
$R_e/10^{-10}$ m	1.6178	1.6107	1.6136	1.6136	1.5998	1.609 048 98 ± 0.000 000 55
$\omega_e/\mathrm{cm}^{-1}$	2338.65	2320.11	2298.64	2298.71	2354.70	2309.095 845 ± 0.000 053
$x_e\omega_e/\mathrm{cm}^{-1}$	38.15	38.09	38.81	38.85		39.6077 ± 0.0064
$D_e/\mathrm{kJ\ mol}^{-1}$	335.7	331.0	302.5	303.7	311.7	308.3 ± 0.2[c]
B_e/cm^{-1}	6.441	6.497	6.475	6.476		6.511 907 129 ± 0.000 000 042
$\alpha_e/\mathrm{cm}^{-1}$	0.164	0.167	0.171	0.172		0.170 450 ± 0.000 022

[a]Based on a potential-energy curve from SFDC-CCSD(T) energies plus HF SOC contributions.

[b]Reference [106].

[c]Reference [226] plus zero-point energy 13.692 430 kJ mol^{-1}.

5.3.3 Analysis of spectral data

A detailed overview of methods to fit experimental data to a potential-energy curve in various functional forms appears elsewhere [201]. We fitted frequencies and wave numbers of pure rotational and vibration-rotational transitions from the available experimental data, summarised in Table 5.4, to Dunham coefficients Y_{kl}. With a minimal number of coefficients, consistent with constraints through parameters c_j, a potential-energy curve,

$$V(z) = c_0 z^2 \left(1 + \sum_j c_j z^j\right), \tag{5.4}$$

was defined that is practically independent of nuclear mass. In equation (5.4) $z = 2(R-R_\mathrm{e})/(R+R_\mathrm{e})$ is a reduced displacement variable. Other coefficients s_j, t_j and u_j, explained below, are related to vibrational and rotational g factors and adiabatic corrections, respectively, for each atomic type, and were included empirically within applicable auxiliary coefficients Z_{kl}[201] to yield the best fit of available experimental data of frequency type. All coefficients Y_{kl} and Z_{kl} beyond the minimal range defined consistently through these radial coefficients are taken to have zero value, but further radial coefficients of types c_j, s_j, t_j and u_j in the several series are merely indeterminate and have not zero value in general. Like c_9 and c_{10}, not listed in Table 5.5 as they pertain to bands for which no experimental intensity data are reported, values of other radial coefficients are irrelevant for the present work.

To take into account extra-mechanical effects due to electrons imperfectly following rotational and vibrational motions of the nuclei, we include parameters u_1, u_3 and u_4 for adiabatic effects, s_0 related to the vibrational g factor at R_e and t_1 and t_3 related to the radial function for the rotational g factor[201]. Parameters u_2 and t_2 that occur in only linear manner were constrained to zero during the fit because, when left freely adjustable, their values were zero within their estimated standard errors. We constrained values of t_0^H and t_0^I to values consistent with the measured rotational g factor, $g_r(R_\mathrm{e}) = 0.096 \pm 0.010$[235] and permanent electric dipole moment[212], as described elsewhere[236]. Values of all these parameters are listed, with their uncertainties as single standard errors, in Table 5.5. With these values of radial parameters, we then calculated values of experimental spectral parameters reported in the latter column of Table 5.3, except D_e that is indeterminate from infrared data.

After deriving this potential-energy curve, we collected all known data [213–221] of intensities of spectral lines in vibration-rotational bands of $^1\mathrm{H}^{127}\mathrm{I}$ into a spreadsheet, converted them to squares of individual vibration-rotational

Table 5.4: Sources of data for derivation of a function for potential energy of HI.

Band	number of lines	ref.	number of lines	ref.	number of lines	ref.
	HI		DI		TI	
$0-0$	2	[227]	3	[227]	1	[228]
$0-0$	11	[229]	9	[230]		
$1-0$	24	[231]	28	[232]		
$2-0$	34	[232]	40	[232]		
$3-0$	34	[232]	39	[232]		
$3-0$			6	[233]		
$4-0$	31	[232]	34	[232]		
$4-0$			4	[233]		
$5-0$	24	[232]	29	[232]		
$5-0$	1	[220]	3	[233]		
$6-0$	30	[234]				
$7-0$	18	[234]				

matrix elements $|\langle \upsilon', J|\mu(R)|0, J''\rangle|^2$, and scrutinised these values taking into account their individual or collective uncertainties of measurement. We transferred data for each band to a Maple worksheet and applied a method − weighted linear regression with criterion of least sum of weighted squares of residuals − to estimate from individual measurements of squares of vibration-rotational matrix elements the square of the pure vibrational matrix element $|\langle \upsilon'|\mu(R)|0\rangle|^2$ and Herman-Wallis coefficients $C_0^{\upsilon'}$ and $D_0^{\upsilon'}$ for each band according to the relation[201]

$$|\langle \upsilon', J|\mu(R)|0, J''\rangle|^2 = |\langle \upsilon'|\mu(R)|0\rangle|^2 \left(1 + C_0^{\upsilon'}\imath + D_0^{\upsilon'}\imath^2\right) \ , \tag{5.5}$$

in which running number $\imath$ is defined to be $\imath = \frac{1}{2}[J'(J'+1) - J''(J''+1)]$. The source of particular data for each band used is identified in Table 5.2 with results of these fits; for band $\upsilon' = 3 \leftarrow \upsilon = 0$, we combined old data[218] with more recent data[215] by scaling the former to be consistent with the latter, because the latter data are sparse.

Assuming a radial function of the form $\mu(x) = \sum_j \mu_j x^j$, to conform to previous notation [237] in which $x = (R - R_\mathrm{e})/R_\mathrm{e}$, we solved a system of linear simultaneous equations

$$\langle \upsilon'|\mu(x)|0\rangle = \sum_j \mu_j x^j \langle \upsilon'|x^j|0\rangle \ , \ j = 0, ..., 5 \tag{5.6}$$

Table 5.5: Values of parameters fitted or constrained in analysis of frequency data of HI and DI.

parameter	value	uncertainty
c_0/m^{-1}	204 699 00	81
c_1	−1.547 358	0.000 197
c_2	0.985 396	0.000 75
c_3	−0.5809	0.0135
c_4	−0.0369	0.074
c_5	−0.446	0.26
c_6	3.08	2.5
c_7	−0.12	6.0
c_8	−42.6	17.
s_0^H	0.6659	0.0025
t_0^H	[0.1908]	
t_1^H	0.0540	0.0164
t_2^H	[0]	
t_3^H	-13.11	1.44
t_0^I	[0.0749]	
$u_1^H/10^6\ \mathrm{m}^{-1}$	-4.4082	0.0161
u_2^H	[0]	
$u_3^H/10^6\ \mathrm{m}^{-1}$	10.96	0.78
$u_4^H/10^6\ \mathrm{m}^{-1}$	41.9	3.7
$R_\mathrm{e}/10^{-10}\ \mathrm{m}^{-1}$	1.609 048 98	0.000 000 55

Values enclosed within brackets are constrained; the uncertainty of R_e includes errors of fundamental constants h and N_A. The maximum range of validity of pertinent radial functions is $R/10^{-10}\ \mathrm{m} = [1.3, 2.3]$.

in which pure vibrational matrix elements $\langle \upsilon' | x^j | 0 \rangle$ are calculated directly from symbolic expressions [201, 238], involving coefficients c_j of potential energy presented in Table 5.5. The resulting radial function for electric dipole moment is

$$\begin{aligned} \mu\,(x)\,/\mathrm{a.u.} &= 0.1759 - 0.030x + 0.2234x^2 \\ &- 0.7925x^3 - 0.2363x^4 + 0.6243x^5. \end{aligned} \tag{5.7}$$

Figure 5.4 presents a curve of this function in R in a range $R/10^{-10}\ \mathrm{m} = [1.25, 2.25]$, with a graphical representation of the theoretically derived function, eqn. 5.3.

We evaluated the signs of $\langle \upsilon' | \mu(R) | 0 \rangle$, indicated with superscript suffix c in Table 5.2, to produce best agreement between calculated values of

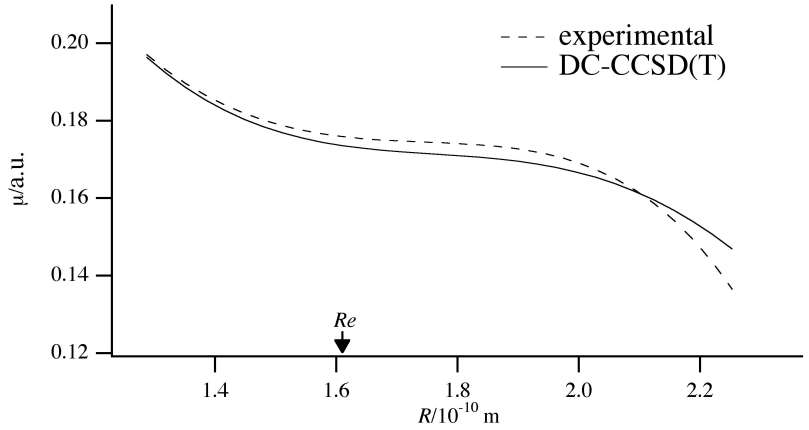

Figure 5.4: Theoretical and experimental radial functions $\mu(R)$ of electric dipole moment from equations 5.3 and 5.7.

Herman-Wallis coefficient $C_0^{v'}$, indicated with suffix d in Table 5.2, and the corresponding experimental values. Calculated values of both $C_0^{v'}$ and $D_0^{v'}$ are based on trial $\mu(x)$ through algebraic expressions [201, 238].

5.4 Discussion

5.4.1 Dipole moment function

The experimental radial function for electric dipole moment, eqn (5.7), agrees satisfactorily with the theoretical one, eqn (5.3). This condition is reflected in the agreement between theoretical values of matrix elements of $\mu(R)$ for vibrational transitions and the experimental values up to $v' = 5$, both shown in the second column of Table 5.2. Most errors are within a few per cent with the largest deviation for $\langle 1|\mu(R)|0\rangle$, that is about 25 per cent too large. That the slope of $\mu(R)$ near R_e is atypically small leads to a large relative error; the absolute error is modest in all computed matrix elements. On this basis we have confidence that predictions for $\langle 6|\mu(R)|0\rangle$ and $\langle 7|\mu(R)|0\rangle$ in the above table will also prove accurate within 10 per cent.

Use of a method better than CCSD(T) to achieve higher-order correlation might further improve agreement with experimental results. Fortuitous cancellation of errors in the CCSD method likely produces agreement with experiment slightly better than with CCSD(T) for the dipole moment at

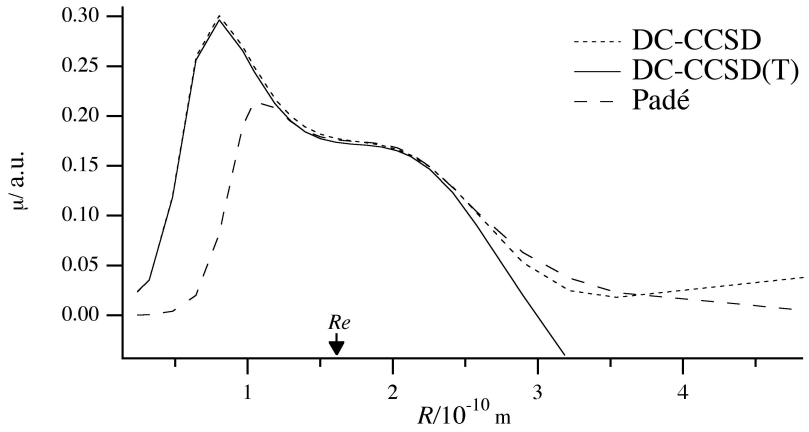

Figure 5.5: Comparison of the DC-CCSD, DC-CCSD(T) and Padé[237] dipole moment $\mu(R)$ over a large range of distance.

R_e. For other coefficients of dipole moment the CCSD(T) results agree better with experiment. For distances with $R/10^{-10}\mathrm{m} > 2.5$, the CCSD method appears superior. In Fig. 5.5 we plot the dipole moment for CCSD, CCSD(T) and the Padé function from 1980[237] in a range $R/10^{-10}\mathrm{m} = [0.24, 4.8]$. The Padé function is a combination of experimental data near R_e with the nonrelativistic two-configuration MCSCF calculations of Ungemach *et al.*[202] for R at long range. The CCSD plot follows the Padé function, with its correct asymptotic behavior, over a greater range of R better than the CCSD(T) curve. This result is likely comparable to the superior behavior of CCSD compared to CCSD(T) for the potential-energy curve of molecules HF and F_2 [239]. The reason is that the (T) correction is based on a fifth-order perturbation expression that for nearly degenerate wave functions diverges. CCSD itself, as an iterative or infinite-order method, is not based on perturbation theory and thus provides a better description at large R. For $R/10^{-10}\mathrm{m} < 1.1$ the coupled-cluster and Padé functions begin to deviate from each other. The coupled-cluster values in this region are probably nearer the true values than the Padé function because the latter, for small R, is based on a functional form that is correct only in a limiting region $R = 0$.

Comparison of the plots based on various Hamiltonians with the curve from experiment, Fig. 5.3, makes clear that relativistic effects are important to render an accurate description of the dipole-moment function of HI. The slope of the scalar relativistic dipole-moment function has the wrong sign at distances larger than R_e; apparently SOC is important not only for a

quantitative description of the dipole moment of HI near R_e but also for a qualitative description of its dependence on internuclear distance. This effect might be due to an avoided crossing allowed through SOC, but analysis of this point is difficult in our calculations. The importance of this spin-orbit interaction furthermore indicates that even inclusion of the two-electron Gaunt interaction in the Hamiltonian might be required to improve on the DC-CCSD(T) results.

The curves for non-relativistic and scalar relativistic CCSD(T) dipole moments of Maroulis[209] and of Iliaš *et al.*[200] show no increase in dipole moment on increasing internuclear distance near R_e. To rationalize this difference with our DC-CCSD(T) results, we plot the SFDC-CCSD(T) curve for the dipole moment of HI in Fig. 5.6. Improving the quality of the basis set raises the curve for dipole moment but also greatly alters the slope of the curve beyond the equilibrium distance, changing it from negative for the $26s20p14d2f$ basis to positive for the large $28s22p17d5f3g2h$ basis. A similar qualitative picture holds for the NR-CCSD(T) method. From these observations we conclude that the negative slopes obtained by Maroulis and by Iliaš *et al.* reflect a cancellation of errors − the use of too small a basis set and the lack of SOC.

The close agreement between the experimental radial function of electric dipole moment of HI and the DC-CCSD(T) function enables us to conclude that previously expressed doubts about the accuracy of the experimental dipole moment on basis of theoretical work are not well founded. The gap between calculation and experiment becomes closed through use of a large basis set, including g and h functions, and the inclusion of spin-orbit coupling.

5.4.2 Spectral parameters

Agreement between the DC-CCSD(T) values and experiment for the spectral parameters, according to Table 5.3, is satisfactory overall. The SFDC-CCSD(T) method also agrees satisfactorily with experiment, except for D_e because it lacks the spin-orbit splitting of the H(^{2}S) + I(^{2}P) asymptote. For all calculated spectral parameters, the SFDC-CCSD(T) values that are corrected with HF SOC contributions result in almost the same values as the full DC-CCSD(T) values, at a much smaller computational cost because single-group symmetry suffices for SFDC-CCSD(T) calculations. Visscher *et al.*[240] calculated the effect of inclusion of the two-electron Gaunt interaction on R_e, ω_e and D_e of HI; the effect found on R_e was an increase 0.1 pm, on ω_e a decrease 2 cm^{-1}, and a negligible effect on D_e. Also shown in this Table are results from Feller *et al.*[106], who used a newly designed large aug-cc-pRV5Z basis set for use with a small-core RECP. For D_e their result agrees

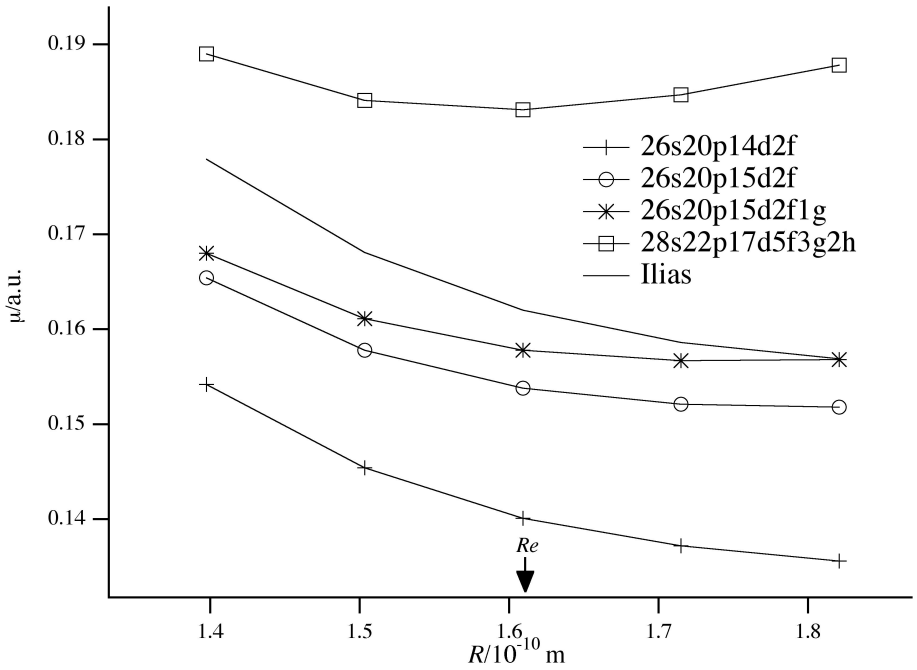

Figure 5.6: SFDC-CCSD(T) dipole moment μ *versus* internuclear distance in a region $R/10^{-10}\mathrm{m} = [1.4, 1.8]$ using various basis sets for iodine; the Iliaš curve is obtained from reference [200]. The position of R_e is indicated with an arrow.

better with experiment than our DC-CCSD(T) value, with deviations 3.4 and 4.6 kJ mol^{-1} respectively. For the calculation of D_e Feller *et al.* applied, besides use of a RECP, scalar relativistic corrections and SOC corrections that are expected to approach the Dirac-Coulomb-Breit limit. Rather than the difference in Hamiltonians, the reason for their superior agreement with experiment is likely the still greater quality of their basis set. For R_e and ω_e their agreement with experiment is worse than ours; two reasons for this condition might be that for these properties they applied no extra relativistic correction, beyond the use of a RECP, and that their FCI estimation was based on a continued-fraction approximation[241], which might in some cases improve results but worsen them in others.

5.5 Conclusions

The satisfactory agreement between quantum-chemical computations and experimentally observable molecular properties of HI, specifically the frequencies and intensities of vibration-rotational transitions, indicates both a mature state of calculations of molecular electronic structure involving atoms of fairly large atomic number and the efficacy of the Dunham approach to analysis of vibration-rotational spectra. Our work provides no support for doubt about the accuracy of the experimental dipole moment because the discrepancy between theory and experiment becomes resolved through use of a large basis set, including g and h functions, and the inclusion of spin-orbit coupling in a variational manner. Our predictions of matrix elements for intensities of vibrational transitions for the fifth and sixth overtone bands of HI can serve as guides for experimental measurements of these properties.

5.6 Acknowledgements

JNPvS and LV thank the Netherlands Organisation for Scientific Research (NWO) for financial support through the 'Jonge Chemici' program, the Dutch National Computing Facilities (NCF) for computer time, and EU COST action D26, WG HAMEC for travel support. JFO thanks Dr. J.-P. Bouanich for helpful discussion.

Chapter 6

Relativistic correction to the dipole moment surface of water

The effect of special relativity on the dipole moment surface of water is calculated. The effect is small and quite constant over the entire surface, about 0.20% - 0.30%. For all calculated points, relativity makes the dipole moment smaller, which means that calculated intensities of the rotation-vibration spectrum of water will be smaller as well.

6.1 Introduction

Despite the availability of quantum chemical methods that allow investigation of large, chemically interesting systems such as for example DNA fragments[242], complexes in solution[243] and large metal clusters[244], calculations on a single water molecule still presents many challenges. These challenges are in the calculation of properties of water as accurately as possible. Especially the description of the bending behavior of water is far from trivial. Upon bending, the oxygen valence electrons rehybridize from sp^3 to sp, causing substantial changes. This is reflected in difficulties in calculating the barrier to linearity of water accurately[245, 246].

The rotation-vibration spectrum of water is perhaps the most important of all molecular spectra. Water spectra are important in several applications. Hot water is a major product of nearly all combustion processes. Transitions of water in these environments can give spatial information on the distribution of water and on the local temperature. This kind of information is very useful, since it allows the monitoring and optimization of the performance of internal combustion processes. Another example of an important area of applications includes the study of the atmosphere of planets (including our

own).

In principle, much of information needed can be obtained from laboratory experiments. However, in practice this is difficult since it is necessary to properly assign all of the transitions in order to model the temperature dependence. An example of difficulties in the interpretation of spectra at high temperatures is given by the spectra of sunspots. Sunspots have a temperature of about 3000°C. The complicated spectra of sunspots have about 50 lines/cm^{-1}. However, experimental databases only allow the assignment of a handful of lines to water, even though many more water lines are present.

Another difficulty for experimental measurements are the numerous weak transitions of water. Worthy of mention in this respect is the status of atmospheric models. At the moment, about 30% more radiation is absorbed by the atmosphere than any 'state of the art' model can account for. A possible explanation of this failure might be the poor representation of the near-infrared, visible and near-ultraviolet absorption features of water in atmospheric databases. Since water is the dominant absorber of radiation in the atmosphere (it is responsible for about 70% of the absorption) it is evident that the ability to model the absorption of water accurately, also at weak transitions, is of extreme importance.

If the right methods are used, the theoretical calculation of the absorption of radiation by water allows a more complete and consistent data set. The calculated high-temperature list of 300 million lines by Partridge and Schwenke[12] may in this context be called very impressive. The largest challenge are the electronic structure calculations that have to be of enormously high quality.

The theoretical calculation of (parts of) the rotation-vibration spectrum require both an accurate potential energy (PES) and dipole moment surface (DMS). The PES determines the position of the lines in the spectrum, *e.g.* the frequencies. The DMS is subsequently needed to obtain the corresponding intensities. A very accurate PES has recently been reported by Polyansky *et al.*[247]. To approach an accuracy better than 1 cm^{-1} on average these authors showed that it was necessary to perform MRCI calculation using 5Z and 6Z basis sets followed by an extrapolation to the complete basis set limit. Corrections that had subsequently to be added are: core correlation effects, relativistic corrections (including the Breit interaction), QED corrections (the Lamb shift), first order diagonal Born-Oppenheimer corrections and second-order Born-Oppenheimer corrections (a non-adiabatic correction).

So far, the effect of relativity has been neglected for the DMS. The purpose of this work is to calculate this relativistic correction. This work is part of a more extensive project, coordinated by Professor Jonathan Tennyson from University College London. The aim of the entire project is to obtain

Table 6.1: Geometries used for the test calculations. Bond lengths are in Å.

	θ	r_1	r_2
equilibrium	104.52°	0.9576	0.9576
near linear	170.00°	0.8000	1.0000
bond compressed	100.00°	0.7500	0.9500
bond stretched	100.00°	0.9500	1.0000

both a more accurate PES and a more accurate DMS. At the moment of writing this chapter the project is still ongoing and spectra still have to be calculated. This chapter is thus not about interesting new features discovered in the rotation-vibration spectrum of water, but is about the calculation of relativistic effects on the dipole moment surface of water. To this end relativistic effects are calculated at different geometry points.

6.2 Methods and computational details

The geometric variables used to construct a DMS of water are the O-H bond distances, r_1 and r_2, and the bond angle, θ. 364 geometry points have been used to construct a relativistic correction to the *ab initio* DMS. The fitting of these points to an analytical representation is not discussed in this thesis[1].

The method applied for the calculation of the relativistic effect on the DMS of water was tested at four geometries that each probe a different region of the surface (see Table 6.1 for the precise coordinates). The water molecule was oriented in such a way that the z-axis was perpendicular to the molecular plane and the x-axis bisects the angle between the two OH bonds. The relativistic effect on the dipole moments is defined as the difference between relativistic and nonrelativistic values. The nonrelativistic calculations are based on the Lévy-Leblond reformulation of the Schrödinger equation[69]. Both relativistic and nonrelativistic calculations are performed using the DIRAC program[41] and employ a nucleus that is modeled by a Gaussian charge distribution[165].

The test calculations were performed at the Hartree-Fock (HF), MP2, CCSD and CCSD(T) levels of theory. In the HF method dipole moments were calculated analytically (as an expectation value) while the correlation contribution to the dipole moments was calculated using a finite-field method with perturbation strengths of ± 0.0002 a.u. No electrons were frozen in the correlated calculations.

[1] This will be discussed in a paper that has to appear.

Table 6.2: Effect of spin-orbit coupling on the dipole moment. SFDC are the spin-free calculations, SOC are the calculations including spin-orbit coupling, SOC-effect indicates the effect of spin-orbit coupling. Given is the magnitude of the dipole moment vector in a.u.

	SFDC	SOC	SOC-effect
equilibrium	0.785 038	0.785 036	−0.000 002
near linear	0.255 316	0.255 314	−0.000 001
bond compressed	0.780 764	0.780 763	−0.000 002
bond stretched	0.819 326	0.819 323	−0.000 002

To isolate the effect of spin-orbit coupling (SOC) on the dipole moment of water we have compared calculations using the full Dirac-Coulomb (DC) Hamiltonian with calculations based on the spin-free formalism of Dyall[51]. These calculations were performed at the HF level using the aug-cc-pVDZ basis of Dunning[248] in uncontracted form. The results are shown in Table 6.2 and indicate that SOC effects are very small. We therefore decided to compute the SOC correction only at the HF level of theory where its inclusion does not increase the computation cost. Inclusion in the correlated relativistic calculations makes the computations more demanding as this prohibits use of single group symmetry.

For efficiency reasons we furthermore neglected contributions from the (SS|SS) part of the Coulomb repulsion operator and from the Gaunt interaction. Calculations with and without inclusion of the (SS|SS) type of two electron integrals indicate that the contribution of this type of integrals is negligible for the dipole moment of water (below 10^{-7} a.u.). The Gaunt (SL|SL) type integrals come in at order α^2 ($\alpha = 1/137....$) which is one order higher than the (SS|SS) integrals that contribute at order α^4.However, the fact that spin-orbit effects are small does indicate that also the spin-other-orbit effects (to which the Gaunt or Breit interaction amounts in a two-component picture) will be small.

Four different basis sets from the correlation consistent family of basis sets were tested, the aug-cc-pVTZ, aug-cc-pVQZ[248], aug-cc-pCVTZ and aug-cc-pCVQZ[249]. These were all decontracted because the standard contraction coefficients are determined using non-relativistic methods and not suitable for our purpose. For the oxygen atom a complication arises in decontracting the aug-cc-pCVXZ sets because the additional tight exponents lie close to other exponents. We resolved this by dropping for the aug-cc-pCVTZ set the two tight s exponents and replacing them individually by exponents that lie in between existing exponents using an even-tempered scheme

$$\alpha_b = \sqrt{\alpha_a \alpha_c}, \tag{6.1}$$

where α_a and α_c are the existing (aug-cc-pVXZ) exponents and α_b is the new tight exponent. For example, the tight s exponent 7.845 from the aug-cc-pCVTZ set has been replaced by 10.199 which is obtained by applying the above formula to the exponents 16.760 and 6.207. The same idea was applied to the three extra s exponent from the aug-cc-pCVQZ set and to two of the three extra p exponents from the same aug-cc-pCVQZ basis. All other extra tight exponents are well separated from others and could be included without modification.

The CCSD(T) results of the basis set study are shown in Table 6.3. The difference, on the relativistic effect, between the aug-cc-pVTZ and aug-cc-pCVQZ is of the order of 1 or 2%. However, the absolute differences, on these relativistic contributions calculated using different basis sets, are very small compared to the total dipole moment. The difference between the aug-cc-pVTZ and aug-cc-pCVQZ relativistic effects is only about 0.003% compared to the total aug-cc-pCVQZ dipole moment. Going from the aug-cc-pVTZ to the aug-cc-pCVTZ basis the difference between the aug-cc-pCVQZ basis is almost halved. Because the number of basis functions of the aug-cc-pCVTZ basis is not much larger than the aug-cc-pVTZ basis we decided to perform the correlated calculations using the aug-cc-pCVTZ basis. Because the HF calculations are relatively fast we have, however, calculated the HF contribution to the relativistic effect on the dipole moment using the largest aug-cc-pCVQZ basis.

In the complete set of geometries used to calculate the dipole moment surface of water there were three geometries that appeared to be problematic for the CCSD(T) method. All coordinates of these geometries have $\theta = 104.52°$, $r_1 = 0.95$ Å, while the r_2 is respectively 3.0, 5.0 and 7.0 Å. These geometries, for which water shows a large multi-configuration character, have been treated separately using the complete active space self-consistent-field (CASSCF) method. The effect of relativity on the dipole moment was calculated using the Mass-Velocity-Darwin (MVD) operator in a perturbative manner. HF test calculations on the geometries in Table 6.1 using the aug-cc-pVDZ basis show that the difference on the relativistic effect between MVD and DC is about 5%. Knowing that these three geometries will not be so important for the intensity calculations we consider this difference between DC and MVD on the small relativistic contribution acceptable. The CASSCF calculations are performed in C_s symmetry with the same active space as used by Partridge and Schwenke[12], six a' and two a'' orbitals and

Table 6.3: Test of different basis sets on the relativistic effect on the dipole moment. All values are calculated using the spin-free CCSD(T) method with neglect of (SS|SS) integrals. Given is the magnitude of the dipole moment vector in a.u.

geometry	aug-cc-pVTZ	aug-cc-pCVTZ	aug-cc-pVQZ	aug-cc-pCVQZ
equilibrium	−0.001 720	−0.001 710	−0.001 703	−0.001 697
near linear	−0.000 150	−0.000 149	−0.000 148	−0.000 147
bond compressed	−0.001 419	−0.001 411	−0.001 405	−0.001 400
bond stretched	−0.001 824	−0.001 813	−0.001 807	−0.001 801

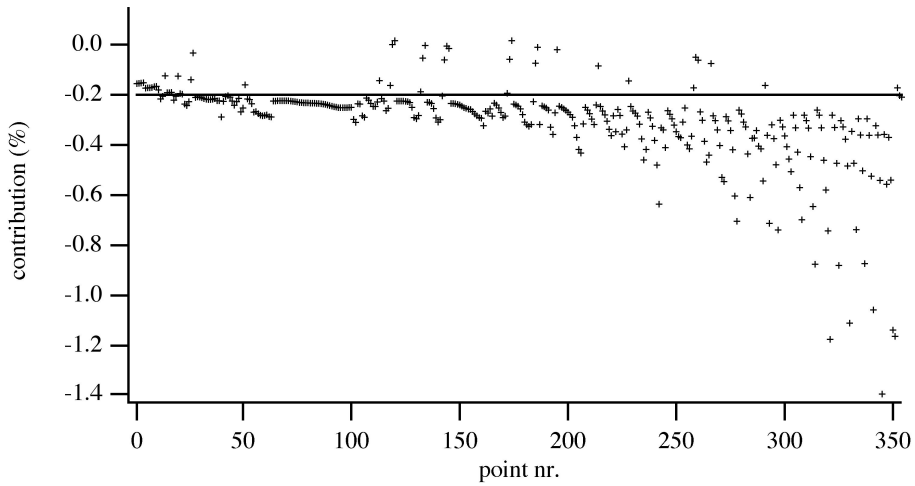

Figure 6.1: Relativistic contribution to the dipole moment, in %, for the geometries used to construct the dipole moment surface.

eight electrons active using the aug-cc-pCVQZ basis with the DALTON electronic structure program[250]. Comparison of the non-relativistic CCSD(T) values with non-relativistic MRCI values for the other geometries of the set confirmed that CCSD(T) should be an adequate method to calculate the relativistic effect for the other 361 points.

6.3 Results and discussion

This section is not extensive, only some very general comments on the results are given. A more detailed description of the effect of relativity on the dipole moment surface and hence the intensities of the rotation-vibration spectrum of water will be given in a paper that has to appear.

In Fig. 6.1 the relativistic contribution, in %, to the x-component of the dipole moment of the calculated points is shown. The points are ordered on increasing r_2. The general observation is that for all points relativity makes the dipole moment smaller and that for most points the effect is on the order of 0.20% - 0.30%. However, when r_2 is larger than 1.2 Å there are numerous points that show a larger relativistic effect (a maximum relativistic effect is found for the point $\theta = 120°$, $r_1 = 1.10$ Å, $r_2 = 1.70$ Å, where the effect is 1.39%). For the y-component a similar trend is observed.

Of the 364 points, 36 are at $r_{\mathrm{OH}} = r_1 = r_2 = 0.95$ Å. In Fig. 6.2 the

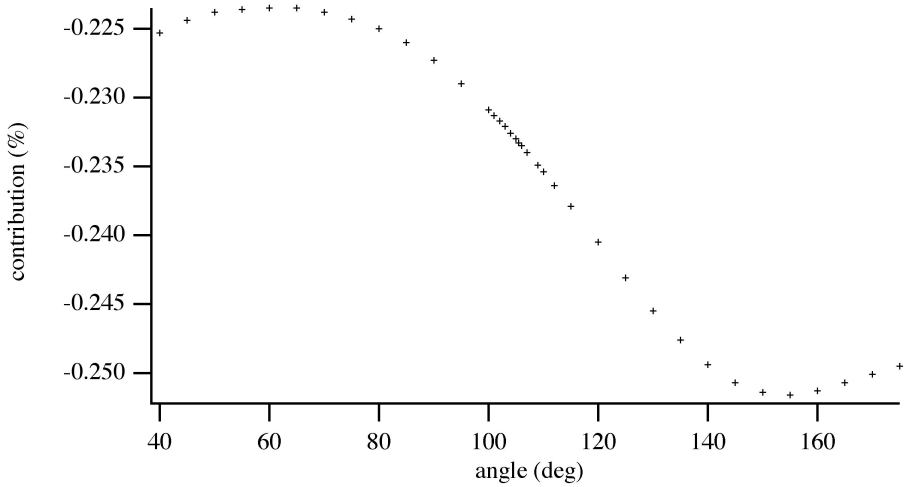

Figure 6.2: Relativistic contribution to the dipole moment, in %, for varying angle (in degrees) using a fixed r_{OH} distance of 0.95 Å

relativistic contribution to the dipole moment, in %, is shown for this bond distance with varying angle. It is apparent that there is, at least for this r_{OH}, a smooth angle dependence.

In Fig. 6.3 the relativistic effect, again in %, is shown as a function of r_{OH}, where the angle is constant at 100° (and $r_1 = r_2$). The increase of the relativistic effect seems to be quite linear with increasing r_{OH} for this angle.

6.4 Conclusions

We have computed the relativistic effect on the dipole moment surface (DMS) of water at the DC-HF level of theory with neglect of (SS|SS) integrals and using the uncontracted aug-cc-pCVQZ basis set. These HF values were supplemented by a correlation contribution calculated using the spin-free CCSD(T) method, also neglecting the (SS|SS) type integrals. The CCSD(T) calculations were performed using the uncontracted aug-cc-pCVTZ basis.

A more detailed discussion of the effect of relativity on the DMS will be given in a coming paper, where the DMS is used to calculate intensities of the rotation-vibration spectrum of water. A general observation is that relativity makes the dipole moment smaller for all calculated points and that the effect is quite constant, on the order of 0.20% - 0.30%. This means that the inclusion of relativistic effects will reduce the intensities of the lines of a

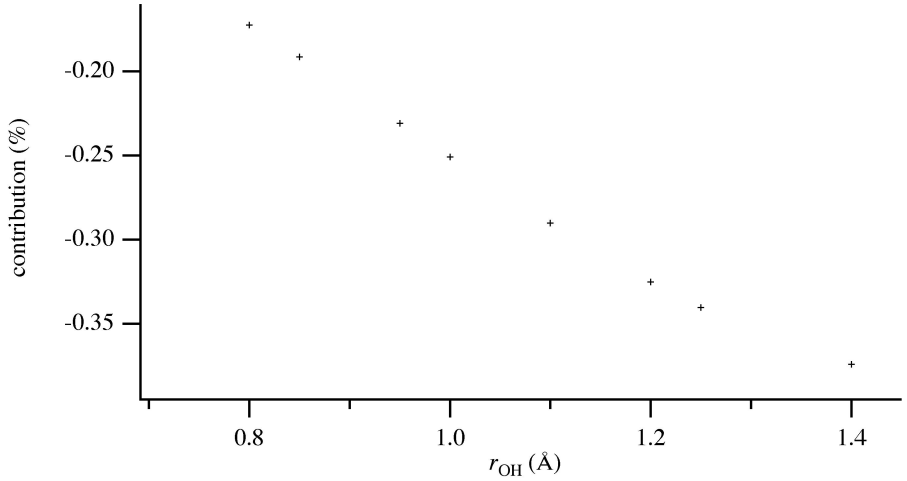

Figure 6.3: Relativistic contribution to the dipole moment, in %, for varying r_{OH} distance using a fixed angle of 100°

calculated rotation-vibration spectrum of water.

6.5 Acknowledgements

The authors gratefully thank the Netherlands Organization for Scientific Research (NWO) for financial support through the 'Jonge Chemici' program. Computer time provided by the National Computing Facilities (NCF) is gratefully acknowledged.

Chapter 7

MP2 calculations on parity-violation interactions in hydrogen peroxyde analogs

The effect of electron correlation on parity-violation energies has been calculated using an implementation of analytical first-order MP2 molecular properties. The calculations have been performed on H_2X_2 (X = O, S, Se, and Te). Electron correlation does not play an essential role for this property in this kind of systems, but the correlation effect is shown to be very geometry dependent.

7.1 Introduction

Parity-violation is a well known phenomenon in nuclear physics[19, 20] and is described in the standard model for electroweak interactions by Glashow, Weinberg and Salam[21–23]. It can also be observed in electronic transitions of atoms[251, 252]. For molecules, the electroweak interactions introduce an energy difference, ΔE_{PV}, between the enatiomers of chiral molecules[253–255]. This energy difference has not yet been detected due to the extremely high precision that needs to be achieved in the experiments. The effect should, however, be observable in molecules which contain heavy atoms[26] and have a rather rigid structure so that ΔE_{PV} is larger than the tunneling splitting[256]. Theoretical calculations serve to propose promising candidates for experimental observation of the PV splittings. Recently Schwerdtfeger and Bast[30] predicted large parity-violation effects in the vibrational spectrum of a number of stable organometallic compounds, that become close to what is detectable in current state of the art experiments[257]. To make

sure that predictions are reliable one needs to consider the size of the errors made in state-of-the-art computational approaches. One source of errors is the normal mode approximation made by Schwerdtfeger and Bast. Recent calculations by Quack and Stohner[258] indicate that results can sometimes be significantly influenced if the effect of anharmonic couplings is taken into account. Another possible source of errors is the (partial) neglect of electron correlation in the calculation of the parity-violation energy hypersurface. Not much is known about the effect of electron correlation on parity-violation energies in molecules. In the non-relativistic regime correlated calculations were performed at the CASSCF and RASCI level by Quack and coworkers[258–260] and at the DFT level by Hennum *et al.*[261]. In such calculations it is not clear how much of the correlation effect is accounted for since a CASSCF calculation will only describe valence correlation and the functionals used in DFT are also optimized for valence correlation. The MP2 approach makes possible to systematically include core electron correlation effects that may be of importance as well. We chose to compute such effects with the new analytical DC-MP2 implementation in some of the simplest stable chiral molecules, the hydrogenperoxide analogs H_2X_2 (X = O, S, Se, Te). Correlated calculations at the four-component level were so far restricted to the lightest members of this series systems due to the use of the finite-field method. We can now extend the work done by Thyssen *et al.* on the H_2O_2 and H_2S_2 molecules by computing the heavier analogues of this series H_2Se_2 and H_2Te_2 as well. These small benchmark molecules are not of direct interest for observation of E_{PV} splittings since the barrier for conversion between the two enantiomers is too low, but serve as a standard test to compare the different theoretical methods. In forthcoming work we will also look at the performance of DC-MP2 and DC-DFT for the calculation of parity-violation effects for the C-F stretching mode of the more interesting class of chiral methyl fluorides.

Because in the DC formalism spin-orbit coupling (SOC) is included in a variational manner we can calculate parity-violation energies simply as a first-order property[26]. In a non-relavistic framework one needs to add SOC explicitly as an extra perturbation so that the parity-violation energies are calculated as a second order property. This more complicated method is followed by most of the other groups[27, 261–263] active in the field.

The operator for the calculation of parity-violation energies, E_{PV}, is the nuclear spin-independent P-odd operator,

$$\hat{H}_p = \frac{G_F}{2\sqrt{2}} \sum_{i,n} Q_{W,n} \gamma_i^5 \varrho_n \left(\mathbf{r}_i\right), \tag{7.1}$$

where the summations run over the electrons i and the nuclei n. G_F =

$1.166\,37 \times 10^{-11}$ MeV^{-2} $= 2.222\,55^{-14}$ a.u. is the Fermi coupling constant, the pseudo-scalar γ^5 chirality operator is given by

$$\gamma^5 = \begin{pmatrix} \mathbf{0} & \mathbf{I} \\ \mathbf{I} & \mathbf{0} \end{pmatrix}, \tag{7.2}$$

where $\mathbf{I}$ and $\mathbf{0}$ are the 2×2 unit and zero matrix respectively. The normalized nucleon density is ϱ_n and $Q_{W,n} = -N_n + Z_n\left(1 - 4\sin^2\theta_W\right)$ is the weak charge of nucleus n with N_n neutrons and Z_n protons. For the terms depending on the Weinberg mixing angle θ_W we used the value $\sin^2\theta_W = 0.2319$.

7.2 Computational details

For completeness we also performed, besides H_2Se_2 and H_2Te_2, calculations on H_2O_2 and H_2S_2. The basis sets for H, O, and S used by Thyssen *et al.*[128] have been used in our study as well. For Se and Te we used similar basis sets. For H this is an uncontracted cc-pVDZ set, for O, S, Se and Te an uncontracted cc-pVDZ + *np* set, where $n = 3$ for O and $n = 2$ for S, Se and Te. The cc-pVDZ sets are the correlation consistent double zeta basis sets developed by Dunning[101] for light elements. For the heavier elements, Se and Te in this case, these basis sets have been developed, following the same recipe, by Dyall[156]. The *np* indicates additional high exponent *p*-functions. These additional exponents were generated as an even-tempered series with ratio = 8.0 to give a better description of the $p_{1/2}$-type spinors.

Calculations have been performed for dihedral angles in the range 0° to 180° using the same bond angles, bond distances and definition of the dihedral angle as used by Laerdahl and Schwerdtfeger[26]. All calculations have been performed in C_2 symmetry. Isotropic Gaussian nuclear charge distributions[165] have been used in all our calculations. To reduce computational cost, we neglected the (SS|SS) type of two-electron integrals in our calculations, as was done also in previous four-component parity-violation calculations[26, 128] on the hydrogen peroxyde analogs.

Besides performing calculations in which all electrons are correlated, Thyssen *et al.*[128] also performed calculations applying a frozen (inactive) core approximation. They found that freezing a $1s$ core hardly changes the results in case of H_2S_2 whereas freezing a $1s2s2p$ core did alter the sign of the correlation contribution. We investigated the effect of frozen cores further, to determine the influence of core correlation, and because we want to apply our method to larger systems, where freezing of the core may be necessary to make the calculations feasible.

Table 7.1: Parity-violation energies for H_2S_2, in a.u., using different active spaces. Results are shown for dihedral angles 15°, 90° and 120°.

Method	15°	90°	120°
Hartree-Fock	-1.083×10^{-17}	-0.580×10^{-17}	0.811×10^{-17}
MP2 (full)	-1.118×10^{-17}	-0.511×10^{-17}	0.939×10^{-17}
correlation contr.	-0.035×10^{-17}	0.069×10^{-17}	0.128×10^{-17}
MP2 (..,1000 a.u.)	-1.118×10^{-17}	-0.511×10^{-17}	0.939×10^{-17}
correlation contr.	-0.035×10^{-17}	0.069×10^{-17}	0.128×10^{-17}
MP2 (..,100 a.u.)	-1.117×10^{-17}	-0.510×10^{-17}	0.937×10^{-17}
correlation contr.	-0.034×10^{-17}	0.069×10^{-17}	0.127×10^{-17}
MP2 (..,50 a.u.)	-1.115×10^{-17}	-0.509×10^{-17}	0.935×10^{-17}
correlation contr.	-0.032×10^{-17}	0.070×10^{-17}	0.125×10^{-17}

7.3 Results and discussion

In Table 7.1 and 7.2 parity-violation energies of H_2S_2 and H_2Se_2 for dihedral angles 15°, 90° and 120° using different active spaces are shown. The active space used in a particular calculation is indicated between brackets, (full) means taking all spinors into account, (..,100 a.u.) means taking into account all occupied spinors and taking virtuals into account with an energy up to 100 a.u., (-63,..,100 a.u.) means the same virtual space but indicates that spinors with an energy lower than -63 a.u. are kept frozen, as well.

The results for H_2S_2 in Table 7.1 indicate that deleting virtuals above 1000 a.u. (taking 73% of the virtuals into account) does not change the results at all. Deleting virtuals above 100 a.u. (52% of the virtuals taken into account) changes the results slightly and deleting virtuals above 50 a.u. (taking 41% of the virtuals into account) changes the correlation contribution by only a few percent, which is still acceptable.

In the case of the H_2Se_2 molecule, Table 7.2, deleting virtuals above 10 000 a.u. (taking 83% of the virtuals into account) does not change the results at all. Removal of virtuals above 1000 a.u. (78% of the virtuals correlated) changes the correlation contribution insignificantly ($< 1\%$). Deleting virtuals in the range 100 - 1000 a.u. (taking 52% of the virtuals into account) has more effect on H_2Se_2 than on H_2S_2. For the angles 90° and 120° the correlation contribution changes by several percent, for $\phi = 15°$ the relative change

Table 7.2: Parity-violation energies for H_2Se_2, in a.u., using different active spaces. Results are shown for dihedral angles 15°, 90° and 120°.

Method	15°	90°	120°
Hartree-Fock	-1.181×10^{-15}	-0.368×10^{-15}	1.336×10^{-15}
MP2 (full)	-1.208×10^{-15}	-0.277×10^{-15}	1.474×10^{-15}
correlation contr.	-0.026×10^{-15}	0.091×10^{-15}	0.138×10^{-15}
MP2 (..,10 000 a.u.)	-1.208×10^{-15}	-0.277×10^{-15}	1.474×10^{-15}
correlation contr.	-0.026×10^{-15}	0.091×10^{-15}	0.138×10^{-15}
MP2 (..,1000 a.u.)	-1.207×10^{-15}	-0.277×10^{-15}	1.473×10^{-15}
correlation contr.	-0.026×10^{-15}	0.091×10^{-15}	0.137×10^{-15}
MP2 (..,100 a.u.)	-1.219×10^{-15}	-0.280×10^{-15}	1.487×10^{-15}
correlation contr.	-0.038×10^{-15}	0.088×10^{-15}	0.151×10^{-15}
MP2 (-63,..,100 a.u.)[a]	-1.219×10^{-15}	-0.280×10^{-15}	1.487×10^{-15}
correlation contr.	-0.038×10^{-15}	0.088×10^{-15}	0.151×10^{-15}
MP2 (-56,..,100 a.u.)[b]	-1.222×10^{-15}	-0.280×10^{-15}	1.490×10^{-15}
correlation contr.	-0.040×10^{-15}	0.087×10^{-15}	0.154×10^{-15}
MP2 (-10,..,100 a.u.)[c]	-1.205×10^{-15}	-0.276×10^{-15}	1.470×10^{-15}
correlation contr.	-0.023×10^{-15}	0.092×10^{-15}	0.134×10^{-15}
MP2 (-7,..,100 a.u.)[d]	-1.228×10^{-15}	-0.277×10^{-15}	1.504×10^{-15}
correlation contr.	-0.047×10^{-15}	0.091×10^{-15}	0.168×10^{-15}
MP2 (-6,..,100 a.u.)[e]	-1.185×10^{-15}	-0.271×10^{-15}	1.445×10^{-15}
correlation contr.	-0.003×10^{-15}	0.097×10^{-15}	0.112×10^{-15}

[a] $1s$ frozen

[b] $1s2s$ frozen

[c] $1s2s2p$ frozen

[d] $1s2s2p3s$ frozen

[e] $1s2s2p3s3p$ frozen

in the correlation contribution is percentually large, but the total effect of electron correlation on E_{PV} is small for this angle. Subsequently freezing the $1s$ spinors of Se does not change the results. Freezing also the $2s$ spinors gives a minor change and subsequently freezing the $2p$ spinors gives again results which are close to the full calculation. This is apparently due to a cancellation of errors as there is no *a priori* reason why these contributions should cancel each other. There is a large difference in the correlation contributions for an $1s2s2p3s$ frozen core and an $1s2s2p3s3p$ frozen core, and we conclude that both frozen cores can not be recommended for Se as the correlation contributions deviates tens of percents from the full result for this property.

The efficiency of the calculations can thus be improved by deleting high lying virtuals but not as much as we observed previously for other properties, see references [127] and [264]. Deleting 30 to 50% of the virtuals gives results which are acceptable. Freezing occupied spinors is also more difficult. In contrast to most other molecular properties almost all electrons have to be taken into account in correlated calculations. From these two conditions we may conclude that correlated parity-violation calculations are very demanding, since much larger active spaces than for the calculation of other first order 1-electron properties is required.

Since our algorithm is not yet fully parallellized, the full reference calculation on H_2Te_2, with 294 large and 692 small component basis functions respectively and 215 virtual Kramers' pairs, is currently not feasible. For the calculations at the different dihedral angles we chose an $1s2s2p$ frozen core and put the threshold for the virtual spinors at 100 a.u. Extrapolation of the results for S and Se indicates that these limits may not be sufficient to obtain a fully converged result, but that the residual error should be small. The threshold for the virtual space at 100 a.u. is furthermore justified by one calculation at $\phi = 120°$ with a virtual space up to 1000 a.u., in which the effect on the correlation contribution of the extended virtual space was found to be only 0.51%.

The results of the full H_2O_2 and H_2S_2 calculations are shown in Table 7.3. For H_2O_2 correlation effects are positive for all angles. The correlation contribution is about 15 to 20% for angles up to approximately 60°, a relative maximum of the correlation contribution occurs in the region where E_{PV} goes through zero, around 100°. For the larger dihedral angles the correlation contribution is smaller, less then 5%. For H_2S_2 the geometric dependence of electron correlation is different from H_2O_2. Correlation effects are negative for dihedral angles up to 60° and positive for larger angles. For the angles up to 60° correlation is not important, it only contributes a few percent. For larger angles electron correlation is, in contrast to H_2O_2, more important, about 10%. Thyssen *et al.*[128] give a graphical representation of their

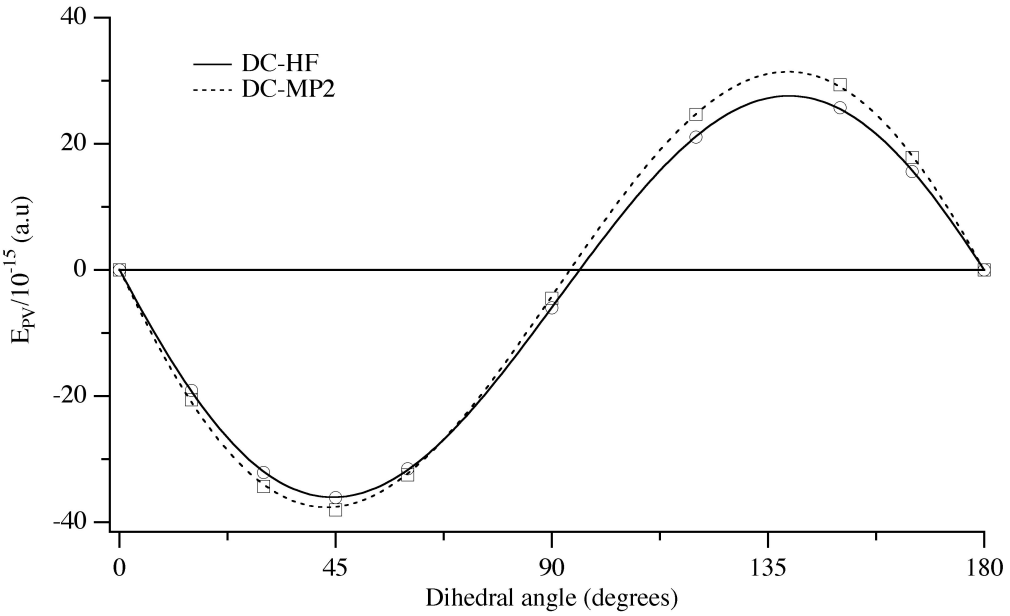

Figure 7.1: Variation of E_{PV} with the dihedral angle in H_2Te_2. The solid and dashed curves are the DC-HF and DC-MP2 values respectively.

results, while explicit values are only given for $\phi = 45°$, for that reason we repeated the finite-field calculations, the results are given in Table 7.3 as well, in parenthesis. Comparing the finite-field values with the analytical values we see that for H_2O_2 the difference between the finite-field method and the analytical method is about 0.01% and 0.05% for HF and MP2 respectively. For H_2S_2 the difference is somewhat larger, for both HF and MP2 about 0.2%. However, overall it can be concluded that for these molecules the overall agreement between the analytical and finite-field methods is satisfactory and that criticism about the applicability of the finite-field method[25] even for molecules containing only light elements is definitely not supported by our results.

For H_2Se_2 and H_2Te_2 the results are shown in Table 7.4. The results for H_2Se_2 are quite similar to the results of H_2S_2. Correlation effects are negative for small angles, although this contribution becomes positive earlier than for H_2S_2. In the region where E_{PV} goes through zero electron correlation seems to be more important than for H_2S_2, but for larger angles the relative contribution is similar as for H_2S_2, about 10%.

The calculated E_{PV} for H_2Te_2, as a function of the dihedral angle, is

Table 7.3: Parity-violation energies for H_2O_2 and H_2S_2, in a.u., as a function of dihedral angle, ϕ. Finite-field values are given in parenthesis.

	ϕ	Hartree-Fock	MP2	corr. contribution
H_2O_2	15°	-3.630×10^{-19}	-3.185×10^{-19}	0.444×10^{-19}
		(-3.630×10^{-19})	(-3.174×10^{-19})	(0.456×10^{-19})
	30°	-6.127×10^{-19}	-5.329×10^{-19}	0.798×10^{-19}
		(-6.127×10^{-19})	(-5.330×10^{-19})	(0.797×10^{-19})
	45°	-6.784×10^{-19}	-5.788×10^{-19}	0.996×10^{-19}
		(-6.783×10^{-19})	(-5.787×10^{-19})	(0.997×10^{-19})
	60°	-5.492×10^{-19}	-4.467×10^{-19}	1.025×10^{-19}
		(-5.492×10^{-19})	(-4.468×10^{-19})	(1.025×10^{-19})
	90°	0.939×10^{-19}	1.666×10^{-19}	0.728×10^{-19}
		(0.939×10^{-19})	(1.664×10^{-19})	(0.725×10^{-19})
	120°	6.942×10^{-19}	7.270×10^{-19}	0.328×10^{-19}
		(6.943×10^{-19})	(7.273×10^{-19})	(0.330×10^{-19})
	150°	6.712×10^{-19}	6.815×10^{-19}	0.103×10^{-19}
		(6.713×10^{-19})	(6.813×10^{-19})	(0.100×10^{-19})
	165°	3.874×10^{-19}	3.920×10^{-19}	0.046×10^{-19}
		(3.875×10^{-19})	(3.925×10^{-19})	(0.051×10^{-19})
H_2S_2	15°	-1.083×10^{-17}	-1.118×10^{-17}	-0.035×10^{-17}
		(-1.085×10^{-17})	(-1.120×10^{-17})	(-0.035×10^{-17})
	30°	-1.826×10^{-17}	-1.874×10^{-17}	-0.048×10^{-17}
		(-1.830×10^{-17})	(-1.878×10^{-17})	(-0.048×10^{-17})
	45°	-2.077×10^{-17}	-2.112×10^{-17}	-0.036×10^{-17}
		(-2.081×10^{-17})	(-2.116×10^{-17})	(-0.036×10^{-17})
	60°	-1.866×10^{-17}	-1.873×10^{-17}	-0.007×10^{-17}
		(-1.870×10^{-17})	(-1.876×10^{-17})	(-0.007×10^{-17})
	90°	-0.580×10^{-17}	-0.511×10^{-17}	0.069×10^{-17}
		(-0.581×10^{-17})	(-0.512×10^{-17})	(0.070×10^{-17})
	120°	0.811×10^{-17}	0.939×10^{-17}	0.128×10^{-17}
		(0.812×10^{-17})	(0.940×10^{-17})	(0.128×10^{-17})
	150°	1.096×10^{-17}	1.216×10^{-17}	0.120×10^{-17}
		(1.098×10^{-17})	(1.218×10^{-17})	(0.120×10^{-17})
	165°	0.667×10^{-17}	0.738×10^{-17}	0.071×10^{-17}
		(0.667×10^{-17})	(0.739×10^{-17})	(0.071×10^{-17})

Table 7.4: Parity-violation energies for H_2Se_2 and H_2Te_2, in a.u., as a function of dihedral angle, ϕ. For H_2Te_2 an $1s2s2p$ frozen core is used, virtuals up to 100 a.u. are taken into account.

	ϕ	Hartree-Fock	MP2	corr. contribution
H_2Se_2	15°	-1.181×10^{-15}	-1.208×10^{-15}	-0.026×10^{-15}
	30°	-1.999×10^{-15}	-2.031×10^{-15}	-0.031×10^{-15}
	45°	-2.263×10^{-15}	-2.275×10^{-15}	-0.012×10^{-15}
	60°	-1.982×10^{-15}	-1.960×10^{-15}	0.022×10^{-15}
	90°	-0.368×10^{-15}	-0.277×10^{-15}	0.091×10^{-15}
	120°	1.336×10^{-15}	1.474×10^{-15}	0.138×10^{-15}
	150°	1.591×10^{-15}	1.718×10^{-15}	0.128×10^{-15}
	165°	0.957×10^{-15}	1.034×10^{-15}	0.077×10^{-15}
H_2Te_2	15°	-1.910×10^{-14}	-2.059×10^{-14}	-0.149×10^{-14}
	30°	-3.212×10^{-14}	-3.432×10^{-14}	-0.220×10^{-14}
	45°	-3.612×10^{-14}	-3.806×10^{-14}	-0.193×10^{-14}
	60°	-3.151×10^{-14}	-3.249×10^{-14}	-0.098×10^{-14}
	90°	-0.603×10^{-14}	-0.447×10^{-14}	0.156×10^{-14}
	120°	2.108×10^{-14}	2.467×10^{-14}	0.359×10^{-14}
	150°	2.571×10^{-14}	2.936×10^{-14}	0.365×10^{-14}
	165°	1.559×10^{-14}	1.782×10^{-14}	0.223×10^{-14}

shown in Fig. 7.1. We see a similar geometry dependence of electron correlation as for H_2S_2 and H_2Se_2, although electron correlation is more important for H_2Te_2 than for the other two molecules. For angles up to 60° electron correlation contributes about 5%, for angles of 120° and larger electron correlation contributes about 10 to 15%. For a dihedral angle of 60° electron correlation has a negative contribution to E_{PV}, just like observed in H_2S_2.

7.4 Conclusions

Our implementation of first-order analytical MP2 properties has been applied to the calculation of parity-violation energies in H_2O_2, H_2S_2, H_2Se_2 and H_2Te_2. The calculations on H_2Se_2 and H_2Te_2 are the first correlated relativistic calculations on parity-violation effects in molecules containing elements from period 4 or 5 of the periodic table. Previous correlated relativistic calculations, using the finite-field method, were, due to numerical instability, restricted to molecules containing lighter elements. Electron correlation does not play a very important role on parity-violation energies for this type of

molecules, roughly ranging from a few percent to about 15%, with a strong geometry-dependence. The calculations indicate that parity-violation energies are quite sensitive to the active space used. Only a few occupied spinors can be kept inactive and this makes correlated parity-violation *ab initio* calculations computationally very intensive. It is therefore interesting to compare the results of four component MP2 to the more economical four component DFT method. Such a comparison between HF, DFT and MP2 for methane analogs is currently undertaken.

7.5 Acknowledgements

JNPvS and LV thank the Netherlands Organization for Scientific Research (NWO) for financial support through the 'Jonge Chemici' program. Computer time provided by the Dutch National Computing Facilities (NCF) and travel support from the EU COST action D23, WG DIRAC and the Danish Natural Science Research Council grant no. 21-02-0467 are also gratefully acknowledged.

Chapter 8

Relativistic second-order many-body and density functional theory for the parity-violation contribution to the C-F stretching mode in CHFClBr

A comparison between four-component Hartree-Fock, second-order Møller-Plesset (many-body) perturbation theory and density functional theory for the calculation of parity-violation effects in the C-F stretching mode of CHFClBr is made. The difference between the methods is large for the total parity-violation energies but modest for vibrational transitions.

8.1 Introduction

The tiny difference in properties between the two enantiomers of a chiral molecule, caused by the electroweak current between electrons and nucleons[254, 255], has not been detected in experiments so far[256]. Perhaps the best strategy to measure these parity-violation (PV) effects in molecules is via vibrational spectroscopy. CO_2 lasers are highly stable, have a high spectral purity and are tunable. A vibrational mode that lies within the tunable range of the CO_2 laser and that shows a high intensity is the C-F stretching mode. CHFClBr has been used in recent years in the experimental search for the manifestation of parity-violation in molecules[257, 265].

Several molecules have been used in theoretical calculations on parity-violation effects[24, 28, 29] of the C-F stretching mode. However, these calculations have been based on four-component Hartree-Fock. The effect of electron correlation has been completely neglected. Not much is known about the effect of electron correlation on parity-violation in molecules yet. Test calculations on H_2X_2 (X = O, S, Se and Te) indicate that the differences between Hartree-Fock (HF), DFT and correlated *ab initio* methods are not so large[128, 261, 266]. The aim of the current research is to compare HF, MP2 and DFT for the calculation of the effect of PV on the vibrational frequencies of the C-F stretching mode of CHFClBr.

8.2 Methods and computational details

All calculations employed the four-component Dirac-Coulomb (DC) Hamiltonian and have been performed using the DIRAC[41] program. As in the previous Dirac-Coulomb Hartree-Fock (DC-HF) calculations on CHFClBr[24] the (SS|SS) type of two-electron integrals were neglected. For all the elements an isotropic nuclear charge distribution was used[165]. The basis sets are also the same as in the previous HF calculations, uncontracted cc-pVDZ + *np* sets[102, 248] augmented by diffuse functions. Calculations have been performed at seven different points along the C-F normal mode, at the equilibrium geometry and at ±0.188 97 a.u., ±0.377 94 a.u. and ±0.944 86 a.u. away from equilibrium. All these geometries correspond to CHFClBr in the *R*-configuration.

The operator for the calculation of parity-violation energies, E_{PV}, is the nuclear spin-independent *P*-odd operator,

$$\hat{H}_p = \frac{G_F}{2\sqrt{2}} \sum_{i,n} Q_{W,n} \gamma_i^5 \varrho_n \left(\mathbf{r}_i\right), \tag{8.1}$$

where the summations run over the electrons i and the nuclei n. $G_F = 1.166\,37 \times 10^{-11}$ MeV^{-2} $= 2.222\,55^{-14}$ a.u. is the Fermi coupling constant, the pseudo-scalar γ^5 chirality operator is given by

$$\gamma^5 = \begin{pmatrix} \mathbf{0} & \mathbf{I} \\ \mathbf{I} & \mathbf{0} \end{pmatrix}, \tag{8.2}$$

where $\mathbf{I}$ and $\mathbf{0}$ are the 2×2 unit and zero matrix respectively. The normalized nucleon density is ϱ_n and $Q_{W,n} = -N_n + Z_n\left(1 - 4\sin^2\theta_W\right)$ is the weak charge of nucleus n with N_n neutrons and Z_n protons. For the Weinberg mixing angle θ_W we used the value $\sin^2\theta_W = 0.2319$.

The MP2 calculations have been performed using our recent analytical first-order property implementation[266]. Due to computational limitations not all spinors have been taken into the active space. The bromine $1s$, $2s$ and $2p$ and the chlorine $1s$ spinors have been left inactive, which means that in total 56 electrons are correlated. The energy threshold for inclusion of virtual spinors has been kept at 100 a.u. The thresholds in both the occupied and virtual space are consistent with those chosen in earlier work on H_2Se_2 and H_2Te_2[266].

The four-component implementation of DFT in DIRAC has been described in references [267] and [211]. The functionals used were LDA[94], the generalized gradient approximations BLYP[95, 96] and PW86[97] and the hybrid functional B3LYP[98]. Standard non-relativistic functionals have been used since relativistic corrections do not lead to large changes in properties[78].

The effect of parity-violation on the C-F stretching mode has been calculated as follows, see also reference [24]. First a normal mode analysis has been applied at the CCSD(T) level using ECPs, obtaining displacement coordinates for the C-F stretching mode. Along this C-F normal coordinate, q, the CCSD(T) potential energy curve V(q) was calculated stepwise. A polynomial fit of V(q) has been used as input for a numerical Numerov-Cooley integration procedure to obtain vibrational wavefunctions $|n\rangle$ (in the rotational groundstate, $J = 0$). Since the parity-violation contribution is so small the natural choice to calculate the effect of parity-violation on the vibrational levels is to use first-order perturbation theory. This means that the following expectation value has to be calculated:

$$E^n_{\mathrm{PV}} = \langle n|E_{\mathrm{PV}}(q)|n\rangle, \tag{8.3}$$

for the vibrational level with quantum number n. For this purpose the parity-violation contributions to the total electronic energy, $E_{\mathrm{PV}}(q)$, are fitted to a polynomial.

8.3 Results

Fig. 8.1 shows the parity-violation energies as a function of the C-F stretching mode, q. It is clear that the different electronic structure methods give quite different results. In Table 8.1 the results at the equilibrium C-F bond distance, $q = 0$, are shown, here the contribution has also been divided in contributions per atom. Apparently electron correlation is important for the absolute parity-violation energies, at $q = 0$ it more than halves the HF E_{PV}.

The large difference in absolute E_{PV}s in CHFClBr is in contrast to the results of the hydrogen peroxyde analogs[128, 261, 266], where HF, DFT and

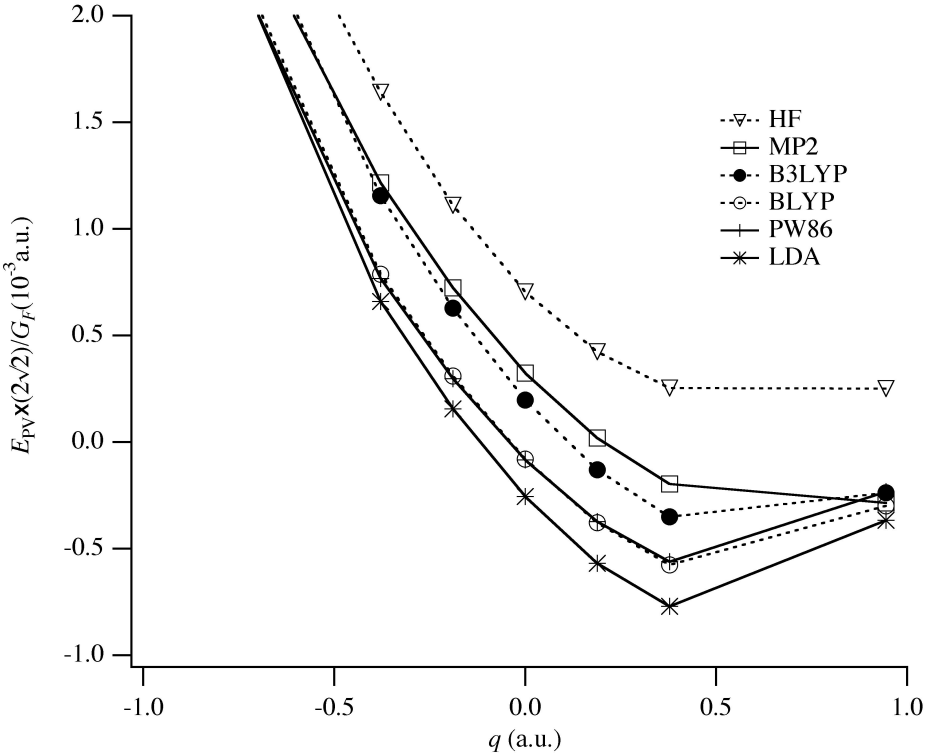

Figure 8.1: Electroweak contribution to the total electronic energy (scaled by $2\sqrt{2}/G_F$) as a function of the C-F stretching normal mode (in a.u.). $q = 0$ defines the equilibrium C-F bond distance.

correlated *ab initio* methods are shown to give quite similar results. It is apparent that the most important contribution to the E_{PV}s come from the heaviest elements, Cl and Br. Also the most important correlation contributions come from these atoms, as shown in Fig. 8.2. The contributions from Cl and Br cancel each other out to some extent.

The question is now how much parity-violation contributes to experimental observables, the vibrational transitions. Table 8.2 shows parity-violation contribution to the first four C-F vibrational modes, these contributions are as expected quite large, as for the absolute E_{PV}s. The E_{PV} differences between different modes, which determine the effect of parity-violation on vibrational transition frequencies, are much smaller, see the last two columns of table 8.2. That the effect of parity-violation on the vibrational transitions of CHFClBr doesn't show a large dependency on the method can easily be

Table 8.1: Parity-violation contribution to the total electronic energy at the equilibrium geometry of CHFClBr ($q = 0$). The contribution per atom is given as well as the total contribution. All values are in a.u.

Atom	HF	MP2	B3LYP	BLYP	PW86	LDA
H	2.811×10^{-24}	6.272×10^{-24}	1.167×10^{-23}	1.433×10^{-23}	1.467×10^{-23}	1.614×10^{-23}
C	5.752×10^{-20}	7.104×10^{-20}	6.890×10^{-20}	6.837×10^{-20}	7.131×10^{-20}	7.736×10^{-20}
F	8.798×10^{-19}	9.158×10^{-19}	1.030×10^{-18}	1.023×10^{-18}	1.002×10^{-18}	1.048×10^{-18}
Cl	-3.598×10^{-18}	-2.895×10^{-18}	-2.835×10^{-18}	-2.170×10^{-18}	-2.009×10^{-18}	-1.702×10^{-18}
Br	8.192×10^{-18}	4.444×10^{-18}	3.280×10^{-18}	4.506×10^{-19}	2.792×10^{-18}	-1.433×10^{-18}
TOTAL	5.530×10^{-18}	2.536×10^{-18}	1.544×10^{-18}	-6.279×10^{-19}	-6.569×10^{-19}	-2.009×10^{-18}

Table 8.2: Parity-violation contribution ($\times 10^{-19}$ a.u.) to the C-F vibrational mode from a normal mode analysis of CHFClBr.

Method	$n=0$	$n=1$	$n=2$	$n=3$	$n=4$	$n=0\rightarrow 1$	$n=1\rightarrow 2$
HF	54.58	53.19	51.90	50.69	49.57	−1.385	−1.295
MP2	24.41	22.55	20.77	19.06	17.41	−1.855	−1.781
B3LYP	14.42	12.44	10.57	8.81	7.17	−1.979	−1.870
BLYP	−7.24	−9.08	−10.81	−12.41	−13.88	−1.843	−1.727
PW86	−7.48	−9.25	−10.89	−12.40	−13.77	−1.760	−1.640
LDA	−21.09	−23.01	−24.79	−26.42	−27.89	−1.915	−1.777

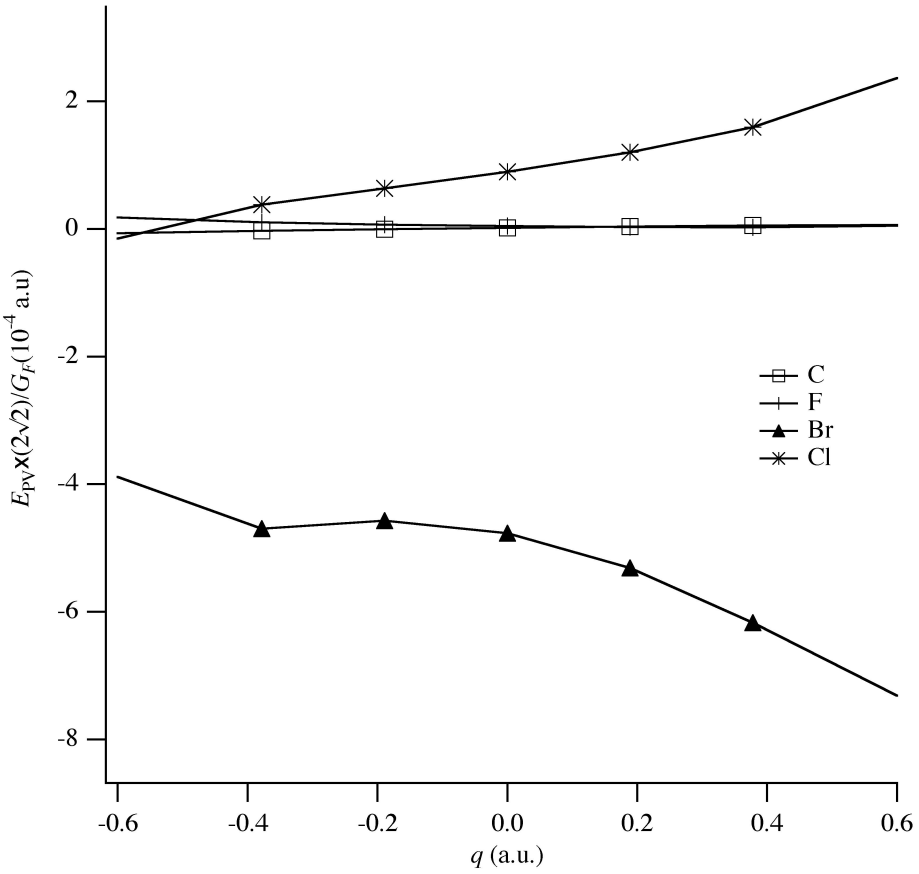

Figure 8.2: Electroweak contribution per atom (scaled by $2\sqrt{2}/G_F$) due to electron correlation as a function of the C-F stretching normal mode. $q = 0$ defines the equilibrium C-F bond distance.

understood from Fig. 8.1. Although the absolute positions of the curves differ, they are all quite parallel around equilibrium. It is not the absolute value of E_{PV} at $q = 0$ that matters, but the relative variation of E_{PV} with distance. If the value of E_{PV} at $q = 0$, for a particular method, is subtracted form the E_{PV}s for the other distances it is clear that the different methods give similar results, this is illustrated for HF, MP2 and LDA in Fig. 8.3.

For the fundamental transition the parity-violation effect varies from -1.39×10^{-19} a.u. for HF to -1.98×10^{-19} a.u. for B3LYP. For MP2 the effect is -1.86×10^{-19} a.u., which is equal to -1.2 mHz. For the frequency difference between the R and S enantiomers we obtain thus $\Delta\nu_{RS} =$

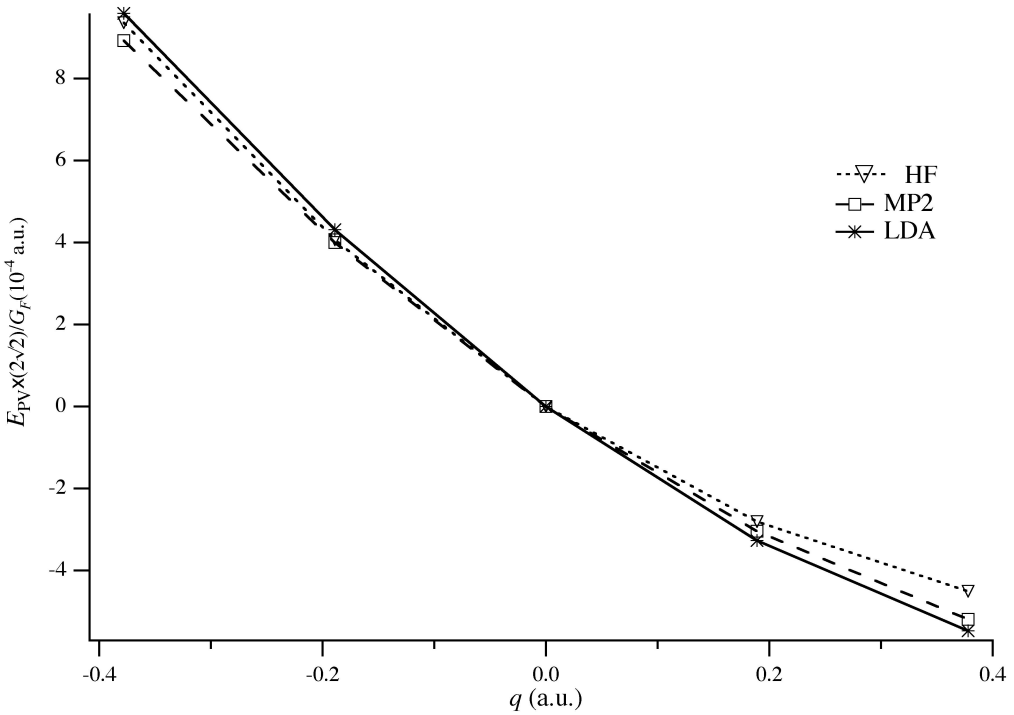

Figure 8.3: Parity-violation energy (scaled by $2\sqrt{2}/G_F$) with respect to the value at equilibrium, $q = 0$, as a function of the C-F stretching normal mode.

$\upsilon_R - \nu_S = -2.4$ mHz. Using $\nu_{\mathrm{C-F}} = 32.29$ THz[268], we obtain the ratio $\Delta\nu_{RS}/\nu_{\mathrm{C-F}} = -7.56 \times 10^{-17}$. This has to be compared with the recent experimental frequency difference sensitivity of 5×10^{-14} obtained by Chardonnet and co-workers[257] for the C-F stretching mode of CHFClBr. This illustrates that the detection of parity-violation effects in molecular spectroscopy presents a great challenge and the resolution of experimental setup has to be improved by several orders of magnitude.

It is difficult to judge which method gives most reliable results. CHFClBr is a molecule for which both DFT and MP2 should perform quite well for standard properties, but since not much is known about the relative performance of these methods for the calculation of parity-violation effects it is difficult to give a ranking here. A test using more molecules seems necessary. Also a comparison with high level coupled-cluster methods is very desirable. However, at the four-component level this requires first the formulation and implementation of formulas for the analytical evaluation of

first-order coupled-cluster properties.

8.4 Conclusions

Relativistic four-component electronic structure methods have been applied to the calculation of parity-violation effects on the C-F stretching mode of CHFClBr. A large absolute difference is seen between Hartree-Fock, MP2 and DFT methods. However, the relative difference between the applied methods is quite small. This results in contributions of parity-violation to vibrational frequencies that are not so method dependent. Tests on a larger number of molecules seems desirable as well as comparison with coupled-cluster methods.

8.5 Acknowledgements

This work was supported by the Marsden Fund managed by the Royal Society of New Zealand. JNPvS and LV thank the Netherlands Organisation for Scientific Research (NWO) for financial support through the 'Jonge Chemici' program and the Dutch National Computing Facilities (NCF) for computer time.

Summary

The availability of computer programs that allow the calculation of properties of molecules is very valuable in chemistry and physics. For example, calculated NMR spectra might be very useful in the elucidation of molecular structures if the experimental spectra are complicated, or if there are uncertainties about the molecules present. Also, theoretical calculations often allow a more detailed understanding of what is really happening in dynamical processes. Many examples can be given where theoretical calculations are worthwhile. For some applications it is sufficient if the model used gives results of reasonable accuracy, while for others theoretical computations are only useful if they are of very high quality. Most of the applications presented in this thesis are of the second type. In general, the aim is to obtain an accuracy as high as possible.

For molecules containing only light elements, to achieve high accuracy in electronic structure calculations, the main 'parameters' of concern are the electronic structure method and the quality of the basis set. When heavy elements are present, or when the electron density in the vicinity of the nuclei is important for the property of interest, the effects of special relativity on the physics have to be taken into account as well.

In this thesis theoretical calculations of first-order molecular properties on small closed-shell molecules are presented. Most of these molecules contain one or more heavy elements. Relativity is incorporated in a rigorous manner in our models by employing the Dirac-Coulomb Hamiltonian, guaranteeing that the most important relativistic effects are taken into account. In most applications careful attention is payed to the use of suitable basis sets. While the most common basis sets in quantum chemistry are energy optimized basis sets, some of the basis sets that are used in this work are specially developed to give good results for the properties of interest. These basis sets are systematically optimized using an even-tempered basis set scheme. The electronic structure method that gives the best results for the investigated systems, within an affordable time, is expected to be the coupled-cluster singles doubles with non-iterative triples method (CCSD(T)). This is thus

the method that has been used in most of the calculations presented here.

The coupled-cluster correlation contribution to the properties has been calculated using the finite-field method, i.e. calculations using different perturbation strengths are performed, and numerical differentiation on the perturbed energies is applied. One of the disadvantages of the finite-field method is that it is not suitable for all molecular properties. The finite-field method can only be applied to the calculation of parity-violation energies if light elements are present. Due to numerical problems it can not be applied for this property if heavier elements are present. Numerical problems can be avoided if analytical formulas are derived for the calculation of properties. In chapter 2 formulas for the analytical evaluation of first-order molecular properties at the second-order Møller-Plesset perturbation theory (MP2) level are presented. The derivation starts from the MP2 correlation energy expression within a Dirac-Coulomb framework which is differentiated with respect to a general perturbation strength parameter, λ.

It is common practice in calculations on systems that contain somewhat heavier elements to include only the valence (and subvalence) electrons in the correlation part of the calculation. High energy virtual spinors (orbitals) can safely be neglected as well. The analytical formalism presented allows for the use of these so-called inactive spinors. Although the inactive spinors do not enter the MP2 energy expression, they show up in the analytical derivative expressions, due to full-relaxation of the active spinors to the perturbation. The same is true for the negative energy spinors: they are not present in the MP2 energy expression but appear in the expressions for the analytical derivative.

The formalism described has been implemented in the four-component electronic structure program DIRAC. Explicit transformation of two-electron integrals to indices that correspond to inactive spinors can be avoided by applying the transformation to these indices in a later stage, i.e. after the formation of the Lagrangian in AO or mixed AO/MO basis. The need to solve a set of coupled equations for each perturbation has been circumvented by use of the Z-vector technique of Handy and Schaefer. The bottleneck of the current implementation is the transformation of two-electron integrals that include small components. This bottleneck might be overcome by neglecting two-electron integrals that include small component basis functions on different nuclei − the one-center approximation. This approximation has already been applied successfully in Dirac-Coulomb Hartree-Fock theory. Further speed up can be obtained by parallelizing the analytical MP2 property code.

This code is used for the calculation of parity-violation energies in chiral molecules. The electroweak neutral current between electrons and nucleons causes a small difference in properties between mirror image molecules. Par-

ity is violated. However, this effect is so small, that, up to now, it is yet to be detected in experiments. Theoretical calculations might help in finding suitable molecules for experiment, and can predict where to look; however, more experience of the effect of different approximations in these molecular calculations has to be gained. For example, not much is known about the effect of electron correlation on parity-violation energies. In chapter 7 the effect of electron correlation has been calculated on H_2X_2 (X = O, S, Se, and Te). Previous correlated relativistic calculations on these systems, employing the finite-field method, were restricted to X = O and S. The newly developed analytical formalism allows calculations on heavier elements. In general, the effect of electron correlation on these systems does not appear to be essential, ranging from a few percent to about 15%. There is, however, a strong geometry-dependence. Compared to other properties, the correlation contribution to this property is very sensitive to the active space used. Only a few occupied spinors can be kept inactive.

A molecule that is more suitable for experimental observation of parity-violation effects is CHFClBr. Currently this molecule is being investigated using molecular beam spectroscopy. Calculations on this molecule are shown in chapter 8. The effect of parity-violation on the C-F stretching mode of CHFClBr is investigated using Hartree-Fock (HF), MP2 and density functional theory (DFT). Although the different methods show quite large differences in the total parity-violation energies, the differences in the fundamental transition frequencies of the C-F stretching mode are not so large. The frequency differences between the two enantiomers of CHFClBr range from 1.8 mHz using HF to 2.6 mHz if B3LYP is employed. MP2 gives 2.4 mHz. However, these numbers indicate that the sensitivity of the current experimental setups has to be improved by roughly a factor thousand to be able to detect this tiny frequency difference between *R*-and *S*-isomers!

The combination of experimental nuclear quadrupole coupling constants (NQCC) at a nucleus with a theoretical value of the electric field gradient (EFG) allows for the determination of the electric quadrupole moment of the corresponding nucleus. This route to obtain a value for the nuclear quadrupole moment (NQM) is called the 'molecular method' since it needs the molecular NQCC and EFG as input. In chapter 3 and 4, new values for the NQM of ^{115}In and ^{127}I are derived.

The new value for the NQM of ^{115}In is 770(8) mb, compared to the old standard value of 810(60) mb. This value is obtained by combining the vibrationally corrected NQCCs of four indium halides with calculated DC-CCSD(T) EFGs at In in these molecules. An extensive and systematic basis set study at the DC-HF level of theory is performed and it is shown that the EFG converges very slowly toward the HF basis set limit, especially for

high angular momentum functions. Relativistic effects are found to be very important, contributing about 10%. Correlation contributions are of the same magnitude but are of opposite sign.

The new recommended value for the NQM of ^{127}I is $-696(12)$ mb, compared to the value of -710(10) mb in the 2001 compilation of NQMs. To get a good insight into the consistency of the NQMs obtained (in principle the value should be independent of the molecule used) we used nine different diatomic molecules. The molecules giving results that deviate most from the average value are the coinage metal containing molecules (CuI, AgI and AuI) and TlI. In contrast to DFT, coupled-cluster methods appear to work quite well for the coinage metals. Relativistic and correlation effects are very large on the EFGs of these systems. The main deficiencies in the theoretical model used are believed to be the neglect of higher order correlation contributions ($\sim 1\%$) and the Gaunt (or Breit) two-electron relativistic interaction ($\sim 0.5\%$). Calculations of the EFG at Au in AuI appear to have failed. This EFG is very small and will need calculations of a higher quality.

Besides the parity-violation energies and EFGs, the third kind of first-order molecular property that is calculated is the dipole moment. In chapter 5 the dipole moment curve of hydrogen iodide (HI) is calculated. In a recent publication the accuracy of the experimentally measured dipole moment of HI was questioned. In this chapter we show that these questions are unwarranted. To show this the DC-CCSD(T) method is used with a set of systematically 'property' optimized basis sets. It is shown that it is very important to use a large enough basis set, that includes several g and h type functions. Also, the variational inclusion of spin-orbit coupling is essential to obtain agreement between theory and experiment. It is found that without the inclusion of spin-orbit coupling, the slope of the dipole moment curve even has the wrong sign close to the equilibrium geometry.

The relativistic effect on the dipole moment surface (DMS) of water is presented in chapter 6. The relativistic contribution to the DMS of water is currently being used as a correction to a highly accurate non-relativistic *ab initio* DMS by a collaborating research group. Together with a state of the art potential energy surface, this should help in the interpretation of high temperature rotation-vibration spectra of water. Rotation-vibration spectra of water have a lot of important applications. As expected, the relativistic effect on the dipole moment of a light molecule like water is very modest. On a large part of the surface the effect is on the order of 0.20% - 0.30%. On the entire surface, relativistic effects make the dipole moment smaller and hence the intensities of the rotation-vibration lines will be lower.

Future Dirac-Coulomb coupled-cluster calculations on first-order properties would certainly benefit from an implementation of analytical formulas.

Besides a reduction in the number of calculations that need to be performed, it would also allow the calculation of coupled-cluster parity-violation energies in systems containing heavier elements. With the formulation and implementation of the formulas for MP2, as presented in this thesis, a first step in this direction has been made.

Samenvatting

Computerprogramma's waarmee eigenschappen van moleculen uitgerekend kunnen worden zijn van grote waarde in de scheikunde en natuurkunde. Theoretisch berekende NMR spectra kunnen bijvoorbeeld goed van pas komen als de experimentele spectra complex zijn of als er onduidelijkheid is over de aard van de aanwezige moleculen. Met behulp van theoretische berekeningen is het ook mogelijk om een beter begrip te krijgen van wat er nu precies gebeurt in dynamische processen. Al met al zijn er vele voorbeelden te noemen waaruit het nut van theoretische berekeningen blijkt. Voor sommige toepassingen is het voldoende wanneer het gebruikte model resultaten geeft die van een redelijke nauwkeurigheid zijn. Voor andere toepassingen zijn berekeningen echter alleen waardevol wanneer ze van een zeer hoge nauwkeurigheid zijn. De meeste resultaten die in dit proefschrift zijn beschreven, zijn van de tweede soort. Het doel is in het algemeen een zo hoog mogelijke nauwkeurigheid te bereiken.

Voor moleculen waarin alleen lichte elementen aanwezig zijn, zijn de belangrijkste 'parameters' om een hoge nauwkeurigheid te bereiken de electronenstructuurmethode die gebruikt wordt, en de kwaliteit van de basisset. Als er echter zware elementen aanwezig zijn of als de electronendichtheid in de nabijheid van de kern belangrijk is voor de eigenschap waar naar gekeken wordt, dan moeten de consequenties die speciale relativiteit op de beweging van de electronen heeft ook in rekening worden genomen.

In dit proefschrift zijn berekeningen van eerste-orde-eigenschappen aan kleine gesloten-schil moleculen beschreven. In de meeste van deze moleculen zijn één of meer zware elementen aanwezig. Relativiteit is op een adequate manier in het gebruikte model verdisconteerd door de Dirac-Coulomb-Hamiltoniaan te gebruiken. Op deze manier kunnen we er zeker van zijn dat de belangrijkste relativistische effecten zijn meegenomen. In de meeste toepassingen is veel aandacht besteed aan het gebruik van goede basissets. Terwijl de meeste basissets die in de quantumchemie worden gebruikt naar energie geoptimaliseerd zijn, zijn sommige basissets die voor dit onderzoek gebruikt zijn speciaal ontwikkeld om een goed resultaat te geven voor de

eigenschap waar op dat moment naar gekeken is. Deze basissets zijn op een systematische manier geoptimaliseerd met behulp van een even-getempereerd basissetschema. Verwacht mag worden dat de electronenstructuurmethode die de beste resultaten oplevert, binnen een veroorloofbare rekentijd, de gekoppeld-clustermethode met enkele, dubbele en niet-iteratief behandelde drievoudige excitaties (CCSD(T)), is. Om die reden is deze dan ook de gebruikte methode in de meeste van de hier beschreven berekeningen.

De bijdrage van de gekoppeld-clustercorrelatie aan de eigenschappen is uitgerekend met behulp van de eindig-veld-methode; dat wil zeggen dat er berekeningen met verschillende verstoringen zijn uitgevoerd en dat er vervolgens numerieke differentiatie op deze verstoorde energieën is toegepast. Een van de nadelen van de eindig-veld-methode is echter dat deze niet toepasbaar is voor alle moleculaire eigenschappen. De eindig-veld-methode kan alleen worden toegepast voor het berekenen van pariteitsverbrekingsenergieën als er lichte elementen aanwezig zijn. Vanwege numerieke problemen kan de eindig-veld-methode niet worden gebruikt voor deze eigenschap als wat zwaardere elementen aanwezig zijn. Deze problemen kunnen worden vermeden als analytische formules voor moleculaire eigenschappen worden gebruikt. In Hoofdstuk 2 worden formules voor het analytisch uitrekenen van eerste-orde eigenschappen voor tweede-orde Møller-Plesset-storingsrekening (MP2) gegeven. De afleiding van deze formules begint bij de Dirac-Coulomb-MP2-correlatieënergieuitdrukking, die wordt gedifferentieerd naar een algemene verstoringssterkteparameter λ.

Het is gebruikelijk om in berekeningen aan systemen die enigzins zware elementen bevatten alleen de valentie- (en soms subvalentie-) electronen in het gecorreleerde gedeelte van de berekening mee te nemen. Hoog energetische, virtuele spinoren (orbitalen) kunnen eveneens worden verwaarloosd. Het analytische formalisme dat is beschreven in dit proefschrift, laat het gebruik van deze zogenaamde inactieve spinoren dan ook toe. Hoewel de inactieve spinoren niet in de MP2-energieuitdrukking voorkomen, verschijnen ze wel in de uitdrukking voor de analytische afgeleide. Dit komt door de volledige relaxatie van de actieve spinoren aan de verstoring. Hetzelfde geldt voor de negatieve-energie spinoren, deze zijn niet present in the MP2-energieuitdrukking maar wel in de uitdrukking voor de analytische afgeleide.

Het beschreven formalisme is geïmplementeerd in het vier-componenten electronenstructuurprogramma DIRAC. Expliciete transformaties van de twee-electronintegralen naar indices die corresponderen met inactieve spinoren kunnen worden vermeden door de transformaties naar deze indices in een later stadium uit te voeren, namelijk na de vorming van de Lagrangiaan in AO- of gemengde AO/MO-basis. Het oplossen van een verzameling gekoppelde vergelijkingen voor iedere verstoring is vermeden door gebruik te maken

van de Z-vector methode van Handy en Schaefer. De flessehals van de huidige implementatie is de transformatie van twee-electronintegralen die kleine-component basisfuncties bevatten. Deze flessehals zou in de toekomst kunnen worden overwonnen door twee-electronintegralen die kleine-component basisfuncties op verschillende kernen bevatten, te verwaarlozen, de zogenaamde één-centrumbenadering. Deze benadering is reeds succesvol toegepast in Dirac-Coulomb-Hartree-Fock-theorie. Verdere versnelling van het programma kan worden behaald door de analytische MP2-eigenschapcode te parallelliseren.

De code is gebruikt voor het uitrekenen van pariteitsverbrekingsenergieën in chirale moleculen. De electro-zwakke neutrale-stroominteractie tussen electronen en nucleonen veroorzaakt een klein verschil tussen de eigenschappen van spiegelbeeldmoleculen. Pariteit is verbroken. Dit effect is echter zo klein, dat het, tot op heden, niet is aangetoond in het laboratorium. Theoretische berekeningen zouden van nut kunnen zijn bij het vinden van geschikte moleculen voor experimenten en zouden vervolgens gebruikt kunnen worden bij het vinden van de verschillen in de spectra van twee spiegelbeeldisomeren. Echter, voordat berekeningen echt van waarde kunnen zijn voor dit onderzoeksgebied moet er meer inzicht worden verworven in de verschillende benaderingen die worden gemaakt. Er is bijvoorbeeld nog niet veel bekend over het effect van electronencorrelatie op pariteitverbrekingsenergieën. In Hoofdstuk 7 wordt het effect dat electronencorrelatie heeft op deze energieën in H_2X_2 (X = O, S, Se, en Te) beschreven. Eerdere gecorreleerde relativistische berekeningen aan deze systemen waren beperkt tot X = O en S. Het nieuwe analytische formalisme maakt het nu mogelijk om aan zwaardere elementen te rekenen. Al met al blijkt het effect van electronencorrelatie op deze systemen echter niet zo groot te zijn, variërend van een paar procent tot ongeveer 15%. Er valt echter wel een sterke geometrieafhankelijkheid te constateren. Vergeleken met andere eigenschappen is de correlatiebijdrage ook erg gevoelig voor de actieve ruimte die gebruikt wordt: slechts weinig bezette spinoren kunnen inactief worden gelaten.

Een molecuul dat meer geschikt is voor het experimenteel aantonen van pariteitsverbrekingseffecten is CHFClBr. Dit molecuul wordt momenteel onderzocht met behulp van molecuulbundelspectroscopie. Resultaten van berekeningen aan dit molecuul zijn te vinden in Hoofdstuk 8. Het effect van pariteitsverbreking op de C-F strekvibratiemodus van CHFClBr is onderzocht met behulp van Hartree-Fock (HF), MP2 en dichtheidsfunctionaaltheorie (DFT). Hoewel de verschillende methoden behoorlijk grote verschillen laten zien in de totale pariteitsverbrekingsenergieën is het verschil in de fundamentele overgangsfrequentie van de C-F strekvibratiemodus niet zo groot. Het verschil tussen de twee enatiomeren van CHFClBr varieert van 1,8 mHz

met HF, 2,4 mHz met MP2 tot 2,6 mHz wanneer B3LYP wordt gebruikt. Deze getallen geven echter aan dat de gevoeligheid van huidige experimentele opstellingen met ongeveer een factor duizend verbeterd moet worden om het frequentieverschil tussen de *R*-and *S*-isomeren te kunnen detecteren!

De combinatie van experimentele kernquadrupoolkoppelingsconstanten (NQCC) op een kern in een molecuul met de electrische veldgradient (EFG) op die kern maakt het mogelijk om het electrische quadrupoolmoment van de desbetreffende kern te bepalen. Deze manier om een waarde van het kernquadrupoolmoment (NQM) te verkrijgen wordt de 'moleculaire methode' genoemd omdat zij de moleculaire NQCC en EFG nodig heeft. In Hoofdstukken 3 en 4 worden nieuwe waarden voor de NQM van ^{115}In en ^{127}I bepaald.

De nieuwe waarde voor de NQM van ^{115}In is 770(8) mb. Deze moet worden vergeleken met de oude standaardwaarde van 810(60) mb. Deze waarde is verkregen door combinatie van de vibrationeel-gecorrigeerde NQCC's van vier indium-halogeniden met uitgerekende DC-CCSD(T) EFG's op In in deze moleculen. Een uitgebreide en systematische basissetstudie op DC-HF niveau liet zien dat de EFG zeer langzaam convergeert naar de HF basissetlimiet, met name voor hoge baanimpulsmomentfuncties. Relativistische effecten zijn, met een bijdrage van ongeveer 10%, zeer belangrijk. Correlatiebijdragen zijn ongeveer even groot, maar zijn tegengesteld van teken.

De nieuwe aanbevolen waarde voor de NQM van ^{127}I is $-696(12)$ mb. De waarde in de samenvatting van NQM's uit 2001 is -710(10) mb. Om inzicht te krijgen in de consistentie van de verkregen NQM's − in principe zou de waarde onafhankelijk moeten zijn van het gebruikte molecuul − zijn er negen verschillende twee-atomige moleculen gebruikt. De moleculen die resultaten geven die het meest van de gemiddelde waarde afwijken, zijn de muntmetaal bevattende moleculen (CuI, AgI en AuI) en TlI. In tegenstelling tot DFT werkt de gekoppeld-clustermethode behoorlijk goed voor de muntmetalen. Relativistische en correlatieëffecten zijn erg groot in deze systemen. De belangrijkste deficiënties in het gebruikte theoretische model zijn waarschijnlijk de verwaarlozing van hogere orde correlatiebijdragen ($\sim 1\%$) en de Gaunt (of Breit) twee-electron relativistische interactie ($\sim 0,5\%$). Berekeningen van de EFG op Au in AuI blijken niet succesvol te zijn. De EFG op goud is erg klein en berekeningen van een hogere kwaliteit zijn nodig.

Een derde eerste-orde-eigenschap, na de pariteitsverbrekingsenergieën en de EFG's, waar aan gerekend is, is het dipoolmoment. In Hoofdstuk 5 wordt het resultaat van de berekening van de dipoolmomentcurve van waterstofjodide (HI) getoond. In een recent artikel werd de nauwkeurigheid van het experimenteel bepaalde dipoolmoment van HI in twijfel getrokken. In dit hoofdstuk wordt aangetoond dat deze twijfels niet gegrond zijn. Om dit te bewijzen is gebruik gemaakt van de DC-CCSD(T)-methode met basissets,

systematisch geoptimaliseerd naar ,,eigenschap". Aangetoond wordt dat het erg belangrijk is een basisset te gebruiken die groot genoeg is en die verscheidene g en h functies bevat. Om overeenstemming van theorie met experiment te verkrijgen is het eveneens essentieel om spin-baan-koppeling op een variationele manier in rekening te nemen. Zonder spin-baan-koppeling mee te nemen heeft de helling van de dipoolmomentcurve zelfs het verkeerde teken rond de evenwichtsgeometrie.

De relativistische effecten op het dipoolmomentoppervlak (DMS) van water zijn te vinden in Hoofdstuk 6. De relativistische bijdrage aan de DMS van water wordt momenteel gebruikt als een correctie op een hoog-nauwkeurige niet-relativistische *ab initio* DMS door een samenwerkende onderzoeksgroep. Samen met een state-of-the-art potentiele-energie-oppervlak moet dit van nut zijn voor de interpretatie van hoge-temperatuur-rotatie-vibratiespectra van water. Rotatie-vibratiespectra van water hebben vele belangrijke toepassingen. Zoals verwacht is het relativistische effect op het dipoolmoment van water zeer gering. Op een groot gedeelte van het oppervlak is het effect ongeveer 0,20% - 0,30%. Over het gehele oppervlak maken relativistische effecten het dipoolmoment kleiner. Dit betekent dan ook dat de intensiteiten van rotatie-vibratielijnen lager zullen zijn wanneer relativistische effecten meegenomen worden.

Toekomstige Dirac-Coulomb gekoppeld-cluster berekeningen aan eerste-orde eigenschappen zullen zeker voordeel hebben van een implementatie van analytische formules. Naast een reductie van het aantal berekeningen dat uitgevoerd moet worden zou het ook betekenen dat pariteitsverbrekingsenergiën aan systemen met zware elementen op gekoppeld-cluster niveau gedaan kunnen worden. Met de uitwerking en de implementatie van een analytisch formalisme voor MP2, zoals beschreven in dit proefschrift, is een eerste stap in deze richting gezet.

Dankwoord

Op deze plaats wil ik alle mensen bedanken die direct dan wel indirect hebben bijgedragen aan het tot stand komen van dit proefschrift.

Allereerst wil ik mijn copromotor Luuk Visscher hartelijk bedanken. Luuk, jouw bijdrage aan dit proefschrift is groot en ik zou niet weten hoe dit boekje er zonder jouw hulp uit zou hebben gezien. Ik ben je dankbaar voor je kritische houding. Ik denk bovendien met veel plezier terug aan het hardlopen in het Amsterdamse Bos tijdens de lunchpauzes op vrijdag in de eerste twee jaar van m'n promotie. Hetzelfde geld voor de KNCV-Run in Amersfoort waar we namens de VU een aantal keer aan hebben deelgenomen.

Mijn promotor Evert Jan Baerends wil ik bedanken voor het kritisch doorlezen van het manuscript en voor de vrijheid die je me hebt geschonken tijdens het onderzoek.

Ivan, my ...! I want to thank you for the fun we had during and outside office hours. You'll have to cope with my daily sneeze for another two years man! I hope that, after Pulp Fiction and The Big Lebowski, we will soon find another 'school of life' movie. I also want to thank you for taking the pictures of my hand.

M'n kamergenoot gedurende de eerste twee jaar, Erik, wil ik bedanken voor z'n gezelschap. Dat jouw ADF berekening aan AuI slechts 10 minuten in beslag nam terwijl mijn coupled-cluster berekening met DIRAC maar liefst 10 dagen duurde heeft mij wel jaloers gemaakt. Gelukkig voor mij bleek DFT voor dit systeem niet succesvol te zijn...

I would like to thank Markus Pernpointner for helping me during the first stage of my PhD with the DIRAC program and initial EFG calculations. Another DIRAC-user that I want to mention is Timo Fleig, thanks for your help and interesting discussions about music and soccer.

I want to thank all the DIRAC-developers for the enjoyable time at the yearly DIRAC-meeting in Denmark. I want to thank Hans Jørgen Jensen for the collaboration during the MP2 gradient project and for the time spend as one of the members of the reading committee. Trond Saue, I want to thank you for useful exchange of data, somehow it appeared that we were often

working on a similar project, fortunately this finally resulted in a joined paper. I also very much appreciate your role as a member of the reading committee.

Ook wil ik de twee Nederlandse leden van de leescommissie, Paul Wormer en Wim Ubachs, bedanken voor het kritisch doorlezen van het manuscript.

I want to thank John Ogilvie for the good contact we had during the HI project, although sometimes your obsession for SI units drove me really crazy. Jonathan Tennyson and Attila Császár, although we never met each other and only had contact via e-mail, I thank you both for the collaboration on the water project. Peter Schwerdtfeger, I would like to thank you for the collaboration on the CHFClBr project.

Paula, hartelijk bedankt voor het ontwerpen van de omslag van dit boekje. Ik wil Drew bedanken voor het verbeteren van het Engels van het inleidende hoofdstuk en de Engelstalige samenvatting. Theodoor wil ik bedanken voor het verbeteren van de Nederlandstalige samenvatting. Myrta, bedankt voor het beantwoorden van allerlei vragen omtrent de promotie.

Marc, heer van het goede leven, aan het stiften? Ja daar kun je wel om lachen... Ik wil je bedanken voor de lol de we hebben gehad op de afdeling. Matthias wil ik bedanken voor de prettige samenwerking gedurende de vakken Inleiding Computer Gebruik en Chemische Informatica. Ik hoop dat onze samenwerking tijdens het katalyseproject ook succesvol zal zijn. I want to thank Andre Gomes for the nice time we had during your visit to Amsterdam. I also want to thank Franco Buda, Jeff Nagle and Steve Wolff for running together in the Amsterdamse Bos during lunchtime on Friday. Manuel, Peter en Marcello wil ik bedanken voor de uren die we samen in verscheidene klimhallen hebben doorgebracht. Pier, ik vind het altijd leuk als je er weer bent op vrijdag, bedankt voor je gesprekken over voetbal en andere zaken. I want to thank Christoph, Johannes and Patricia for watching movies together in the coffee room. Verder wil ik alle andere (ex-)leden van de afdeling bedanken voor de goede sfeer (deze lijst is met het uitdijen van de groep inmiddels te lang geworden om helemaal uit te schrijven).

Arjen en Janneke wil ik bedanken voor de gezamenlijke lunches op de woensdagen.

Naast mijn collega's aan de VU wil ik ook nog een aantal andere mensen bedanken voor de interesse die ze in mijn werk hebben getoond en het bezorgen van de broodnodige afleiding naast het onderzoek. Vrienden uit Heerhugowaard e.o.: Lennard & Liseth, Jurgen & Annemarie, Rob & Lucienne, Gert-Jan & Emmy, Frank & Patty en Geco. M'n vrienden uit Amsterdam: Adem, Heiko, Ismail en Richard. En last but not least, m'n ouders en broertje Bas.

List of publications

1. J. N. P. van Stralen and L. Visscher, "The nuclear quadrupole moment of ^{115}In from molecular data", J. Chem. Phys. **117**, 3103 (2002).

2. J. N. P. van Stralen and L. Visscher, "Molecular relativistic electric field gradient calculations suggest revision of the value of the nuclear electric quadrupole moment of ^{127}I", Mol. Phys. **101**, 2115 (2003).

3. J. N. P. van Stralen, L. Visscher, and J. F. Ogilvie, "Theoretical and experimental evaluation of the radial function for electric dipole moment of hydrogen iodide", Phys. Chem. Chem. Phys. **6**, 3779 (2004).

4. J. N. P. van Stralen, L. Visscher, C. V. Larsen, and H. J. Aa. Jensen, "First order MP2 molecular properties in a relativistic framework", *accepted for publication in Chem. Phys.*

5. P. Schwerdtfeger, T. Saue, J. N. P van Stralen, and L. Visscher, "Relativistic second-order many-body and density functional theory for the parity-violation contribution to the C-F stretching mode of CHFClBr", *accepted for publication in Phys. Rev. A.*

Bibliography

[1] J. Gauss, in *Modern Methods and Algorithms of Quantum Chemistry*, edited by J. Grotendorst (NIC series, Jülich, 2000), vol. 3.

[2] T. Helgaker, M. Jaszuński, and K. Ruud, Chem. Rev. **99**, 293 (1999).

[3] Y. Yamaguchi, Y. Osamura, J. D. Goddard, and H. F. Schaefer III, *A New Dimension to Quantum Chemistry. Analytic Derivative Methods in Ab Initio Molecular Electronic Structure Theory* (Oxford University Press, Oxford, 1994).

[4] E. A. C. Lucken, *Nuclear Quadrupole Coupling Constants* (Academic Press, London, 1969).

[5] P. J. Hore, *Nuclear Magnetic Resonance* (Oxford University Press, Oxford, 1995).

[6] C. J. Evans, A. Lesarri, and M. C. L. Gerry, J. Am. Chem. Soc. **122**, 6100 (2000).

[7] P. Pyykkö, Mol. Phys. **99**, 1617 (2001).

[8] M. Pernpointner, P. Schwerdtfeger, and B. A. Hess, J. Chem. Phys. **108**, 6739 (1998).

[9] V. Kellö and A. J. Sadlej, Phys. Rev. A **60**, 3575 (1999).

[10] P. R. Bunker and P. Jensen, *Molecular Symmetry and Spectroscopy,* 2nd edition (NRC Research Press, Ottawa, 1998).

[11] J. Tennsyon, in *Computational Molecular Spectroscopy*, edited by P. R. Bunker and P. Jensen (Wiley, Chisester, 2000).

[12] H. Partridge and D. W. Schwenke, J. Chem. Phys. **106**, 4618 (1997).

[13] J. Tennyson and O. L. Polyansksy, Contemp. Phys. **39**, 283 (1998).

[14] P. Pulay and W. Meyer, J. Chem. Phys. **57**, 3337 (1972).

[15] Y. Yamaguchi, M. Frisch, J. Gaw, H. F. Schaefer III, and J. S. Binkley, J. Chem. Phys. **84**, 2262 (1986).

[16] F. Hund, Z. Phys **43**, 805 (1927).

[17] H. Primas, *Chemistry, Quantum Mechanics and Reductionism* (Springer-Verlag, Berlin, 1981).

[18] M. Quack, Angew. Chem **101**, 588 (1989).

[19] T. Lee and C. Yang, Phys. Rev. **104**, 254 (1956).

[20] C. S. Wu, R. W. Hayward, D. D. Hoppes, and H. R. P., Phys. Rev. **105**, 1413 (1957).

[21] S. L. Glashow, Nuc. Phys. **22**, 579 (1961).

[22] S. Weinberg, Phys. Rev. Lett. **19**, 1264 (1967).

[23] A. Salam, in *Proceedings of the 8th Nobel Symposium*, edited by N. Svartholm (Almqvist and Wiksell, Stockholm, 1968), p. 367.

[24] P. Schwerdtfeger, J. K. Laerdahl, and C. Chardonnet, Phys. Rev. A **65**, 2508 (2002).

[25] R. Berger, in *Relativistic Electronic Structure Theory – Part 2: Applications*, edited by P. Schwerdtfeger (Elsevier, Amsterdam, 2004), p. 188.

[26] J. K. Laerdahl and P. Schwerdtfeger, Phys. Rev. A **60**, 4429 (1999).

[27] R. A. Hegstrom, D. W. Rein, and P. G. H. Sandars, J. Chem. Phys. **73**, 2329 (1980).

[28] P. Schwerdtfeger, J. Gierlich, and T. Bollwein, Angew. Chem. Int. Ed. **42**, 1293 (2003).

[29] R. Bast and P. Schwerdtfeger, Phys. Rev. Lett. **91**, 023001 (2003).

[30] P. Schwerdtfeger and R. Bast, J. Am. Chem. Soc. **126**, 1652 (2004).

[31] P. Schwerdtfeger, *Relativistic Electronic Structure Theory – Part 1: Fundamentals* (Elsevier, Amsterdam, 2002).

[32] P. Schwerdtfeger, *Relativistic Electronic Structure Theory – Part 2: Applications* (Elsevier, Amsterdam, 2004).

[33] P. A. M. Dirac, Proc. Roy. Soc. (London) **A117**, 610 (1928).

[34] P. A. M. Dirac, Proc. Roy. Soc. (London) **A126**, 360 (1929).

[35] M. H. Mittleman, Phys. Rev. A **24**, 1167 (1981).

[36] J. D. Talman, Phys. Rev. Lett. **57**, 10914 (1986).

[37] I. P. Grant and H. M. Quiney, Adv. At. Mol. Phys. **23**, 37 (1987).

[38] H. M. Quiney, H. Skaane, and I. P. Grant, Adv. Quant. Chem. **32**, 1 (1999).

[39] G. Breit, Phys. Rev. **34**, 553 (1929).

[40] J. A. Gaunt, Proc. Roy. Soc. (London) **A122**, 513 (1929).

[41] DIRAC, a relativistic *ab initio* electronic structure program, Release 3.2 (2000), written by T. Saue, V. Bakken, T. Enevoldsen, T. Helgaker, H. J. Aa. Jensen, J. K. Laerdahl, K. Ruud, J. Thyssen, and L. Visscher (http://dirac.chem.sdu.dk).

[42] L. Visscher, Ph.D. thesis, Rijksuniversiteit Groningen (1993).

[43] J. Thyssen, Ph.D. thesis, University of Southern Denmark (2001).

[44] J. G. Snijders, Ph.D. thesis, Vrije Universiteit Amsterdam (1979).

[45] L. Visscher, Chem. Phys. Lett. **253**, 20 (1996).

[46] T. Saue and H. J. A. Jensen, J. Chem. Phys. **111**, 6211 (1999).

[47] L. Visscher, Theor. Chem. Acc. **98**, 68 (1997).

[48] G. T. de Jong and L. Visscher, Theor. Chem. Acc. **107**, 304 (2002).

[49] J. K. Pedersen and H. J. A. Jensen (2004), to be published.

[50] L. Visscher, J. Comp. Chem. **23**, 759 (2002), equation (12) of this reference contains an error in the expression for $G_{pqr\bar{s}}$. The correct expression is:
$G_{pqr\bar{s}} = \left(G^{02}_{pqrs} - G^{13}_{pqrs}\right) + i\left(G^{03}_{pqrs} + G^{12}_{pqrs}\right)$.

[51] K. G. Dyall, J. Chem. Phys. **100**, 2118 (1994).

[52] W. Kutzelnigg, Int. J. Quant. Chem. **25**, 107 (1984).

[53] L. Visscher and E. van Lenthe, Chem. Phys. Lett. **306**, 357 (1999).

[54] W. Kutzelnigg, Z. Phys. D **11**, 15 (1989).

[55] W. Kutzelnigg, Z. Phys. D **15**, 27 (1990).

[56] H. A. Bethe and E. E. Salpeter, *Quantum Mechanics of One- and Two-electron atoms* (Springer, Berlin, 1957).

[57] V. Kellö, A. J. Sadlej, and B. A. Hess, J. Chem. Phys. **105**, 1995 (1996).

[58] M. Douglas and N. M. Kroll, Ann. Phys. **82**, 89 (1974).

[59] B. A. Hess, Phys. Rev. A **32**, 756 (1985).

[60] B. A. Hess, Phys. Rev. A **33**, 3742 (1986).

[61] G. Jansen and B. A. Hess, Phys. Rev. A **39**, 6016 (1989).

[62] C. Chang, M. Pélissier, and P. Durand, Phys. Scr. **34**, 394 (1986).

[63] E. van lenthe, E. J. Baerends, and J. G. Snijders, J. Chem. Phys. **99**, 4597 (1993).

[64] R. van leeuwen, E. van lenthe, E. J. Baerends, and J. G. Snijders, J. Chem. Phys. **101**, 1272 (1994).

[65] E. van lenthe, E. J. Baerends, and J. G. Snijders, J. Chem. Phys. **101**, 9783 (1994).

[66] E. van Lenthe, Ph.D. thesis, Vrije Universiteit Amsterdam (1996).

[67] L. L. Foldy and S. A. Wouthuysen, Phys. Rev. **78**, 29 (1950).

[68] S. Faas, J. G. Snijders, J. H. van lenthe, E. van lenthe, and E. J. Baerends, Chem. Phys. Lett. **246**, 632 (1995).

[69] J. M. Lévy-Leblond, Commun. Math. Phys. **6**, 286 (1967).

[70] L. Visscher and T. Saue, J. Chem. Phys. **113** (2000).

[71] G. Y. Hong, M. Dolg, and L. M. Li, Chem. Phys. Lett. **334**, 396 (2001).

[72] M. Dolg, in *Relativistic Electronic Structure Theory – Part 1: Fundamentals*, edited by P. Schwerdtfeger (Elsevier, Amsterdam, 2002), p. 793.

[73] E. J. Baerends, W. H. E. Schwarz, P. Schwerdtfeger, and J. G. Snijders, J. Phys. B **23**, 3225 (1990).

[74] M. Pernpointner and P. Schwerdtfeger, Chem. Phys. Lett. **295**, 347 (1998).

[75] L. Visscher, O. Visser, P. J. C. Aerts, H. Merenga, and W. C. Nieuwpoort, Comput. Phys. Commun. **81**, 120 (1994).

[76] K. G. Dyall, in *Relativistic and Correlation Effects in Molecules and Solids*, edited by G. L. Malli (Plenum, New York, 1994), p. 17.

[77] I. P. Grant and H. Quiney, Int. J. Quant. Chem. **80**, 283 (2000).

[78] S. Varga, E. Engel, W. D. Sepp, and B. Fricke, Phys. Rev. A **59**, 4288 (1999).

[79] W. J. Liu, G. Y. Hong, D. D. Dai, L. M. Li, and M. Dolg, Theor. Chem. Acc. **96**, 75 (1997).

[80] T. Yanai, T. Nakajima, Y. Ishikawa, and K. Hirao, J. Chem. Phys. **114**, 6526 (2001).

[81] R. McWeeny, *Methods of molecular quantum mechanics,* 2nd edition (Academic Press, London, 1989).

[82] T. Helgaker, P. Jørgensen, and J. Olsen, *Molecular Electronic Structure Theory* (Wiley, Chichester, 2000).

[83] B. O. Roos and P.-O. Widmark, *European Summerschool in Quantum Chemistry 2003* (Lund University, Lund, 2003).

[84] W. Koch and M. C. Holthausen, *A Chemist's Guide to Density Functional Theory* (Wiley-VCH, Weinheim, 2000).

[85] M. Feyereisen, G. Fitzgerald, and A. Komornicki, Chem. Phys. Lett. **208**, 359 (1993).

[86] M. Schütz, G. Hetzer, and H.-J. Werner, J. Chem. Phys. **111**, 5691 (1999).

[87] S. Saebø and P. Pulay, J. Chem. Phys. **115**, 3975 (2001).

[88] H.-J. Werner, F. R. Manby, and P. J. Knowles, J. Chem. Phys. **118**, 8149 (2003).

[89] M. Schütz and H.-J. Werner, J. Chem. Phys. **114**, 661 (2001).

[90] M. Schütz and F. R. Manby, Phys. Chem. Chem. Phys. **5**, 3349 (2003).

[91] J. Gauss and J. F. Stanton, J. Chem. Phys. **116**, 1773 (2002).

[92] K. Raghavachari, G. W. Trucks, J. A. Pople, and M. Head-Gordon, Chem. Phys. Lett. **157**, 479 (1989).

[93] E. J. Baerends and O. V. Gritsenko, J. Phys. Chem. A. **101**, 5383 (1997).

[94] S. H. Vosko, L. Wilk, and M. Nusair, Can. J. Phys. **58**, 1200 (1980).

[95] A. D. Becke, Phys. Rev. A **38**, 3098 (1988).

[96] C. T. Lee, W. T. Yang, and R. G. Parr, Phys. Rev. B. **37**, 785 (1988).

[97] J. P. Perdew and Y. Wang, Phys. Rev. B. **33**, 8800 (1986).

[98] A. D. Becke, J. Chem. Phys. **98**, 1372 (1993).

[99] T. Nakajima, T. Yanai, and K. Hirao, J. Comp. Chem. **23**, 847 (2002).

[100] K. Fægri, Jr., Theor. Chem. Acc. **105**, 252 (2001).

[101] T. H. Dunning, Jr., J. Chem. Phys. **90**, 1007 (1989).

[102] D. E. Woon and T. H. Dunning, Jr., J. Chem. Phys. **98**, 1358 (1993).

[103] D. Feller, J. Chem. Phys. **98**, 7060 (1993).

[104] W. Klopper, J. Chem. Phys. **102**, 6168 (1995).

[105] A. Halkier, W. Klopper, T. Helgaker, and P. Jørgensen, J. Chem. Phys. **111**, 4424 (1999).

[106] D. Feller, K. A. Peterson, W. A. de Jong, and D. A. Dixon, J. Chem. Phys. **118**, 3510 (2003).

[107] K. A. Peterson, D. Figgen, E. Goll, H. Stoll, and M. Dolg, J. Chem. Phys. **119**, 11113 (2003).

[108] R. Raffenetti, J. Chem. Phys. **59**, 5936 (1973).

[109] J. A. Pople, R. Krishnan, H. B. Schlegel, and J. S. Binkley, Int. J. Quant. Chem. Symp. **13**, 225 (1979).

[110] N. C. Handy and H. F. Schaefer III, J. Chem. Phys. **81**, 5031 (1984).

[111] N. C. Handy, R. D. Amos, J. F. Gaw, J. E. Rice, and E. D. Simandiras, Chem. Phys. Lett. **120**, 151 (1985).

[112] J. E. Rice, R. D. Amos, N. C. Handy, T. J. Lee, and H. F. Schaefer III, J. Chem. Phys. **85**, 963 (1986).

[113] C. M. Aikens, S. P. Webb, R. L. Bell, G. D. Fletcher, M. W. Schmidt, and M. S. Gordon, Theor. Chem. Acc. **110**, 233 (2003).

[114] M. J. Frisch, M. Head-Gordon, and J. A. Pople, Chem. Phys. Lett. **166**, 275 (1990).

[115] M. J. Frisch, M. Head-Gordon, and J. A. Pople, Chem. Phys. Lett. **166**, 281 (1990).

[116] F. Haase and R. Ahlrichs, J. Comp. Chem. **14**, 907 (1993).

[117] I. D. B. Nielsen, Chem. Phys. Lett. **255**, 210 (1996).

[118] G. D. Fletcher, A. P. Rendell, and P. Sherwood, Mol. Phys. **91**, 431 (1997).

[119] F. Weigend and M. Häser, Theor. Chem. Acc. **97**, 331 (1997).

[120] A. El Azhary, G. Rauhut, P. Pulay, and H.-J. Werner, J. Chem. Phys. **108**, 5185 (1998).

[121] P. Schwerdtfeger, T. Fischer, M. Dolg, G. Igel-Mann, A. Nicklass, H. Stoll, and A. Haaland, J. Chem. Phys. **102**, 2050 (1988).

[122] P. Norman, B. Schimmelpfennig, K. Ruud, H. J. A. Jensen, and H. Ågren, J. Chem. Phys. **116**, 6914 (2002).

[123] M. Kaupp, V. G. Malkin, O. L. Malkina, and D. R. Salahub, Chem. Phys. Lett. **235**, 382 (1995).

[124] J. Vaara, O. L. Malkina, H. Stoll, V. G. Malkin, and M. Kaupp, J. Chem. Phys. **114**, 61 (2001).

[125] V. Kellö and A. J. Sadlej, J. Chem. Phys. **93**, 8122 (1990).

[126] L. Visscher, T. Enevoldsen, T. Saue, and J. Oddershede, J. Chem. Phys. **109**, 9677 (1998).

[127] J. N. P. van Stralen and L. Visscher, J. Chem. Phys. **117**, 3103 (2002).

[128] J. Thyssen, J. K. Laerdahl, and P. Schwerdtfeger, Phys. Rev. Lett. **85**, 3105 (2000).

[129] M. Head-Gordon, Mol. Phys. **96**, 673 (1999).

[130] J. Gauss and D. Cremer, in *Advances in quantum chemistry*, edited by P. O. Löwdin (Academic Press, San Diego, 1992), vol. 23, p. 205.

[131] P. Jørgensen and T. Helgaker, J. Chem. Phys. **89**, 1560 (1988).

[132] T. Helgaker and P. Jørgensen, Theor. Chim. Acta **75**, 111 (1989).

[133] K. G. Dyall, Chem. Phys. Lett. **224**, 186 (1994).

[134] G. W. Trucks, E. A. Salter, C. Sosa, and R. J. Bartlett, Chem .Phys. Lett. **147**, 359 (1988).

[135] J. Gerratt and I. M. Mills, J. Chem. Phys. **49**, 1719 (1968).

[136] G. A. Aucar, T. Saue, L. Visscher, and H. J. A. Jensen, J. Chem. Phys. **110**, 6208 (1999).

[137] L. N. Labzowsky, Sov. Phys. JETP **32**, 94 (1971).

[138] J. Sapirstein, Phys. Scr. **36**, 801 (1987).

[139] T. Saue and L. Visscher, in *Theoretical chemistry and physics of heavy and superheavy elements*, edited by U. Kaldor and S. Wilson (Kluwer academic publisher, Dordrecht, 2003), chap. 6.

[140] T. Saue and H. J. A. Jensen, J. Chem. Phys. **118**, 522 (2003).

[141] H. A. Kramers, Proc. Acad. Sci. Amsterdam **33**, 959 (1930).

[142] L. Visscher, T. J. Lee, and K. G. Dyall, J. Chem. Phys. **105**, 8769 (1996).

[143] T. Saue, Ph.D. thesis, University of Oslo (1996).

[144] M. Abe, T. Yanai, T. Nakajima, and K. Hirao, Chem. Phys. Lett. **388**, 68 (2004).

[145] P. Pyykkö, Z. Naturforsch. A **47**, 189 (1992).

[146] C. Belfrage, S. Hörbäch, C. Levinson, I. Lindgren, H. Lundberg, and S. Svanberg, Z. Phys. A **316**, 15 (1984).

[147] R. M. Sternheimer and R. F. Peierls, Phys. Rev. A **3**, 837 (1971).

[148] R. Leiberich and P. C. Schmidt, Z. Naturforsch. A **45**, 368 (1990).

[149] W. Y. Lee, S. Bernow, W. Y. Chen, S. C. Cheng, D. Hitlin, J. W. Kast, E. R. Macagno, A. M. Rushton, and C. S. Wu, Phys. Rev. Lett. **23**, 648 (1969).

[150] E. van Lenthe and E. J. Baerends, J. Chem. Phys. **112**, 8279 (2000).

[151] W. Gordy and R. L. Cook, *Microwave Molecular Spectra* (Wiley, New York, 1970).

[152] E. A. C. Lucken, in *Advances in Nuclear Quadrupole Resonance*, edited by J. A. S. Smith (Wiley, New York, 1983), vol. 5.

[153] A. Halkier, H. Koch, O. Christiansen, P. Jørgensen, and T. Helgaker, J. Chem. Phys. **107**, 849 (1997).

[154] K. G. Dyall and K. Fægri, Jr., Theor. Chem. Acc. **94**, 39 (1996).

[155] K. G. Dyall, I. P. Grant, C. T. Johnson, F. A. Parpia, and E. P. Plummer, Comput. Phys. Commun. **55**, 425 (1989).

[156] K. G. Dyall, Theor. Chem. Acc. **99**, 366 (1998).

[157] V. Kellö, P. Pyykkö, and A. J. Sadlej, Chem. Phys. Lett. **346**, 155 (2001).

[158] M. Pernpointner and L. Visscher, J. Chem. Phys. **114**, 10389 (2001).

[159] J. Hoeft and K. P. R. Nair, Z. Phys. D **29**, 203 (1994).

[160] J. Hoeft, Chem. Phys. Lett. **155**, 273 (1989).

[161] J. Hoeft and K. P. R. Nair, Chem. Phys. Lett. **164**, 33 (1989).

[162] B. Schenk, E. Tiemann, and J. Hoeft, Z. Naturforsch. A **25**, 1827 (1970).

[163] L. Visscher and K. G. Dyall, J. Chem. Phys. **104**, 9040 (1996).

[164] A. K. Wilson, D. E. Woon, K. A. Peterson, and T. H. Dunning, Jr., J. Chem. Phys. **110**, 7667 (1999).

[165] L. Visscher and K. G. Dyall, Atom. Data Nucl. Data Tabl. **67**, 207 (1997).

[166] W. A. de Jong, L. Visscher, and W. A. Nieuwpoort, J. Mol. Struct.: THEOCHEM **458**, 41 (1999).

[167] M. Pernpointner, P. Schwerdfeger, and B. A. Hess, Int. J. Quant. Chem. **76**, 371 (2000).

[168] V. Kellö, A. J. Sadlej, P. Pyykkö, D. Sundholm, and M. Tokman, Chem. Phys. Lett. **304**, 414 (1999).

[169] J. Bieroń, P. Pyykkö, D. Sundholm, V. Kellö, and A. J. Sadlej, Phys. Rev. A **64**, 2507 (2001).

[170] J. Eberz, U. Dinger, G. Huber, H. Lochmann, R. Menges, R. Neugart, R. Kirchner, O. Klepper, T. Kühl, D. Marx, et al., Nucl. Phys. A **464**, 9 (1987).

[171] T. G. Eck and P. Kusch, Phys. Rev. **106**, 958 (1957).

[172] H. Haas and H. M. Petrilli, Phys. Rev. B. **61**, 13588 (2000).

[173] V. Kellö and A. J. Sadlej, Chem. Phys. Lett. **174**, 641 (1990).

[174] V. Kellö and A. J. Sadlej, Mol. Phys. **89** (1996).

[175] R. K. Harris, E. D. Becker, S. M. C. De Menezes, R. Goodfellow, and P. Granger, Pure Appl. Chem. **73**, 1795 (2001).

[176] L. M. Reynard, C. J. Evans, and M. C. L. Gerry, J. Mol. Spectrosc. **205**, 344 (2001).

[177] P. Schwerdtfeger, M. Pernpointner, and J. K. Laerdahl, J. Chem. Phys. **111**, 3357 (1999).

[178] E. R. Cohen and B. N. Taylor, J. Phys. Chem. Ref. Data **17**, 1795 (1988).

[179] F. Matsushima, S. Kakihata, and K. Tagaki, J. Chem. Phys. **94**, 2408 (1991).

[180] H. S. P. Müller and M. C. L. Gerry, J. Chem. Phys. **103**, 577 (1995).

[181] E. Tiemann and T. Möller, Z. Naturforsch. A **30**, 986 (1975).

[182] K. P. R. Nair, E. Tiemann, and J. Hoeft, Z. Naturforsch. A **32**, 1053 (1977).

[183] A. D. Buckingham, J. Chem. Phys. **36**, 3096 (1962).

[184] M. E. Radzig and B. M. Smirnov, *Reference Data on Atoms, Molecules and Ions* (Springer-Verlag, Berlin, 1985).

[185] P. Pyykkö and M. Seth, Theor. Chem. Acc. **96** (1997).

[186] M. Pernpointner, J. Phys. B **35**, 383 (2002).

[187] M. Pernpointner, P. Schwerdtfeger, and B. A. Hess, Int. J. Quant. Chem. **76**, 371 (2000).

[188] B. A. Hess and U. Kaldor, J. Chem. Phys. **112**, 1809 (2000).

[189] K. Fægri, Jr. and L. Visscher, Theor. Chem. Acc. **105**, 265 (2001).

[190] A. J. Sadlej, Czech. Chem. Commun. **53**, 1995 (1988).

[191] A. Pizlo, G. Jansen, B. A. Hess, and W. von Niessen, J. Chem. Phys. **98**, 3945 (1993).

[192] J. K. Laerdahl, T. Saue, and K. Fægri, Jr., Theor. Chem. Acc. **97**, 177 (1997).

[193] I. Malkin, O. L. Malkina, and V. G. Malkin, Chem. Phys. Lett. **361**, 231 (2002).

[194] V. Kellö, A. J. Sadlej, and P. Pyykkö, Chem. Phys. Lett. **329**, 112 (2000).

[195] A. Halkier, H. Larsen, J. Olsen, P. Jørgensen, and J. Gauss, J. Chem. Phys. **110**, 734 (1999).

[196] J. P. Perdew, Phys. Rev. B **33**, 8822 (1986).

[197] J. P. Perdew, K. Burke, and M. Ernzerhof, Phys. Rev. Lett. **77**, 3865 (1996).

[198] C. J. Evans and M. C. L. Gerry, J. Mol. Spectrosc. **203**, 105 (2000).

[199] R. J. Powers, P. Martin, G. H. Miller, R. E. Welsh, and D. A. Jenkins, Nucl. Phys. A **230**, 413 (1974).

[200] M. Iliaš, V. Kellö, T. Fleig, and M. Urban, Theor. Chem. Acc. **110**, 176 (2003).

[201] J. F. Ogilvie, *The vibrational and rotational spectrometry of diatomic molecules* (Academic press, London, 1998).

[202] S. R. Ungemach, H. F. Schaefer III, and B. Liu, J. Mol. Spectrosc. **66**, 99 (1977).

[203] H.-J. Werner, E. Reinsch, and P. Rosmus, Chem. Phys. Lett. **78**, 311 (1981).

[204] P. Schwerdtfeger, L. V. Szentpály, K. Vogel, H. Silberbach, H. Stoll, and H. Preus, J. Chem. Phys. **84**, 1606 (1986).

[205] D. A. Chapman, K. Balasubramanian, and S. H. Lin, J. Chem. Phys. **87**, 5325 (1987).

[206] D. A. Chapman, K. Balasubramanian, and S. H. Lin, Phys. Rev. A **38**, 6098 (1988).

[207] M. Dolg, Mol. Phys. **88**, 1645 (1996).

[208] E. van Lenthe, J. G. Snijders, and E. J. Baerends, J. Chem. Phys. **105**, 6506 (1996).

[209] G. Maroulis, Chem. Phys. Lett. **318**, 181 (2000).

[210] A. Alekseyev, H.-P. Liebermann, D. B. Kokh, and R. J. Buenker, J. Chem. Phys. **113**, 6174 (2000).

[211] O. Fossgaard, O. Gropen, M. C. Valero, and T. Saue, J. Chem. Phys. **118**, 10418 (2003).

[212] F. A. van Dijk and A. Dymanus, Chem. Phys. Lett. **5**, 387 (1970).

[213] G. Ameer and W. M. Benesch, J. Chem. Phys. **37**, 2699 (1962).

[214] P. Niay, P. Bernage, C. Coquant, and A. Fayt, J. Mol. Spectrosc. **72**, 168 (1978).

[215] H. Riris, C. B. Carlisle, D. E. Cooper, L.-G. Wang, T. F. Gallagher, and R. H. Tipping, J. Mol. Spectrosc. **146**, 381 (1991).

[216] M. O. Bulanin, A. V. Domanskaya, and K. Kerl, J. Mol. Spectrosc. **218**, 75 (2003).

[217] W. M. Benesch, J. Chem. Phys. **39**, 1048 (1963).

[218] P. C. Meyer, C. Haeusler, and P. Barchewitz, J. Phys. **26**, 305 (1965).

[219] M. O. Bulanin, A. V. Domanskaya, I. M. Grigoriev, and K. Kerl, J. Mol. Spectrosc. **223**, 67 (2004).

[220] P. Niay, P. Bernage, C. Coquant, and R. Houdart, Can. J. Phys. **56**, 727 (1978).

[221] C. Haeusler, Ph.D. thesis, University of Paris (1965).

[222] J. A. Pople, Rev. Mod. Phys. **71**, 1267 (1999).

[223] P. Pyykkö, Chem. Rev. **88**, 563 (1988).

[224] J. N. P. van Stralen and L. Visscher, Mol. Phys. **101**, 2115 (2003).

[225] R. J. Le Roy, LEVEL 7.4: A computer program for solving the radial Schrödinger equation for bound and quasibound levels. University of Waterloo Chemical Physics Research Report No. CP-642-R, 2001.

[226] M. W. Chase, J. Phys. Chem. Ref. Data Monogr. **9** (1998).

[227] F. C. de Lucia, P. Helminger, and W. Gordy, Phys. Rev. A **3**, 1849 (1971).

[228] B. Rosenblum and A. H. Nethercot, Phys. Rev. **97**, 84 (1955).

[229] K. V. Chance, T. D. Varberg, K. Park, and L. R. Zink, J. Mol. Spectrosc. **162**, 120 (1993).

[230] T. D. Varberg, J. C. Roberts, K. A. Tuominen, and K. M. Evenson, J. Mol. Spectrosc. **191**, 384 (1998).

[231] A. Goldman, K. V. Chance, M. T. Coffey, J. W. Hannigan, W. G. Mankin, and C. P. Rinsland, J. Mol. Spectrosc. Radiat. Transfer **162**, 120 (1998).

[232] P. Guelachvili, P. Niay, and P. Bernage, J. Mol. Spectrosc. **85**, 253 (1981).

[233] P. Niay, P. Bernage, H. Bocquet, and R. Houdart, J. Mol. Spectrosc. **77** (1979).

[234] T. Katayama, F. Matsushima, and H. Sasada, J. Mol. Spectrosc. **167**, 236 (1994).

[235] C. A. Burris, J. Chem. Phys. **30**, 976 (1959).

[236] J. F. Ogilvie, J. Oddershede, and S. P. A. Sauer, Adv. Chem. Phys. **111**, 475 (2000).

[237] J. F. Ogilvie, W. R. Rodwell, and R. H. Tipping, J. Chem. Phys. **73**, 5221 (1980).

[238] F. M. Fernandez and J. F. Ogilvie, MapleTech **5**, 42 (1998).

[239] X. Li and J. Paldus, J. Chem. Phys. **108**, 637 (1998).

[240] L. Visscher, J. Styszyñski, and W. A. Nieuwpoort, J. Chem. Phys. **105**, 1987 (1996).

[241] D. Z. Goodson, J. Chem. Phys. **116**, 6948 (2002).

[242] C. Fonseca Guerra, F. M. Bickelhaupt, J. G. Snijders, and E. J. Baerends, Angew. Chem **111**, 3120 (1999).

[243] I. A. C. Infante and L. Visscher, J. Com. Chem. **25**, 386 (2004).

[244] P. Nava, M. Sierka, and R. Ahlrichs, Phys. Chem. Chem. Phys. **5**, 3372 (2003).

[245] G. Tarczay, A. G. Császár, W. Klopper, V. Szalay, W. D. Allen, and H. F. Schaefer III, J. Chem. Phys. **110**, 11971 (1999).

[246] E. F. Valeev, W. D. Allen, H. F. Schaefer III, and A. G. Császár, J. Chem. Phys. **114**, 2875 (2001).

[247] O. L. Polyansky, A. G. Császár, S. V. Shirin, N. F. Zobov, P. Barletta, J. Tennyson, D. W. Schwenke, and P. J. Knowles, Science **299**, 539 (2003).

[248] R. A. Kendall, T. H. Dunning Jr, and R. J. Harrison, J. Chem. Phys. **96**, 6796 (1992).

[249] D. E. Woon and T. H. Dunning Jr, J. Chem. Phys. **103**, 4572 (1995).

[250] DALTON, T. Helgaker, H. J. Aa. Jensen, P. Jørgensen, J. Olsen, K. Ruud, H. Ågren, T. Andersen, K. L. Bak, V. Bakken, O. Christiansen, P. Dahle, E. K. Dalskov, T. Enevoldsen, B. Fernandez, H. Heiberg, H. Hettema, D. Jonsson, S. Kirpekar, R. Kobayashi, H. Koch, K. V. Mikkelsen, P. Norman, M. J. Packer, T. Saue, P. R. Taylor, and O. Vahtras, Oslo University, Norway, http://www.kjemi.uio.no/software/dalton/dalton.html.

[251] M.-A. Bouchiat, J. Guena, L. Hunter, and L. Pottier, Phys. Lett. B **117**, 358 (1982).

[252] M.-A. Bouchiat and C. Bouchiat, Rep. Prog. Phys. **60**, 1351 (1997).

[253] Y. Yamagata, J. Theor. Biol. **11**, 495 (1966).

[254] D. Rein, J. Mol. Evol. **4**, 15 (1974).

[255] V. S. Letokhov, Phys. Lett. A **53**, 275 (1975).

[256] M. Quack, Angew. Chem. Int. Ed. **41**, 4618 (2002).

[257] M. Ziskind, C. Daussy, T. Marrel, and C. Chardonnet, Eur. Phys. J. D **20**, 219 (2002).

[258] M. Quack and J. Stohner, J. Chem. Phys. **119**, 11228 (2003).

[259] R. Berger and M. Quack, J. Chem. Phys. **112**, 3148 (2000).

[260] M. Quack and J. Stohner, Phys. Rev. Lett. **84**, 3807 (2000).

[261] A. C. Hennum, T. Helgaker, and W. Klopper, Chem. Phys. Lett. **354**, 274 (2002).

[262] P. Lazzeretti and R. Zanasi, Chem. Phys. Lett. **279**, 349 (1997).

[263] A. Bakasov, T.-K. H. Ha, and M. Quack, J. Chem. Phys. **109**, 7263 (1998).

[264] J. N. P. van Stralen, L. Visscher, and J. F. Ogilvie, Phys. Chem. Chem. Phys. **6**, 3779 (2004).

[265] C. Daussy, T. Marrel, A. Amy-Klein, C. T. Nguyen, C. J. Bordé, and C. Chardonnet, Phys. Rev. Lett. **83**, 1554 (1999).

[266] J. N. P. van Stralen, L. Visscher, C. V. Larsen, and H. J. A. Jensen, Chem. Phys. *accepted* (2004).

[267] T. Saue and T. Helgaker, J. Comp. Chem. **23**, 814 (2002).

[268] A. Beil, D. Luckhaus, and M. Quack, Ber. Bunsenges. Phys. Chem. **100**, 1853 (1996).